Sonochemical and Impregnated Co-W/γ-Al_2O_3 Catalysts: Performances and Kinetic Studies on Hydrotreatment of Light Gas Oil

A Thesis submitted to the College of Graduate Studies and Research in Partial

Fulfillment of the Requirement for the

Degree of Master of Science

in the Department of Chemical Engineering

University of Saskatchewan

Saskatoon

By

Santosh K Vishwakarma

COPYRIGHT

ABSTRACT

γ-Al_2O_3 supported Co-W based catalysts with varying Co (1 - 3 wt %) and W (7 - 13 wt %) loadings were prepared using impregnation and sonochemical methods. All prepared catalysts were characterized with elemental analysis, BET analysis, X-ray diffraction (XRD), NH_3 temperature programmed desorption (TPD), temperature programmed reduction (TPR) and thermogravimetry analysis (TGA).

The performances of all the synthesized catalysts were tested at a pressure of 8.9 MPa, LHSV of 2 h^{-1} and temperatures of 340, 350 and 360 °C in a laboratory trickle bed microreactor for hydrodesulphurization (HDS) and hydrodenitrogenation (HDN) of light gas oil (LGO) derived from Athabasca bitumen. The performance tests with impregnated catalysts indicated a maximum in activity for HDS and HDN reactions (sulfur and nitrogen conversions at 93.0 and 57.1 % at 360 °C) for Co(3 wt %)-W(10 wt %)/γ-Al_2O_3 whereas the performance tests with sonochemically prepared catalysts showed a maximum in activity (sulfur and nitrogen conversions at 87.9 and 42.5 % at 360 °C) for Co(3 wt %)-W(11.5 wt %)/ γ-Al_2O_3. These two catalysts were selected for detail performance, optimization and kinetic studies. The effects of reaction temperature (340 - 380 °C), pressure (7.6 - 10.3 MPa), liquid hourly space velocity (1.5 - 2.0 h^{-1}) and hydrogen gas/gas oil ratio (400 - 800 mL/mL) were examined on HDS and HDN of LGO with these catalysts. The reaction kinetics for HDS was best fitted with a Power Law model whereas same for HDN was found to be best represented by a Langmuir-Hinshelwood model with a reasonable accuracy ($0.90 < R^2 < 0.95$). The activation energy for HDS of LGO were 14 and 12 kJ/mol for selected impregnated and sonochemically

prepared catalysts whereas the same for HDN were 0.9 and 14 kJ/mol for these catalysts, respectively.

Calculation showed that the fitted HDS rate expressions were apparent and HDN rate expressions were intrinsic under existing reaction conditions. It also showed that the pore diffusion resistances for both HDS and HDN increased with an increase in reaction temperature from 340 to 380 °C.

ACKNOWLEDGEMENT

I wish to acknowledge the inputs and contributions of a number of persons who helped me in diverse ways to bring this thesis to fruition.

First and foremost, I render my sincere gratitude to my supervisors, Dr. A. K. Dalai and Dr. J. Adjaye for their invaluable assistance and guidance in my entire experimental work and in my thesis write up. I am grateful for the time and efforts taken by them to read and correct the written materials.

Secondly, I wish to express my profound gratitude to the members of my advisory committee: Dr. H. Wang and Dr. T. Pugsley for their immense contribution and guidance. Other personalities whose efforts I want to acknowledge are my MSc degree level course instructors. They include: Dr. D. Y. Peng and Dr. R. Evitts. The knowledge imparted by them served as the basis for the entire work.

Assistances from Mr. R. Blondin and Dr. V. Sundaramurthy are also highly acknowledged. Finally, the financial assistance from NSERC is also gratefully acknowledged.

TABLE OF CONTENTS

LIST OF TABLES

LIST OF FIGURES

NOMENCLATURE

a	constant, dimensionless
c	constant, dimensionless
C_A	concentration of compound A, mol/cc
C_F	concentration of aromatic compounds in light gas oil, mol/cc
C_{iF}	concentration of i^{th} species in feed, mol/cc
C_{iP}	concentration of i^{th} species in reaction product, mol/cc
C_N	concentration of nitrogen species in light gas oil, mol/cc
C_S	concentration of sulfur species in light gas oil, mol/cc
D_{iL}	diffusivity of hydrogen in gas oil, cm^2/s
$d_{P,T}$	gas oil density at operating pressure and temperature, g/cc
$f(p_H)$	expression involving hydrogen partial pressure in Langmuir-Hinshelwood model, dimensions depend on specific rate expression
k	general definition of rate constant, dimensions depend on the specific rate expression
k'	general definition of rate constant, dimensions depend on the specific rate expression
K_F	adsorption equilibrium constant for aromatic compounds present in light gas oil, atm^{-1}
k_i	reaction rate constant for reactant i, dimensions depend on the specific rate expression
K_j	adsorption equilibrium constant for species j, MPa^{-1}
k_{hds}	rate constant for HDS of light gas oil, $mol^{0.43}$- $m^{1.71}$/s-kg cat.

K_{hds}	adsorption equilibrium constant for sulfur species in light gas oil, m^3/mol
k_{iL}	liquid film side mass transfer coefficient between hydrogen and light gas oil, cm/s
LHSV	liquid hourly space velocity, h^{-1}
m	exponent in Langmuir-Hinshelwood model, dimensionless
n	exponent in power law and Langmuir-Hinshelwood models, dimensionless
p_H	partial pressure of hydrogen, MPa
p_{H_2S}	partial pressure of H_2S, MPa
p_i	partial pressure of reactant i, MPa
p_j	partial pressure of reactant j, MPa
$-r_A$	rate of reaction for compound A, mol/s- kg cat
$-r_i$	rate of conversion of reactant i, mol/s-kg cat
r_{hdn}	rate of conversion of nitrogen species in light gas oil, mol/s-cc of cat
r_{hds}	rate of conversion of sulfur species in light gas oil, mol/s-cc of cat
S_{SN}	selectivity of sulfur compounds with respect to the nitrogen compounds, dimensionless
X_i	conversion of i^{th} species, dimensionless
β	factor defined as the ratio of the maximum temperature difference that can exist between the catalyst pellet external surface to its core, dimensionless
Φ_S	modulus for HDS of LGO, dimensionless
Φ_N	modulus for HDN of LGO, dimensionless

1 INTRODUCTION

In line with the worldwide trend in reduction in sulfur levels of fossil fuels, the Canadian Diesel Fuel Regulations mandated a reduction in the highway diesel sulfur content to 15 ppm from a previous level of 500 ppm starting from June 1, 2006 (Canada Gazette, Sulfur in diesel fuel regulation, 2002). The introduction of this stringent environmental regulation, coupled with the refractory feeds (containing very high amounts of less reactive sulfur, nitrogen and aromatic compounds and thus very hard to convert) such as gas oils derived from oil sands, has put a lot of pressure on the refiners to explore ways to meet this new challenge.

Traditionally, the oil industry uses the hydrodesulphurization process at commercial scale for reduction of sulfur in petroleum oils. Typically, commercial HDS catalysts are heterogeneous bimetallic systems which are prepared using the impregnation method. These catalysts consist of MoS_2 supported on γ-Al_2O_3, containing Co or Ni promoters that operate at a temperature of approximately 400 °C and result in the sulfur removal to 300 ppm.

It has been seen that the method of catalyst synthesis has remarkable impact on its properties. The different methods of catalyst synthesis include impregnation method, co-precipitation method, chemical vapor deposition method and sonochemical method. Out of these, the impregnation and the co-precipitation methods are most widely used throughout the industry. The chemical vapor deposition and the sonochemical methods are newer methods and are currently being investigated for synthesis of new highly active catalysts.

This thesis discusses the use of sonochemical method for synthesis of Co-W/γ-Al_2O_3 catalysts and comparison of their performances with those of catalysts synthesized using impregnation method on HDS and HDN of LGO derived from Athabasca bitumen.

1.1 Knowledge Gaps

It can be seen (see literature review) that there are not many reports on the performances of sonochemically synthesized catalysts for HDS and HDN of light gas oil derived from Athabasca bitumen in open literature. The reports in open literautre also indicate a lack of information on the performances of Co-W/ γ-Al_2O_3 catalysts on HDS and HDN of LGO derived from Athabasca bitumen. And finally, they show a lack of information on the kinetic study of HDS and HDN of LGO with the sonochemically synthesized catalysts.

1.2 Hypotheses

The following hypotheses were outlined for this work:

- It was expected that sonochemical method of synthesis of catalysts would give higher metal dispersion on support and hence result in higher activity in synthesized catalysts.
- As cobalt and tungsten show good performances for HDS and hydrogenation reactions respectively, therefore it was expected that both the metals together would improve overall HDS and HDN activity of the catalyst.

1.3 Research Objective

The overall objective was to synthesize Co-W/γ-Al_2O_3 catalysts using sonochemical and impregnation methods and then to examine and to compare their

performances for HDS and HDN of LGO derived from Athabasca bitumen. This objective was achieved in three different phases as mentioned below.

- **Phase 1: Catalysts Synthesis and their Characterization**

The objective of this phase was to synthesize Co-W/γ-Al_2O_3 catalysts using sonochemical and impregnation methods and study their physicochemical properties using various characterization methods such as elemental analysis, thermogravimetry analysis, BET surface area and pore size distribution, X-ray diffraction, temperature programmed desorption of NH_3 and temperature programmed reduction.

- **Phase 2: Catalysts Performance Evaluation and Screening**

The objective of this phase was to evaluate and to compare the performances of impregnated and sonochemically prepared catalysts at fixed reaction pressures and liquid hourly space velocity (LHSV) with different reaction temperatures for HDS and HDN reactions using LGO derived from Athabasca bitumen as feed.

- **Phase 3: Catalyst Performance and Optimization Studies, Development of Rate Equation and Post Reaction Characterization**

The objective of this phase was to study the effects of reaction temperature, pressure, LHSV and hydrogen gas/gas oil ratio on HDS and HDN of light gas derived from Athabasca bitumen using selected sonochemically synthesized and impregnated Co-W/γ-Al_2O_3 catalysts. The data obtained with the HDS and HDN performance studies were used for determination of reaction rate kinetics using Power Law and Langmuir - Hinshelwood models. The BET surface area and pore volume analysis of selected spent catalysts were done to investigate the effect of change in surface area and pore volumes upon reaction. The selected spent catalysts were also characterized using TGA with air to

obtain the information on the coke deposited upon the catalysts during the course of reaction studies. These estimated properties were explained with the HDS and HDN activity shown by catalysts.

2 LITERATURE REVIEW

This chapter presents a review of the literature pertinent to this work with a special emphasis on the concepts of hydrodesulphurization and hydrodenitrogenation of model compounds and real feeds. It also includes the effects of preparation methods on the properties of the synthesized catalysts. The different kinetic models are also discussed.

2.1 Types of Sulfur and Nitrogen Compounds in Petroleum

The sulfur content of petroleum varies from less than 0.05 to more than 8 wt % but generally falls in the range 1 to 4 wt %. The distribution of sulfur containing constituents in petroleum includes the following types (Speight, 2000):

- Non thiophenic molecules i.e. sulfides.
- Thiophenes.
- Benzothiophenes.
- Dibenzothiophenes.
- Benzonaphthothiophenes.
- Dinaphthothiophenes.

The sulfur-heterocyclic compounds in the mid distillate range are primarily the thiaclane derivative, benzothiophene derivatives and dibenzothiophene derivatives. These are major contributors in vacuum gas oil fractions (Speight, 2000). Figure 2.1 shows structural formulas of some of the sulfur compounds found in petroleum oil.

Nitrogen compounds in the crude oils usually vary from 0.1 to 1.0 wt % and these are concentrated in the fractions heavier than those containing sulfur. These compounds are

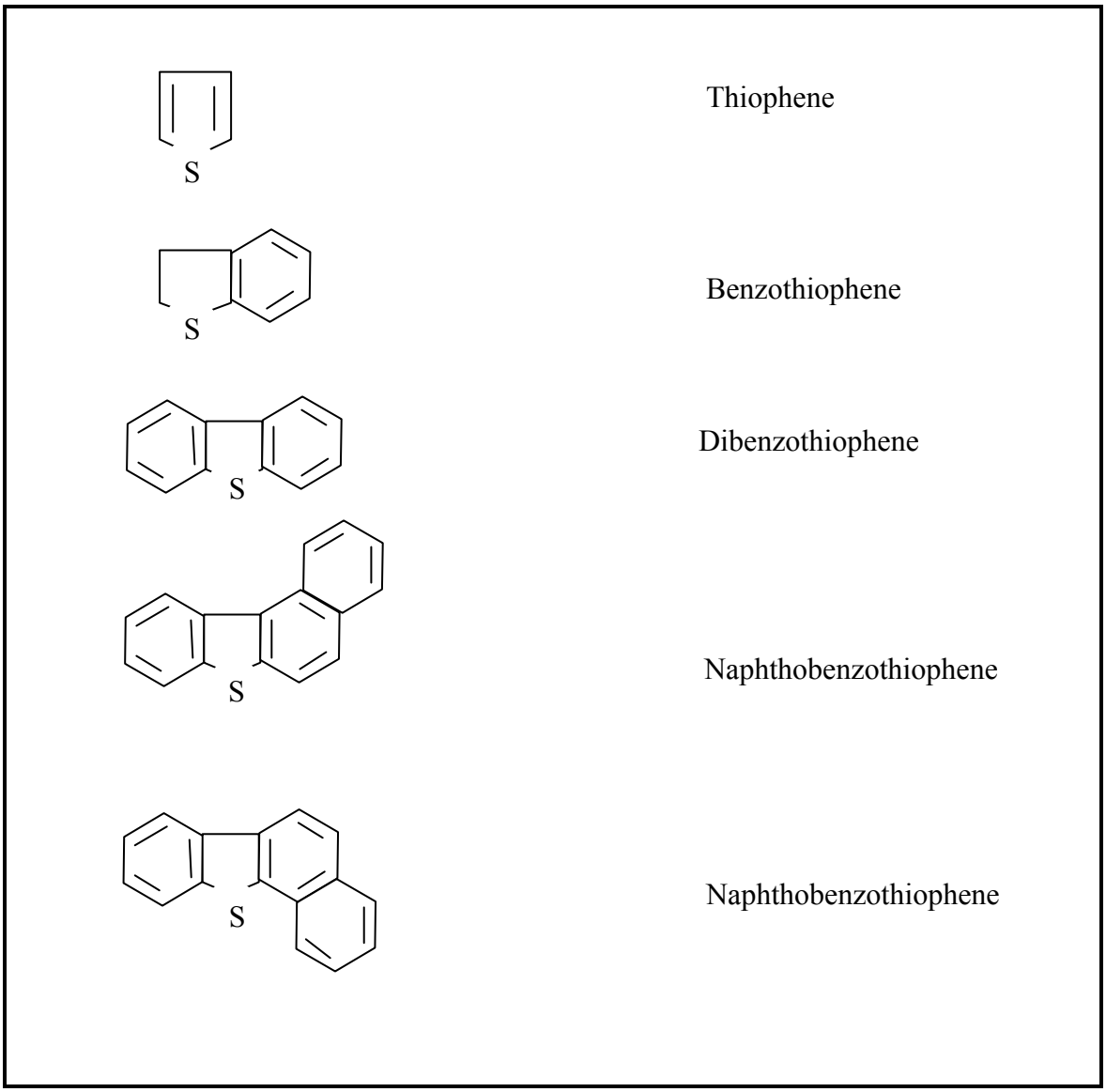

Figure 2.1: Some of the heterocyclic compounds found in petroleum oil (Speight, 2000).

mainly present as the heterocyclic aromatic compounds. Other types of nitrogen containing molecules such as aliphatic amines and nitriles, also contain a small amount of nitrogen. The heterocyclic nitrogen compounds are basically found in two forms:

- Basic nitrogen compounds such as pyridine and quinoline containing a six-ringed structure. These compounds roughly constitute one third of total nitrogen compounds present in petroleum oil.
- Non basic compounds such as pyrrole, indoles and carbazoles containing a five-ringed structure (Speight, 2000; Clausen et al., 1996).

Figure 2.2 shows the structural formulas of some of the nitrogen compounds present in petroleum oils.

2.2 Reactivity of Sulfur and Nitrogen Compounds

Research has indicated that the reactivity of sulfur compounds in petroleum oils depends on the molecular size and on the structure of the sulfur containing compounds and is reported to be in the following order.

Alkyl sulfides>Thiophene>Benzothiophene>Dibenzothiophene

Alkyl sulfides, which typically are sulfides, disulfides and thiols are quite reactive and readily desulfurized. Thiophenic compounds are the least reactive compounds for HDS. A study by Singhal et al. (1981) shows that among organosulfur compounds; dibenzithiophene (DBT) has the least HDS reactivity. The substituent groups attached to the thiophenic compounds retard the HDS reactivity. This could be attributed to the steric hindrance of substituents and to the electronic effects on adsorption of reactant onto the catalyst and the subsequent reaction (Gray et al., 1994). The HDS reactivity decreases

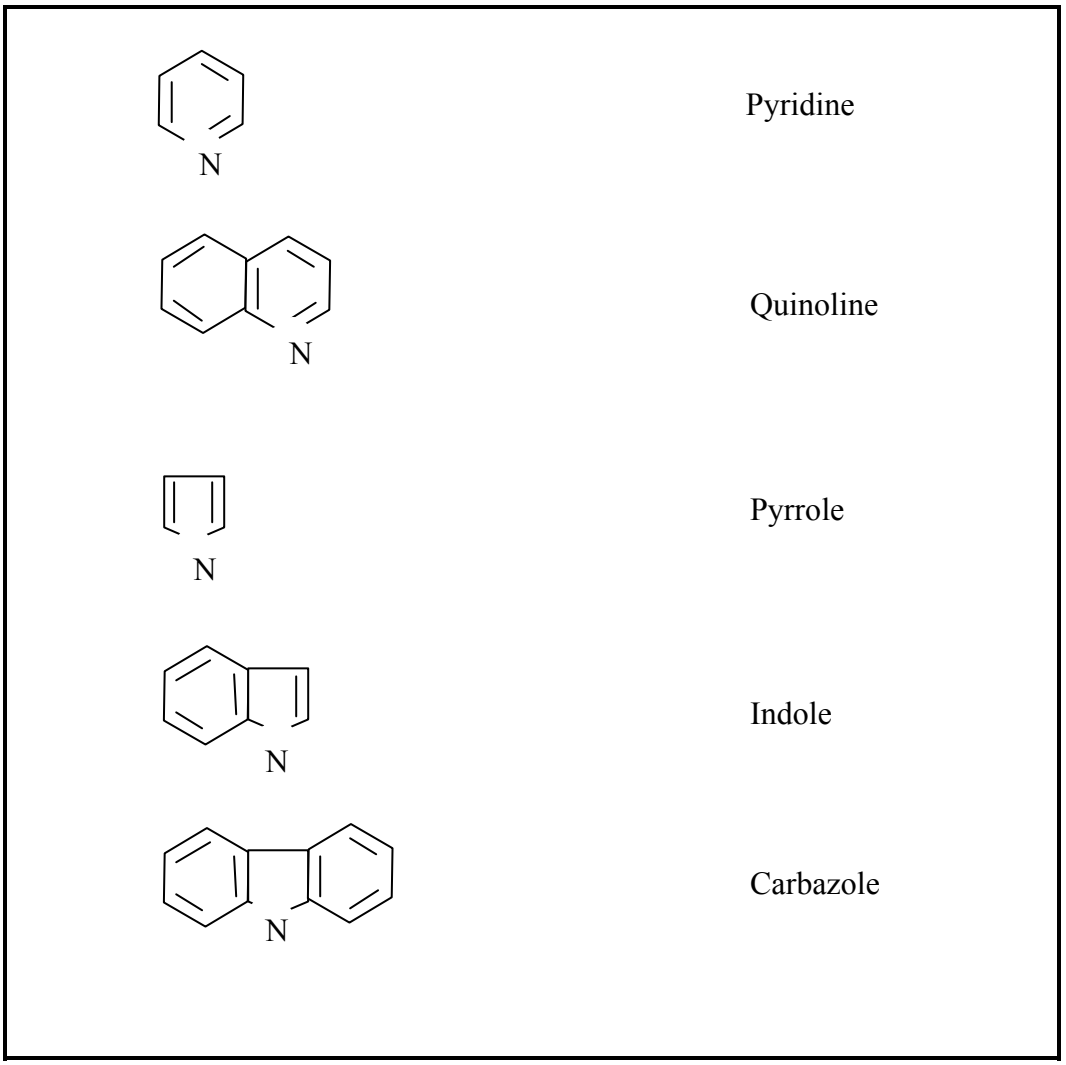

Figure 2.2: **Some of the nitrogen compounds in petroleum oils (Speight, 2000).**

further with the presence of methyl substituents at 4 and 6 positions as in 4, 6 dimethyl dibenzothiophene (4, 6 DMDBT). This may be attributed to the steric hindrance to the ability of the molecule to adsorb on the surface of the catalyst. 4, 6 DMDBT remains intact until the final stages of desulfurization and acts as the limiting reactant for the HDS reactions (Clausen et al., 1996). Zhang and Qian (1997) report a study with model compounds which shows the first order rate constants for HDS of DBT, 4 Methyl benzothiophene (4, MBDT) and 4, 6 DMDBT as 12, 4.5 and 1.5 h^{-1} at 350 °C indicating the order of their decreasing reactivity. The reactivity of thiophenic compounds also decreases with an increase in the number of aromatic rings (Ma et al., 1994c). For higher analogues of dibenzothiophenes, hydrogenation of one of the aromatic rings is preceded by HDS (Clausen et al., 1996).

The conversion of thiophenic compounds can occur by two main pathways:

- Direct removal of sulfur molecule from the aromatic ring namely hydrogynolysis.
- Saturation of the aromatic ring followed by removal of sulfur molecule.

Figure 2.3 shows the proposed mechanisms for conversion of 4, 6 DMDBT via two above-mentioned pathways. In the first pathway, the sulfur molecule is first removed and then the saturation of the aromatic ring takes place, whereas in the second pathway, first the saturation of the aromatic ring takes place and then the removal of sulfur molecule takes place (Breysse et al., 2003). Either mechanism can be followed, depending upon the reaction conditions and type of catalyst being used. For example, the initial aromatic ring saturation route is followed at high hydrogen pressure (Girgis and Gates, 1999). However, the direct sulfur removal route is the most favored reaction

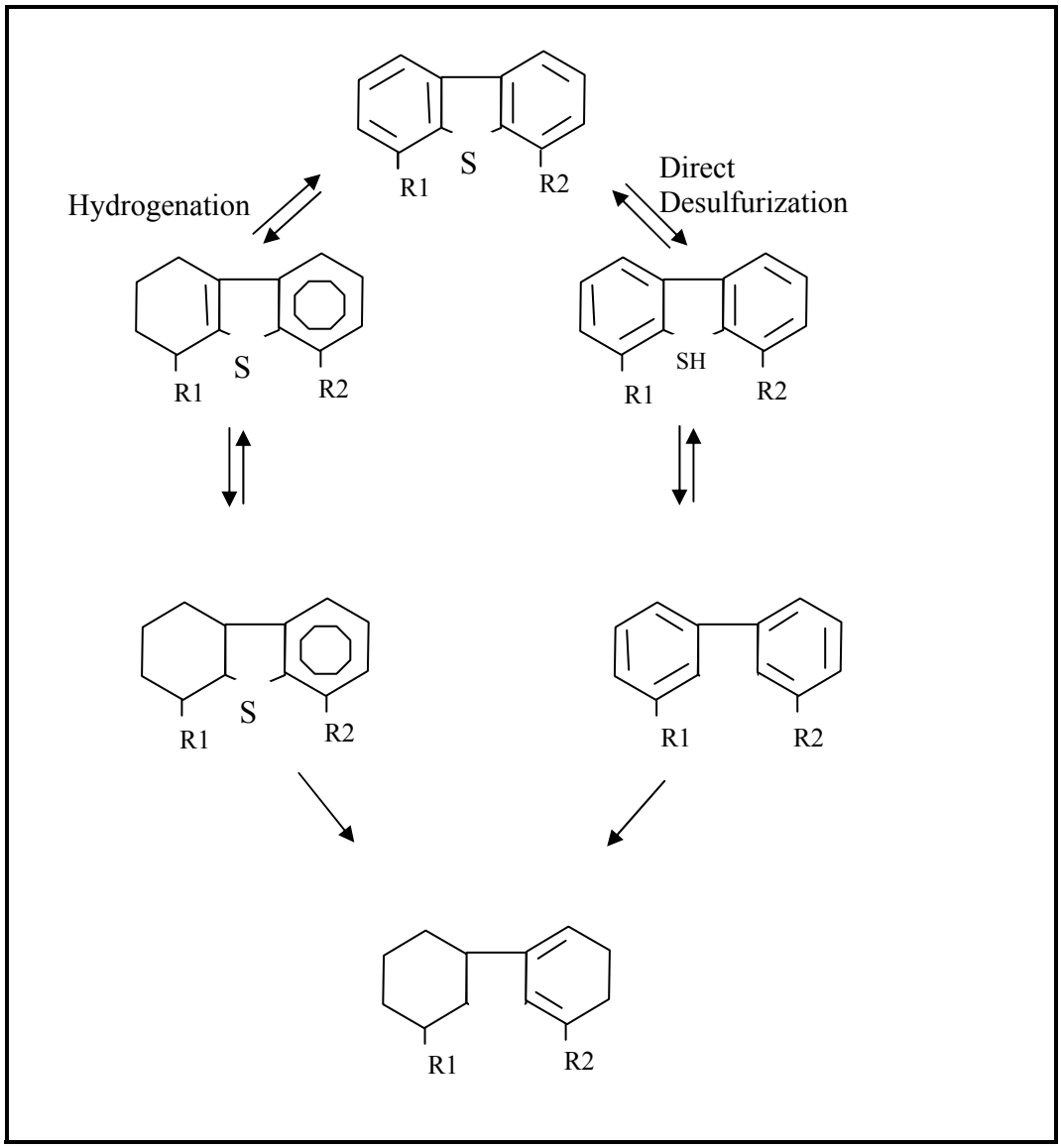

Figure 2.3: Proposed mechanism of HDS of 4, 6 DMDBT (Breysse et al., 2003).

pathway under moderate HDS conversions. But, the highly substituted DBT's follow initial ring saturation route before sulfur removal as they are limited by steric hindrance.

The HDN of aliphatic amines and nitriles is very fast and these are hydrodenitrogenated fully. The HDN of heterogeneous nitrogen compounds generally requires hydrogenation of nitrogen containing aromatic ring before removal of nitrogen molecule. The reactivity of such compounds can be ordered as follows (Clausen et al., 1996): Quinoline>Pyridine>Isoquinoline>Indole>Pyrrole

The HDN of heterocyclic compounds proceeds through a single step and starts with the hydrogenation of the aromatic ring before the removal of the nitrogen molecule (Clausen et al., 1996). Since hydrogenation of the aromatic ring is a strong function of hydrogen partial pressure, the operating pressures used in industry are high enough to force the equilibrium towards saturation of ring and make HDN independent of ring saturation step (Girgis and Gates, 1991).

The non-basic nitrogen compounds such as carbazole and their substituted homologues are less reactive than their basic counterparts such as pyridine and quinoline due to the presence of localized lone electron pairs (Ho, 1988). Among carbazoles, the doubly substituted 1, 8 carbazole is the most refractory nitrogen compound (Zeuthen et al., 2001). During HDN, non basic compounds are first converted to basic form during the hydrogenation step and then the removal of the nitrogen molecule from the ring takes place as shown below.

Non Basic compounds ⟶ Basic Nitrogen compound ⟶ N removed Hydrocarbon

2.3 Challenges of Removal of Sulfur and Nitrogen

The desulphurization of gas oils with current industrial catalysts involves many challenges such as:

- Inhibition of HDS and HDN by H_2S.
- Inhibition of HDS by competitive adsorption of nitrogen compounds.
- Reduction in hydrogen partial pressure along with the increase in H_2S concentration as the reaction progresses along the reactor.

Reports on HDS of model compounds and real feeds have shown that H_2S inhibits the conversion of sulfur compounds. The H_2S produced during the HDS occupies the hydrogenation and desulfurization active sites and stays on the sites due to high adsorption co-efficient (Kabe et al., 2001). In a study about the effect of H_2S on HDS of DBT and 4, 6 DMDBT, H_2S was observed to inhibit the conversion of both DBT and 4, 6 DMDBT. The reactions were carried out at a pressure of 5.1 MPa, temperatures of 240 and 260 °C, LHSV of 7.0 h^{-1} and a hydrogen gas to oil ratio as 1100 NL/L. Same study also indicates that the inhibition effect increases with an increase in H_2S partial pressure (Zhang and Qian, 1997). Studies conducted by Sie (1999) also indicate that the HDS of real feedstock is highly inhibited by H_2S.

The HDS of DBT and 4, 6 DMDBT is severely inhibited by the presence of nitrogen compounds. Yang et al. (2005) prepared light cycle oil feeds with different concentrations of nitrogen by removing the nitrogen by adsorption using a silica column. Their results show that the temperature required to achieve 50 wt % conversion for HDS decreases by 5 and 25 °C for DBT and 4,6 DMDBT as the nitrogen concentration is decreased from 744.9 mg/L to 16.5 mg/L, respectively. They also show that nitrogen

compounds and 4, 6 DMDBT compete for the same active sites for conversion and indicate that HDN is enhanced by removal of nitrogen compounds.

A study done by Zeuthen et al. (2001) shows that alkyl substituted carbazoles are the least reactive nitrogen compounds. However, the HDS is most severely inhibited by basic nitrogen compounds. They also indicate that the HDS of sterically hindered sulfur compounds and HDN of carbazoles mainly take place through hydrogenation of the aromatic ring on the same catalytic sites. In their study for the effects of nitrogen compounds on HDS of gas oils, Alvarez et al. (2006) removed the nitrogen compounds using a proprietary adsorbent from straight run gas oil and studied it for HDS using a batch reactor. They report an increase in HDS conversions with a decrease in nitrogen compounds concentrations in gas oil, indicating the inhibition from nitrogen compounds or NH_3 formed as the result of their HDN.

Commercial HDS reactors are down-flow trickle bed reactors with co-current flow of hydrogen gas and oil feed. These reactors show the highest sulfur conversion values at the outlet which is where the highest H_2S concentrations (indicating highest H_2S inhibition and lowest H_2 partial pressures) are encountered. It is noteworthy to know from section 2.2 that higher conversion zone encounters the presence of the least reactive compounds such as DBT, 4, 6 DMDBT and carbazoles also. All these factors coupled together make the conversion of sulfur species very difficult.

2.4 Effects of Reaction Conditions on HDS and HDN

The rates of HDS and HDN normally increase with the increase in the reaction temperature typically up to 400 °C. A further increase in reaction temperature leads to severe side reactions such as hydrocracking and reforming (Gray et al., 1994). Besides, at

higher reaction temperatures (>400 °C), the HDS of DBT series compounds proceeds through hydrogenation of the aromatic ring which is reversible in nature. This causes an increase in the rate of reverse reaction also with an increase in reaction temperature and puts a thermodynamic limitation on the overall HDS process. A study for thermodynamic limitation on hydrogenation of 4, 6 DMDBT shows that it is favoured only at temperatures <260 °C and is completely unfavoured at temperatures >400 °C (Whitehurst et al., 1998). Due to this limitation, high reaction temperatures do not lead to a corresponding increase in HDS and HDN conversions.

The rates of HDS and HDN also increase with an increase in hydrogen partial pressure. Since the HDN proceeds through the saturation of aromatic rings, an increase in pressure leads to an increase in HDN if hydrogenation of the aromatic ring is the rate limiting step. High hydrogen pressure also leads to the dilution of H_2S and to an increase in HDS (Whitehurst et al., 1998). In addition, high hydrogen pressure also reduces the rate of coke formation on the catalyst surface (Girgis and Gates, 1991).

2.5 Catalysts for Hydrotreating

The most common combinations for gas oil hydrotreating catalysts are Co-Mo and Ni-Mo supported on highly porous γ-Al_2O_3 and are prepared using impregnation method. The concentration of the metals are usually 1-4 wt % for Co/Ni and 8-16 wt % for Mo. Typical support materials are alumina and silica-alumina of which γ-Al_2O_3 is more common. The impregnated catalysts show large sheets of multi-stacked MoS_2 with edge and corner defects providing active sites for HDS and utilize only a fraction of potentially active sites. Besides, these catalysts show a maximum in HDS activity for a Mo loading of approximately 12 wt %. A further increase in metal loading leads to the

formation of clusters of the catalyst metals having lower dispersion which do not display increased catalytic activity (Clausen et al., 1996). This indicates that creating smaller particles of MoS_2 resulting in an increase in edge and corner defects should improve the activity of HDS catalysts (Daage and Chianelli, 1994). Since these catalysts are active in sulfide form, they are sulfided before the use for HDS. The sulfidation is normally carried out using H_2S or low boiling sulfur-containing compounds such as dimethyl di-sulfide, carbon-di-sulfide and butanethiol. Sulfidation is done within a temperature range of 180-350 °C and a pressure greater than 10 MPa. The extent of sulfidation is dependent upon the temperature, H_2S partial pressure and H_2/H_2S ratio. Texier et al. (2005) carried out the sulfidation studies with Co-Mo/Al_2O_3 and Ni-Mo/Al_2O_3 and indicate that the sulfidation is more favourable at lower temperatures (around 423 K) with H_2S as the sulfiding agent. In their study with straight run gas oil, Marroquin et al. (2004) sulfided the Ni-Mo commercial catalyst at three temperatures of 290, 320 and 350 °C using a liquid phase sulfiding agent. Their study indicates that catalysts sulfided at higher temperature show higher HDS activity. These studies indicate that sulfidation at two levels of temperatures would probably be the best for ensuring the completion of sulfidation of catalysts.

Various models have been proposed for structural information of sulfided Co-Mo or Ni-Mo phases and the promotional effects of Co/Ni sulfides on Mo sulfides in the prepared catalysts. These include a monolayer model (Schuit and Gates, 1973), an intercalation model (Voorhoeve, 1971), a contact synergy model (Delmon, 1979) and a Co-Mo-S /Ni-Mo-S model (Topsoe et al 1984). Of these four, the Co-Mo-S /Ni-Mo-S model is the most widely accepted (Clausen et al., 1996). Topsoe et al. (1984) show that, during the synthesis of a supported Co-Mo-S/γ-Al_2O_3, various species are formed. They

used Mossbauer spectroscopy to show that active sites for sulfur removal constitute only a fraction (~ 10 wt %) of all the Co or Ni sites. Their study indicates that among three phases of cobalt, namely Co_9S_8, Co-Mo-S and Co on Al_2O_3, only Co-Mo-S is active for HDS and HDN. It further shows that Co-Mo-S phase consists of Co decorating the corners of MoS_2 hexagonal plane. They also propose that Co-Mo-S catalyst has two different types of sites for HDS: sulfur removal sites and hydrogenation sites. They name these as Type I and Type II sites. Figure 2.4 indicates the pictorial representation of the two types of sites. Type I sites are located on monolayered slabs and are considered to promote HDS through direct sulfur removal from thiophenic compounds. Type II sites are located on multilayered slabs and are considered to be more reactive than Type I sites due to the ease in accessibility especially for sterically hindered molecules such as 4, 6 DMDBT.

Among the commercial HDS catalysts, Co-Mo/γ-Al_2O_3 and Ni-Mo/γ-Al_2O_3 are most common. The Co-Mo based catalyst is highly selective for HDS whereas Ni-Mo based catalyst is more selective for HDN and hydrogenation. As a result, Ni-Mo based catalysts result in higher hydrogen consumption than Co-Mo based catalysts for the same extent of HDS with identical feed. However, Ni-Mo based catalysts indicate a better activity for HDS of higher boiling fractions than Co-Mo based catalysts (Ma et al., 1994c). The reports in open literature indicate that cobalt promoted tungsten based catalysts have been relatively less explored for HDS and HDN reactions. In one of the studies, the Co–W/γ-Al_2O_3 catalysts were prepared using the impregnation method and tested for HDS of coal derived liquids. The study indicated that Co(0.6 wt %)-W(9.0 wt %)/ γ-Al_2O_3 showed comparable performance with Ni(3.4 wt %)-Mo(19.8 wt %)/γ-Al_2O_3

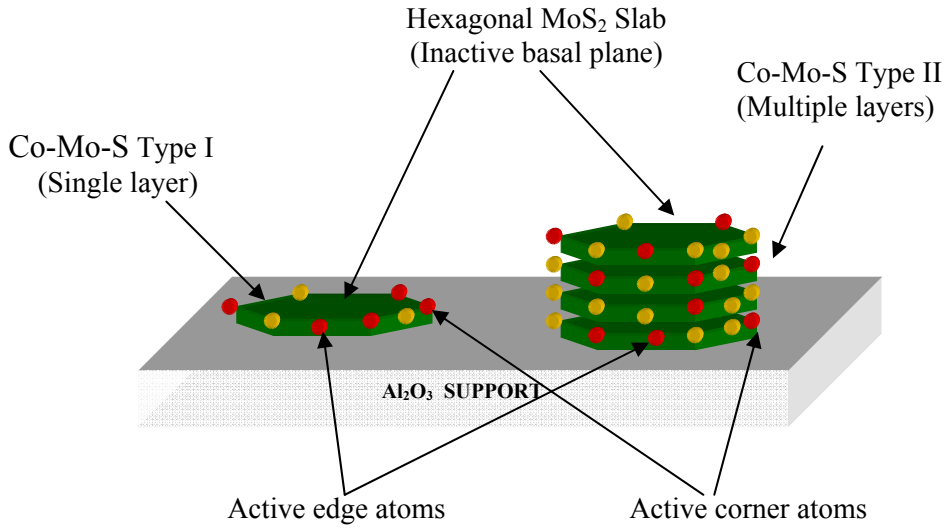

Figure 2.4: Type I and Type II Co-Mo-S sites in Co-Mo/γ-Al_2O_3 hydrotreatment catalysts.

(Mauchausse et al., 1992). In another study, Suvanto et al. (1999) prepared Co-W/γ-Al_2O_3 using the chemical vapor deposition method. Their results conclude that the prepared catalysts have much lower sulfidation temperatures and better performances for HDS of thiophene than those prepared using impregnation method. These reports indicate that Co-W/γ-Al_2O_3 catalysts hold good potential for HDS of LGO.

2.5.1 Conventional Preparation

Traditionally, preparation of Co-Mo/γ-Al_2O_3 or Ni-Mo/ γ-Al_2O_3 catalyst is done by the impregnation method. Usually the co or sequential impregnation method is employed for incorporation of Co/Ni and Mo metals to the support. Desired qualities in the catalyst can be achieved by careful adjustment of the pH of the solution, sequence of the metal impregnation and various other parameters (Satterfield, 1991). The typical loading values for Mo ranges from 8 to 15 wt % for the catalysts prepared using theimpregnation method. This corresponds to a monolayer surface coverage for an alumina support with a typical surface area of 250 m^2/g (Clausen et al., 1996). A further increase in the metal loading leads to formation of bulk species. A XPS study of sulfided Co-Mo catalysts estimates the coverage of alumina by Mo by measuring the Mo/Al intensity ratio in the spectra. It shows that with an increase in Mo concentrations up to 15 wt %, the Mo/Al intensity ratio increases linearly and then levels off. This study shows Mo loadings higher than 15 wt % lead to the formation of bulk MoS_2 (Clausen et al., 1996). Typical values for Co/Ni loadings range from 2 to 4 wt %. As the Co/Ni loading is increased (Co or Ni/ Mo > 0.4) on a constant Mo surface, Co-Mo-S phase first increases linearly then formation of Co_9S_8 phase starts to takes place (Dhas et al., 2001).

2.5.2 Sonochemical Preparation

Ultrasonic waves are the longitudinal waves with frequencies in the range of 20 kHz to 10 MHz (Suslick, 2000). When these waves pass through liquids they result in a phenomenon called cavitation (Suslick, 2000). This acoustic cavitation results in the formation, growth and finally collapse of the bubbles of volatile component present in the liquid. These bubbles have a very short life span and their collapse results in localized spots of pressure (up to 200 MPa), temperatures (up to 5000 K) and cooling rates (10^9 K/s) in the liquid undergoing sonication (Suslick, 2000). The high cooling rate hinders the organization and crystallization of sonication products and yields amorphous, nanosized products.

In this process of catalyst synthesis, the solutes (volatile compounds of the metals to be deposited on the support) and catalyst supports are mixed in a non-volatile solvent. The ultrasonic treatment is applied to this mixture to attain a high dispersion of the catalyst metals on the support (Dhas et al., 2001, Landau et al., 2000). One study reports the use of this method of synthesis to produce supported nanometer sized particles of Mo and Co oxides which are further treated to form the HDS catalysts. The $Mo(Co)_6$/$Co(CO)_3NO$ are used as the precursors for metals deposited on Al-MCM-41(Landau et al., 2000). In another study, Dhas et al. (2001) report the sonochemical synthesis of supported nanosized HDS Co-Mo-S/Al_2O_3, Ni-Mo-S/Al_2O_3 and Co-Ni-Mo/Al_2O_3 catalysts. This study compares the properties of impregnated and sonochemically prepared catalysts and shows that lattice fringes of MoS_2 layers in impregnated catalysts are mostly composed of multi-stacked layers with no wrinkled fringes. It also indicates that sonochemically prepared supported catalysts have short

lengths of wrinkles layers that are highly disordered and have only a minimal stacking. The authors conclude that the disordered, fractured and defective nature of sonochemically prepared MoS_2 has higher dispersion which is desirable for higher HDS activity. In their work they also study the HDS of thiophene vapors in a flow microreactor and that of DBT in a batch reactor over sonochemically prepared catalysts and compare their performances with impregnated catalysts at reaction temperature of 375 °C and pressure of 3.4 MPa. Comparing the turnover numbers over the two catalysts, they conclude that the sonochemically prepared catalysts have higher activities for HDS of thiophene and DBT than the comparable micrometer sized commercial catalysts. They also indicate that the Co-Ni-Mo phase formed is more active than Co-Mo and Ni-Mo for conversion of thiophene and DBT.

In their study with sonochemically synthesized $MoS_2/\gamma\text{-}Al_2O_3$ catalysts, Lee et al. (2003) show that even at increased metal loadings (approximately 25 wt %) in the prepared catalysts, multisulfides are not formed and the activity of the catalyst keeps increasing with an increase in metal loading. Mahajan et al. (2004) carried out a study involving the sonochemical synthesis of unsupported MoS_2, Co-Mo-S and Co-S. They indicate that sonochemically prepared catalysts are much more active than the similar commercially available catalysts for conversion of DBT. Gusta et al., (2005) synthesized $Co\text{-}Mo/\gamma\text{-}Al_2O_3$ using sonochemical and co-impregnation methods and carried out their study in a trickle bed microreactor with light gas oil derived from Athabasca bitumen. Their study indicates that sonochemically synthesized catalyst show about 6 wt % more conversion for HDS than the impregnated catalysts.

It can be seen that all the reports show positive results for HDS and indicate a great potential for HDS of real feedstock such as gas oil derived from oil sands.

2.6 Kinetics of Removal of Sulfur and Nitrogen

The kinetics of removal of the sulfur compounds and other impurities has very important effect on optimizing process variables and selection of catalyst for the HDS and HDN processes. Traditionally, the kinetics of removal of sulfur compounds has been studies in two ways, namely Power Law model and Langmuir - Hinshelwood Hougen Watson model (Knudsen et al., 1999). The power law model is overall in nature and does not account for the individual steps taking part in the reaction whereas the Langmuir model incorporates the detail mechanism in rate equation. Most of the HDS kinetic studies have been done with thiophenic model compounds as they are the least reactive compounds in petroleum. The HDN kinetic studies have been done with quinoline and pyridine (Girgis and Gates, 1991).

2.6.1 Power Law Model

The HDS reaction can be expressed by Equation 2.1.

$$\text{R-S} \rightarrow \text{R-H} \qquad (2.1)$$

The Power Law kinetics for HDS as in Equation 2.1 can be expressed by Equation 2.2:

$$-r_A = kC_A^n \qquad (2.2)$$

The kinetic studies with sulfur or nitrogen model compounds typically follow 1st order kinetics (Speight, 2000). The HDN of gas oils also have been found to follow first order kinetics (Aoyagi et al., 2003). For moderate HDS of gas oils, the orders of reactions have been well documented and reported to be in the range of 1 to 2. The order of reaction depends upon the type and distribution of the sulfur and nitrogen compounds in the feed

and the type of the catalyst used. Bej et al. (2002) did a study with oil sands derived gas oils and obtained a reaction order of 1.5 for the HDN. Similarly, Callejas and Martinez (1999) obtained half order kinetics for HDN of Maya residue.

Trytten et al. (1990) did a study with narrow boiling cuts of coker gas oil over a Ni-Mo catalyst in a CSTR at 400 °C, 13.9 MPa. The study indicates that the HDS follows first order kinetics. It, however, shows different values of rate constants for different boiling ranges. It also concludes that the higher molecular weight cuts show a lower rate constant for both HDS and HDN. This indicates that the rate kinetics depends upon the molecular weight of the species undergoing HDS. Since the real feeds are composed of different molecular weight compounds which show different rate kinetics, sometimes it is not possible to express the overall HDS and HDN using a single expression. A similar conclusion has been made by Sie (1999) also. The use of two first order kinetics is reported in literature for the HDS of real feeds. Studies also indicate that the Power Law model is valid only for moderate desulphurization of real feeds. In such a study, Chen and Ring, (2004) indicate that at higher temperature the hydrogenation of a thiophene ring becomes limiting and the simple power law model fails to represent the rate of HDS.

2.6.2 Langmuir - Hinshelwood Model

The Langmuir-Hinshelwood general rate equation is given by:

$$-r_i = \frac{k_i p_i}{(1+\sum K_j p_j)^n} f(p_H) \qquad (2.3)$$

Where r_i is the rate of conversion of reactant i , k_i is the reaction rate constant , p_i is the partial pressure ,K_j and p_j are the adsorption constants and partial pressures of all adsorbed species involved in the rate determining step and n is a constant (1 or 2). In this

analysis usually one step is assumed to be rate determining and all the other steps are assumed to be in equilibrium.

The HDS reaction stoichiometry can be expressed by the Equation 2.4.

$$\text{R-S} + \text{H}_2 \rightarrow \text{R-H} + \text{H}_2\text{S} \qquad (2.4)$$

In HDS, shown by Equation 2.4, this is assumed to be the reaction between adsorbed organic species and adsorbed hydrogen molecules (Clausen et al., 1996). The $f(p_H)$ term refers to a function of hydrogen partial pressure. If hydrogen is adsorbed on a different type of site from the organic reactant an inhibition term and different order in hydrogen need to be considered. This leads to the following expression:

$$f(p_H) = \frac{K_H p_H^a}{(1 + K_H p_H^b)^c} \qquad (2.5)$$

Where the constant a can have values of ½ or 1 , b of ½ or 1 and c of 1 or 2, depending on the rate limiting step of the reaction and whether the hydrogen is adsorbed associatively or dissociatively (Clausen et al., 1996). As per a study for very deep desulfurization of gas oils by Knudsen et al. (1999), following equation can be used for describing the kinetics:

$$-r_S = \frac{kC_S^n p_H}{1 + K_{H_2S} p_{H_2S}} + \frac{k' C_S^m p_H}{1 + K_F C_F} \qquad (2.6)$$

In Equation 2.6, the first term represents the direct sulfur removal route, which is enhanced by the increase in the partial pressure of hydrogen and inhibited by the presence of H_2S. The second term represents the hydrogenation route, which is also enhanced by an increase in the hydrogen pressure but inhibited by the presence of aromatic compounds and in particular by the compounds like carbazole (Knudsen et al., 1999).

Most Langmuir-Hinshelwood models are derived with the hydrogynolysis of C-S bond as the rate limiting step. Gates et al. (1979) studied the kinetics of HDS of thiophene. They assume two different sites for hydrogynolysis and hydrogenation as the H_2S affects the rates of hydrogynolysis and hydrogenation differently. In a similar study with DBT, Froment et al. (1986) also assume two catalytic sites for reaction, namely one for hydrogenation and other for hydrogenolysis. For this analysis they assume the rate of surface reaction as the limiting step. They also assume the dissociative adsorption of hydrogen molecule on both the sites. Leglise et al. (1996) consider the rate limiting step as the dearomatization of thiophenes. In their study they assume the same sites for adsorption of thiophene and H_2S.

Satterfield and Yang (1983) studied the kinetics of quinoline and their results indicate that HDN is inhibited by ammonia, aromatic amines and decahydroquinoline. They model the reaction using a Langmuir-Hinshelwood rate expression. They model the kinetics of HDN of quinoline with a single site as well as dual site assumptions and conclude that dual site model is better. Yui (1989) studied the kinetics of HDN of quinoline and fitted the Langmuir –Hinshelwood model. They calculate the adsorption co-efficient as 2.5 MPa^{-1} at 78.9 MPa.

3 EXPERIMENTAL

This chapter describes the experimental procedures and details used in this work and includes the following,

- Preparation and characterization of Co-W/γ-Al_2O_3 using sonochemical and impregnation methods.
- Reaction studies using light gas oil derived from Athabasca bitumen (obtained from Syncrude Canada Ltd., sulfur content: 15950 ppmw and total nitrogen content: 209 ppmw) on different impregnated and sonochemically synthesized Co-W/γ-Al_2O_3 catalysts.
- Post reaction characterization.

3.1 Catalyst Preparation using the Sonochemical Method

The Co-W/γ-Al_2O_3 catalysts were synthesized using the sonochemical method. Tungsten hexacarbonyl (97 %, Sigma Aldrich, U. S.) and cobalt octacarbonyl (stabilized with 1-5 % hexane; Alfa Aesar, U. S.) were used as precursors for tungsten and cobalt metals due to their low decomposition temperatures (<50 °C for cobalt octacarbonyl and <150 °C for tungsten hexacarbonyl). γ-Al_2O_3 (from Sud chemie India Ltd.) was used as the support for the catalysts. n-Hexadecane (99 % ; Sigma Aldrich, U. S.) was used as solvent due to its low vapour pressure at catalyst synthesis conditions (0.000054 MPa at 90 °C as compared to 0.187 MPa for n-hexane at same temperature).

The γ-Al_2O_3 support was calcined at 500 °C for 2 h to remove the moisture before being used in actual preparation. In a typical preparation procedure a slurry of cobalt octacarbonyl, tungsten hexacarbonyl and γ-Al_2O_3 in hexadecane was irradiated with high intensity ultrasound (Sonics and Materials, Model VCF1500, 20 kHz, 1500 W/cm^{-2}) in a

flowing air atmosphere for 10 h. The temperature of the mixture was observed to increase rapidly to about 100 °C during the course of sonication. The mixture temperature was controlled by a water bath. All syntheses were done using a VCF1500 ultrasonic processor with 12.7 cm long and 2.5 cm o. d. titanium probe directly immersed into the sonicating mixture (See table 3.1 for the details of the catalysts prepared). The syntheses were performed in a custom made steel reactor (16 cm long and 6 cm diameter, with air inlet, outlet and thermocouple at the top) under an air atmosphere for getting the oxide phases of tungsten and cobalt metals. The catalyst synthesis setup involved a reactor, gas mass flowmeter, temperature indicator and a source of air. Figure 3.1 depicts the setup used for sonochemical synthesis of catalysts.

Values for power input, sonication time and sonication temperature were optimised for 1 wt % Co and 10.7 wt % W loading on γ-Al_2O_3 and final values used were 225 W, 10 h and 90 °C respectively. The optimization of these parameters was done on the basis of maximum conversion of tungsten carbonyl into oxide form and was based on the visible tungsten carbonyl present in the resultant slurry. The resulting blackish slurry was filtered and the thick paste obtained from filtration was washed several times with hot hexadecane to remove the remaining unconverted tungsten carbonyl. The paste was then washed with hexane to remove the remaining hexadecane. The resulting powder was then dried in ambient air for 6 h for removal of hexane. Finally, the powder was heated at 500 °C for 5 h to remove blackish carbonaceous deposits. The temperature of 500 °C was selected on the basis of TGA study done with these catalysts which showed negligible weight loss at this temperature for all the sonochemically synthesized catalysts.

Table 3.1: List of catalysts synthesized for the study.

Method of Synthesis	Co wt %	W wt %
Sonochemical	1	13
	2	13
	3	7
	3	10
	3	13
	4*	18*
Impregnation	1	13
	2	13
	3	7
	3	10
	3	13

*** As impreganted catalysts show a maximum in activity typically for Co(3 wt %)-W(10 wt %)/γ-Al_2O_3 (Clausen et al., 1996), So Co (4 wt %)-W(18 wt %)/γ-Al_2O_3 was not prepared using this method.**

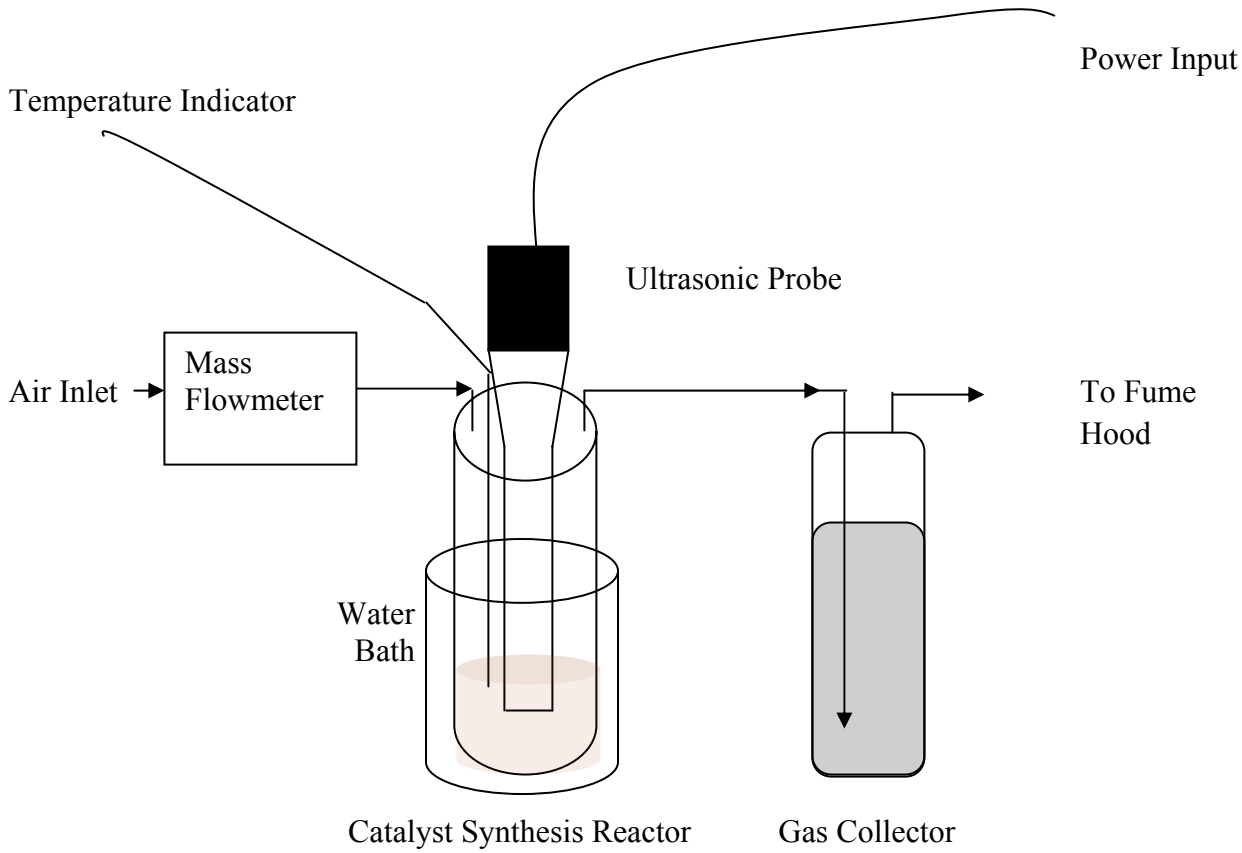

Figure 3.1: Schematic for sonochemical synthesis of catalysts.

3.2 Catalyst Preparation using the Impregnation Method

Another set of Co-W/γ-Al_2O_3 catalysts was synthesized using the incipient wetness co-impregnation method with the metal loadings equivalent to the sonochemically prepared catalysts. In this method, an ammoniacal solution was prepared using required amount of ammonium metatungstate [$(NH4)_6H_2W_{12}O_{40}.xH_2O$] and cobalt nitrate [Co $(NO_3)_2.6H_2O$]. γ-Al_2O_3 (calcined at 500 °C for 2 h before synthesis) was then impregnated with the above solution and dried for 12 h at 120 °C. The catalyst was then calcined at 600 °C for 6 h.

3.3 Catalyst Characterization

Catalyst characterization was carried out to identify their physical and chemical properties. Different characterization techniques included: elemental analysis using inductively coupled plasma–mass spectrometer (ICP-MS), thermogravimetry analysis (TGA), BET surface area, pore volume and pore size measurement, temperature programmed reduction (TPR), temperature programmed desorption (TPD) and x-ray diffraction.

3.3.1 Elemental Analysis

All synthesized catalysts were analyzed for elemental composition, namely, Co and W. Sonochemically synthesized catalysts were additionally analyzed for C and H.

Co and W were identified using inductively coupled plasma - mass spectrometer (ICP-MS). A catalyst sample (0.05 g) was dissolved in hydrofluoric acid (48-51 %) at a temperature of 100-150 °C for three days. After cooling, samples were further dissolved in concentrated HNO_3 to ensure the complete dissolution of the metals. The final solution was prepared using 0.2 N HNO_3 and analyzed with a mass spectrometer.

Sonochemically synthesized catalysts were analyzed for carbon and hydrogen using Elementstar, model vario EL II analyzer. About 25 mg of catalyst was put in a tin foil and combusted in an oxygen atmosphere. The gases thus formed were separated using specific adsorption columns. These separated gases were then determined in succession using thermal conductivity detector with He as the carrier gas.

3.3.2 Thermogravimetry Analysis

All sonochemically synthesized samples were analyzed with PerkinElmer Pyris Diamond TG DTA SII machine. Approximately 20 mg of sample was heated in flowing air at 50 mL/min and temperature was increased linearly @10 °C/min. The weight loss of the sample was measured and data were collected using online data acquisition system.

3.3.3 BET surface area, Pore volume and Pore Size Distribution

BET surface area, pore volume and pore size measurements of catalysts were performed using Micrometrics adsorption equipment (Model ASAP 200, Micrometrics Instruments Inc., Norcross, GA USA) using N_2 gas (99.995 % pure, obtained from Praxair, Mississauga, ON, Canada). About 0.20 g of sample was used for each analysis. Catalyst samples were evacuated at 200 °C for 4 h in a vacuum of 5×10^{-4} atm to remove all the adsorbed moisture from the catalyst surface before analysis. The adsorption and desorption isotherms used in the evaluation of BET surface area were obtained at the boiling temperature of liquid nitrogen (78 °K). The pore volume and pore sizes were determined using BJH algorithm (developed by Barrett–Joyner–Halenda, using Kelvin equation for calculation of pore volume and pore sizes) for adsorption and desorption of nitrogen.

3.3.4 X-Ray Diffraction

XRD studies were performed on the calcined samples to identify the crystalline species present. Analyses were performed using a Rigaku diffractometer (Rigaku, Tokyo, Japan) with Cu Kα radiation filtered by a graphic monochromator at a setting of 40 kV and 130 mA. The powdered samples were spread on a glass slide with acetone and dried at room temperature. The X-ray diffraction analyses were carried in the scanning angle range of 5 to 90 ° at a scanning speed of 5 °/min.

3.3.5 Temperature Programmed Desorption

TPD analyses were performed using Quantachrome equipment (chemBET 3000, Qunatachrome Corporation, FL USA). TPD of adsorbed ammonia was done for qualitative measurement of acidic sites on synthesized catalysts. For analysis, about 0.2 g of sample was placed in a quartz U tube in an electrical heater. The sample was then degassed in flowing helium at a temperature of 400 °C for 1 h and cooled down to 100 °C at rate of 10 °C/min. Ammonia was then adsorbed on the sample at a temperature of 100 °C for 30 minutes. Then the sample was cooled down to room temperature at a rate of 10 °C/min in helium. Finally, the TPD was run from room temperature to 650 °C @ 10 °C/min. The amount of ammonia was measured using a thermal conductivity detector (TCD) which measured the change of the resistance of sensing element caused by the change in its temperature.

3.3.6 Temperature Programmed Reduction

All synthesized catalysts were analyzed using TPR with hydrogen to study their reducibility. Analyses were performed using Quantachrome equipment (chemBET 3000, manufactured by Qunatachrome Corporation, FL USA). About 0.1 g of catalyst sample

was placed in a U shaped quartz tube and degassed at 200 °C for 1 h under flowing helium atmosphere in an electrical furnace with precise temperature control. The sample was then cooled to room temperature. The sample was then heated from room temperature to a level of 950 °C at a linearly programmed rate of 5 °C/min. The entire heating was done in a reducing gas stream of 3 mol % H_2 in N_2 (Praxair, Mississauga, ON, Canada) with a flow of 35 mL/min. H_2 consumption was measured using a thermal conductivity detector.

3.3.7 X-Ray Photoelectron Spectroscopy

Based on the catalyst screening test results nine catalysts were selected and analyzed with XPS to identify the dispersion of the metals on the support (see section 4.1.7 for details of the catalysts). A Leybold Max200 X-ray photoelectron spectrometer was used for these analyses. Al Kα was used as the photon source for all the metal oxides. Al Kα was generated at 15 kV and 20 mA. The pass energy for the scan was set at 192 eV. All XPS spectra were corrected to the Cls peak at 285 eV.

3.4 Catalyst Performance Test

All synthesized catalysts were tested for HDS and HDN reactions in a trickle bed micro reactor using light gas oil. The schematic diagram of the experimental setup is given in Figure 3.2. The system comprises of hydrogen gas and liquid feed sections, a high pressure reactor and a heater equipped with a temperature controller (Eurotherm, model No. 2216e). The setup also consists of a mass flow controller (Brooks Instrument, Model no. 0152c) for hydrogen gas flow measurement to the reactor, a scrubber for removing the ammonia from the reactor effluent and a high pressure liquid gas separator.

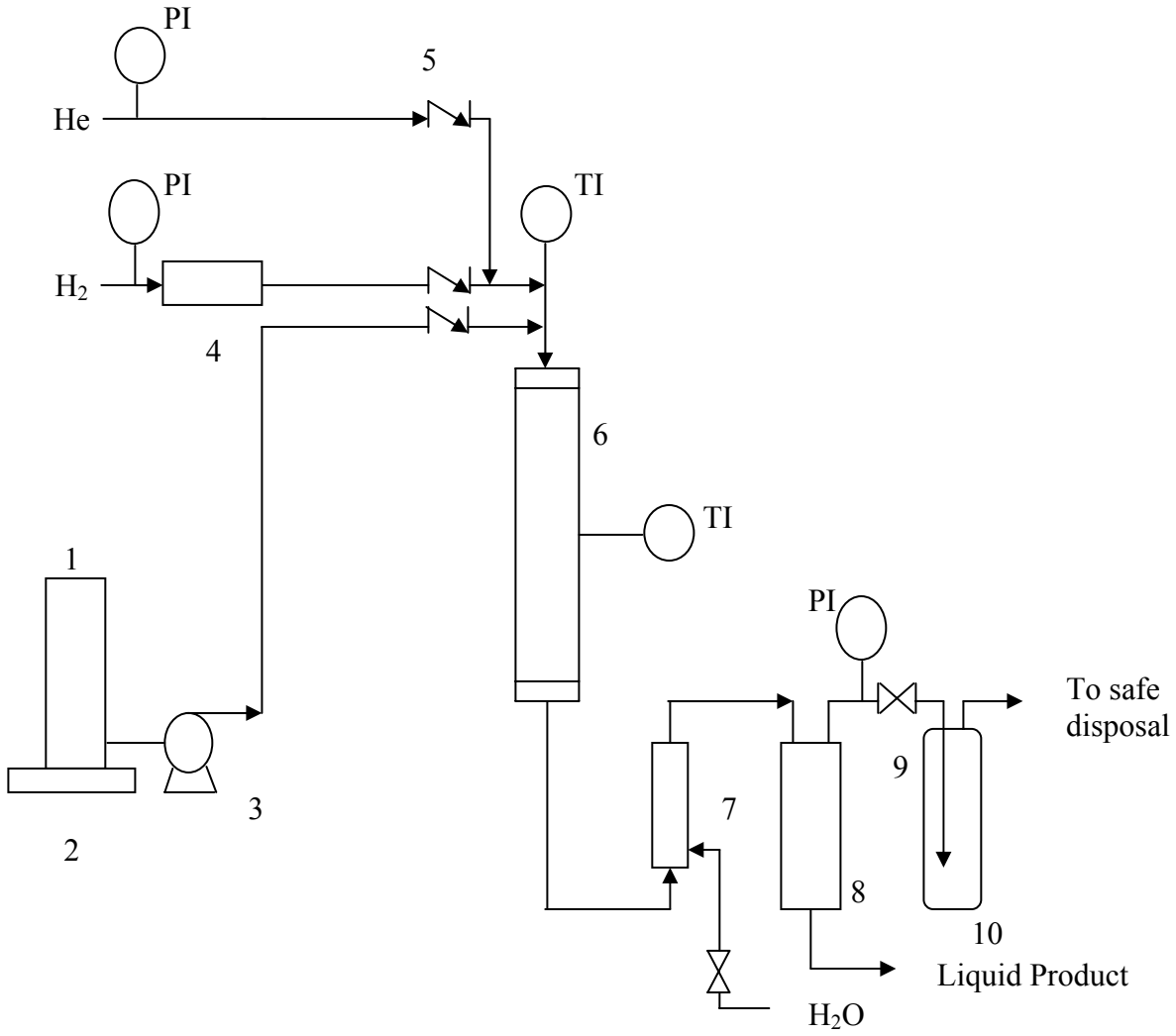

Figure 3.2: Schemctic diagram of experimental set up for reaction. (1) Liquid feed tank; (2) weighing balance; (3) liquid feed pump; (4) mass flowmeter for hydrogen; (5) check valve; (6) reactor and furnace assembly; (7) water scrubber; (8) high pressure gas liquid separator; (9) back pressure regulator; (10) H_2S scrubber.

The length and internal diameter of the reactor were 240 and 14 mm, respectively. The reactor was loaded with a bed of catalyst (average particle diameter ~ 1.7 mm) diluted with 90 mesh silicon carbide to minimize the axial dispersion in the study with commercially sized catalyst in the trickle bed microreactor. The reactor was loaded in nine separate layers. The bottom of the reactor was loaded to a depth of 22 mm with 3 mm size glass bead followed by a 25 mm layer of 16 mesh size silicon carbide. These were followed by two 10 mm layers of silicon carbide of 46 and 60 mesh sizes, respectively. After these layers, 3.8 g of catalyst was loaded along with 12 mL 90 mesh of silicon carbide. Catalyst and silicon carbide were loaded in alternate layers in the reactor and mildly vibrated intermittently. After this, the top part of the catalyst bed was loaded with three 8 mm layers of silicon carbide 60 mesh, 46 mesh, 16 mesh and 20 mm of 3 mm size glass beads. The schematic diagram of the catalyst bed is given in Figure 3.3.

After loading the reactor it was put in the reaction setup and 50 mL of water was injected into the scrubber to remove the NH_4HS formed due to presence of H_2S and NH_3. The unit was pressure tested with helium at 10.3 MPa after which the reactor pressure was decreased to 8.9 MPa. Helium was then flowed through the reactor at a rate of 50 mL/min and reactor temperature was raised to 100 °C. Sulfidation of catalysts was started after the reactor temperature was increased to 100 °C. The sulfidation of catalysts was carried out using 2.9 vol % of butanethiol in straight run atmospheric gas oil. The initial rate of sulfiding solution was kept high (around 2.5 mL/min) for wetting the catalyst bed. After passing the sulfiding solution for 2 h at this rate the flow was decreased to a LHSV of 1 h^{-1}. Hydrogen flow was then started at 600 mL/mL of oil at STP and helium flow to

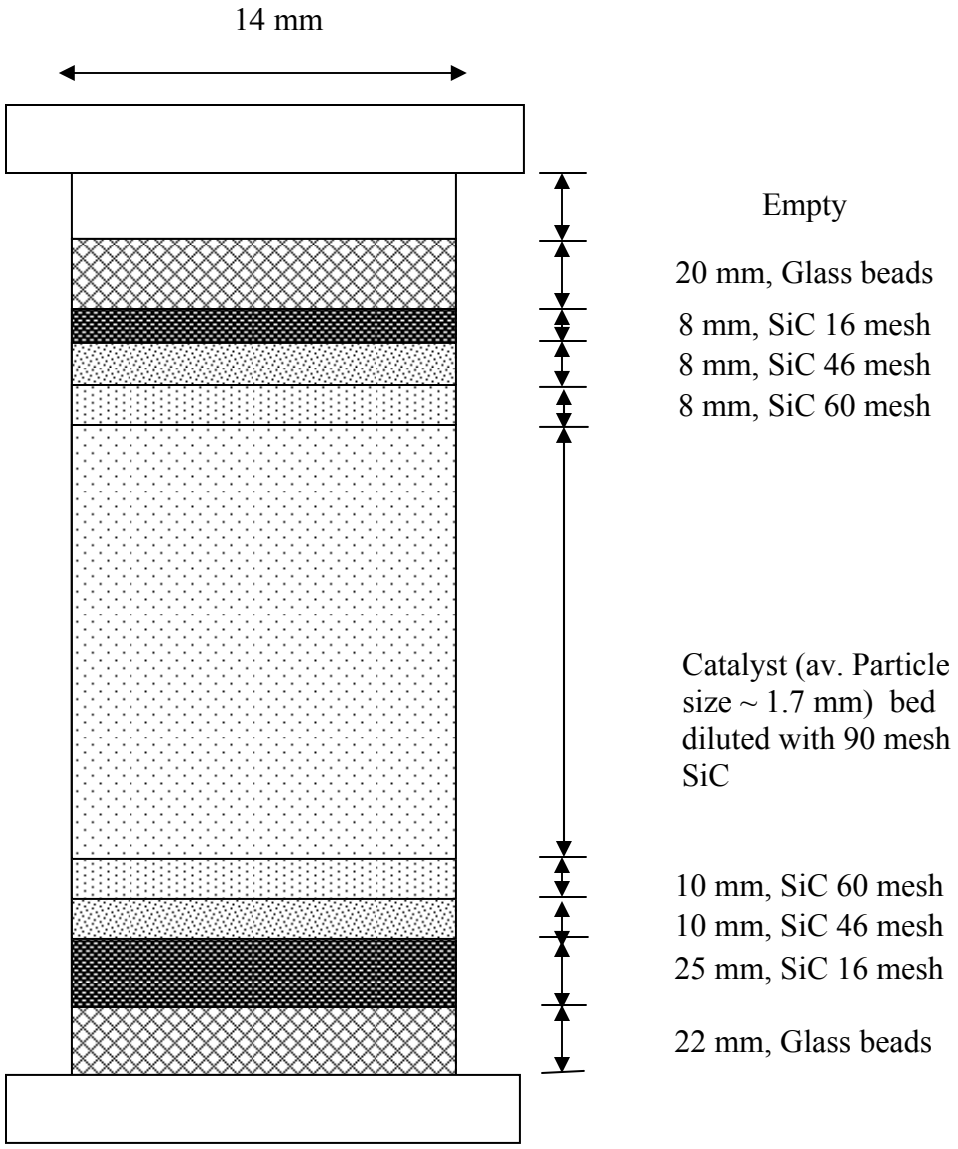

Figure 3.3: Catalyst bed in trickle bed reactor with different layers of packing.

reactor was then stopped. The temperature of the reactor was then increased to 193 °C and maintained for 24 h. After this the temperature of the reactor was again increased to 343 °C and maintained for another 24 h. The completion of sulfidation was ensured by checking the H_2S breakthrough (concentration > 10,000 ppm) in the product gases.

After completion of sulfidation, the catalyst was precoked by passing light gas oil at LHSV of 2 h^{-1} at 375 °C. Precoking was done for 5 days to stabilize the activity of the catalysts. Initial screening of the catalysts was done at three temperature levels of 340, 350 and 360 °C. These temperature levels were selected for getting the sulfur and nitrogen conversions within the reasonable range from the screening studies. Samples were collected at an interval of 12 h. The reaction products were stripped by sparging nitrogen through them for 2 h to ensure the removal of NH_3 and H_2S gases. The stripped samples were then analyzed for nitrogen and sulfur content.

3.5 Analysis of Reaction Products

The total sulfur and nitrogen content of HDS and HDN reaction products were measured using an Antek 9000NS analyzer. For analysis, the sample was first combusted in an oxygen atmosphere at 1050 °C. The gases from the product of combustion were analyzed for sulfur and nitrogen using fluorescence (ASTM 5453-06 method) and chemiluminescence (ASTM D4629 method) techniques, respectively. The details of the measurement are described in sections 3.5.1, 3.5.2 and 3.5.3.

3.5.1 Use of N, S analyzer

The samples were introduced into the nitrogen and sulfur analyser using a 5 microlitre injection. The injection chamber was maintained at 5 °C. The sample was injected into a quartz sample boat through a septum containing the quartz wool to

increase the surface area for the sample to adhere to. Argon was used as carrier gas and oxygen was used as combustion gas for the analysis of nitrogen and sulphur compounds. The flow rate of argon and oxygen were maintained at 140 mL/min and 450 mL/min, respectively. The mixture of carrier gas and combustion gas was used to sweep the sample into the pyrolysis tube. The gases resulting from combustion were passed through a membrane drying system to remove all water and then to the detector module for quantification.

3.5.2 Quantification of Total Nitrogen Compounds

In the combustion chamber of the analyser, nitric oxide was produced as a result of combustion of samples. The NO produced was contacted with ozone to produce NO_2. As the metastable species (NO_2) decayed, it emitted a photon of light at certain wavelength and was detected by chemiluminescence detector. The chemiluminescence was specific for nitrogen and proportional to the amount of nitrogen in the original sample.

3.5.3 Quantification of Sulfur Compounds

The samples were combusted in an oxygen rich atmosphere in the combustion chamber to form SO_2. Water formed during combustion was removed and combustion gases were exposed to ultraviolet (UV) radiation. The SO_2 absorbed the energy from UV radiation and formed excited sulphur dioxide, which caused some electrons to shift to higher energy levels. As the electrons returned to their original orbits, the extra energy was released in form of photons at specific wavelength and detected by UV detector. This fluorescence signal was specific to sulfur and was proportional to the amount of sulphur in the sample.

3.6 Post Reaction Characterization

All spent catalysts were washed with hexane in order to remove the volatiles present on the surface of the catalysts. Selected spent catalysts were characterized using TGA and BET surface area analysis to determine the extent of deposition of coke on the catalysts and the reduction in BET surface area and pore volumes upon reaction. The detailed procedures for these characterizations are given in section 3.3.

4 RESULTS AND DISCUSSION

This chapter describes and discusses the results obtained from different experimental studies. The in depth catalyst characterization results using various techniques including ICP, BET surface area, pore volume and pore size measurement, TPR, TPD, XRD are given in section 4.1. Section 4.2 describes the relation between catalyst properties and HDS and HDN activities with LGO in a trickle bed reactor. Section 4.3 describes the performance and optimization studies on the two selected catalysts. Section 4.4 discusses the post reaction characterization of spent catalysts and the kinetic studies are described in section 4.5.

4.1 Syntheses of Catalysts and their Characterization

4.1.1 Elemental Analysis

Table 4.1 shows the elemental analyses of prepared catalysts. It can be seen that for all the catalysts, the measured metal concentrations are less than the target ones. For example, for a catalyst of theoretical Co and W metal loadings of 3 and 13 wt % the actual loadings are only 2.8 and 11.0 wt %. These lower metal loadings may be contributed in part to the diffusional limitations of metals inside pores which do not allow all the Co and W to come in contact with the alumina support during synthesis of catalysts and hinder the deposition of metals. It was also observed that the sonochemical process of catalyst synthesis led to heating of the sonicating mixture, resulting in vaporization and loss of metal precursor compounds along with the flowing air. This led to lower metal loadings in synthesized catalysts than the targeted ones. A thermogravimetry analysis performed on tungsten carbonyl indicated an evaporation rate of 0.513 mg/min at 90 °C which was the operating temperature for synthesis of

Table 4.1: Summary of elemental analysis of synthesized Co-W/γ–Al_2O_3 catalysts prepared using impregnation and sonochemical methods.

Method of Synthesis	Cobalt wt%		Tungsten wt %		C and H analysis on Sonochemically prepared catalysts	
	Theor.	Actual	Theor.	Actual	C wt %	H wt %
Impregnated *	3	3.1	13	12.2	-	-
Sonochemical*	0	0	0	0	1.9	1.2
	1	1.0	13	10.7	3.1	1.2
	2	2.0	13	12.3	3.4	1.4
	3	3.0	7	8.0	2.8	1.2
	3	2.8	13	11.0	3.6	1.3
	3	3.0	13	11.5	5.3	1.5
	4	4.0	18	15.4	5.7	1.4

*** All the impregnated and sonochemically prepared catalysts shall be denoted by "Imp x/y" and "Sono x/y" respectively, where x and y indicate the actual cobalt and tungsten loadings in wt % for that catalyst.**

sonochemically prepared catalysts. This indicated that there was a loss of tungsten carbonyl during syntheses of the catalysts due to evaporation at a rate indicated by TG study.

Sonochemically prepared catalysts were additionally analyzed for carbon and hydrogen content. None of the impregnated catalysts was analyzed for carbon and nitrogen contents. Table 4.1 shows a carbon content of 2.8 to 5.7 wt % and hydrogen content of 1.2 to 1.5 % for all synthesized catalysts. A similar analysis on γ–Al_2O_3 sonicated under similar conditions shows a carbon and hydrogen contents of 1.9 and 1.2 wt %, respectively. The presence of these carbon and hydrogen impurities may be due to the decomposition of solvent and deposition on the surface of prepared catalyst during long sonication hours (Yu et al., 2002).

4.1.2 BET Surface Area, Pore Volume and Pore Size Measurement

The BET surface area, pore volume and pore size distribution of synthesized catalysts are given in Table 4.2. It can be observed from the table that surface area, pore volume and pore diameters of both types of catalysts decrease with the incorporation of Co and W in γ–Al_2O_3. The surface area of sonochemically prepared catalysts ranges from 145 to 188 m^2/g while for impregnated catalysts it ranges from 183 to 188 m^2/g. This indicates that, for comparable metal loadings, sonochemically prepared catalysts show more reduction in surface area than impregnated catalysts. This decrease in the surface area is primarily due to the blockage of the pores of alumina with the deposited metals (Lewandowski and Sarbak, 1997). The reduction in surface area can additionally be attributed to the vigorous agitation provided by formation and collapse of bubbles of solute vapors caused by cavitation in case of sonochemically prepared catalysts.

Table 4.2: BET surface area, adsorption pore volume and macropore volume of prepared catalysts.

Catalyst	BET surface area, m^2/g	Total pore volume, cc/g	Macropore volume		Mesopore volume	
			cc/g	% contribution to total pore volume	cc/g	% contribution to total pore volume
γ-Al_2O_3	200	0.64	0.015	2.3	0.63	97.7
Sono 1/10.7	164	0.48	0.060	12.5	0.42	87.5
Sono 2/12.3	168	0.50	0.080	16.0	0.42	84.0
Sono 3/8	188	0.51	0.035	6.9	0.48	93.1
Sono 2.8/11	185	0.53	0.054	10.2	0.48	89.8
Sono 3/11.5	177	0.54	0.055	10.2	0.49	89.8
Sono 4/18	145	0.44	0.045	10.2	0.40	89.8
Imp 1/13	186	0.51	0.024	4.7	0.49	95.3
Imp 2/13	187	0.51	0.023	4.5	0.49	95.5
Imp 3/7	183	0.52	0.014	2.7	0.51	97.3
Imp 3/10	186	0.53	0.020	3.8	0.51	96.2
Imp 3.1/12.2	183	0.50	0.011	2.2	0.49	97.8

It can be seen from Figure 4.1 that impregnated catalysts show hysteresis loops slightly different than those displayed by sonochemically synthesized catalysts. Impregnated catalysts display hysteresis loops classified as type H1 which are associated with strongly interlinked particles leading to narrow pore size distributions, whereas sonochemically synthesized catalysts show hysteresis loops classified as type H3 which are associated with pores of non uniform sizes (Lynch, 2003). This indicates that the sonochemical method of synthesis of catalysts leads to a change in the pore size distributions of prepared catalysts.

Table 4.2 shows that γ-Al_2O_3 has a macropore (average pore diameter > 50 nm) volume of 0.015 cc/g which corresponds to 2.3 % of total pore volume. The table also indicates that impregnated catalysts display the macropores with a pore volume in the range of 0.01 to 0.02 cc/g which form 2-3% of the total pore volume. These values of pore volumes are very close to the one of γ-Al_2O_3. It can also be observed from Table 4.2 that sonochemically prepared catalysts show an increase in the number of macropores with a cumulative macropore volume in the range of 0.035 to 0.08 cc/g, which correspond to 7-16 % of total pore volume. A comparison of these results indicates that the sonochemical method of synthesis of catalysts leads to a greater increase in the volume of macropores than the impregnation method. This can be explained on the basis of phenomenon of cavitation which takes place as sonic waves are introduced to the mixture in the catalysts synthesis procedure (Dhas et al., 2001; Yu et al., 2002). It is known that high ultrasonic energy imparted to liquids leads to cavitation, which is the generation and collapse of vapor bubbles during the rarefaction and compression cycles of these waves. This cavitation may result in the collapse of some of the mesopores and

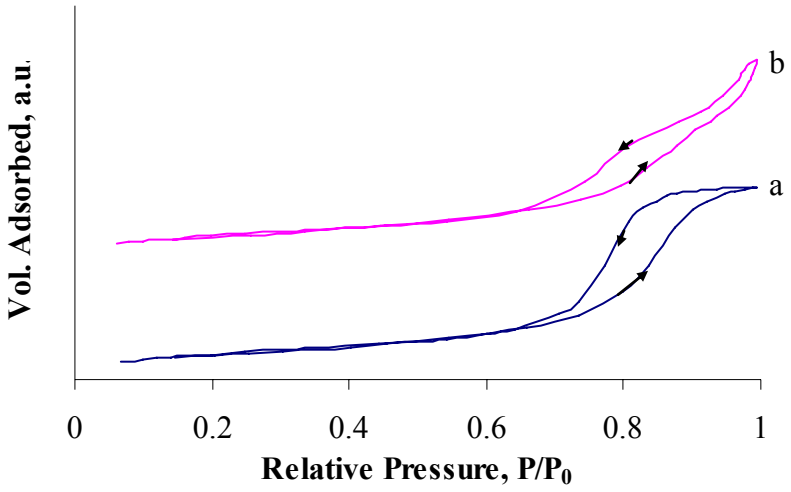

Figure 4.1: Hysteresis loops displayed by (a) Imp 3.1/12.2; (b) Sono 3/11.5.

generation of macropores.

4.1.3 Thermogravimetry Analysis

All sonochemically synthesized catalysts were tested with thermogravimetry analysis in the presence of air. Figures 4.2a and 4.2b show weight losses at 60, 275 and 525 °C by analyzed catalysts. The peak at less than 100 °C can be assigned to evaporation of water present in the sample. Figure 4.3 shows the differential themogravimetry analysis for tungsten carbonyl. This chart indicates a strong peak at 150 °C which means that $W(CO)_6$ vaporizes in this temperature range. There is no peak observed in this temperature range in Figures 4.2a and 4.2b indicating the absence of tungsten carbonyl in sonochemically prepared catalysts. This shows that filtration and washing leads to complete removal of unconverted tungsten carbonyl from prepared catalysts. Figure 4.2 also shows a strong peak at 275 °C, which corresponds to the vaporization of hexadecane used as the solvent during synthesis of the catalysts. It indicates that the synthesized hexane-washed catalysts still had some solvent left, which evaporated at its' boiling point. The broad peak at around 460 °C shows the presence of free carbon, which may have come from the decomposition of solvent during long sonication time used for synthesis of catalysts (Yu et al., 2002).

4.1.4 X-Ray Diffraction

All the synthesized catalysts were characterized with X-ray diffraction (XRD) analysis to identify the different crystalline phases present. The XRD patterns of impregnated and sonochemically prepared catalysts are shown in Figures 4.4 and 4.5,

a

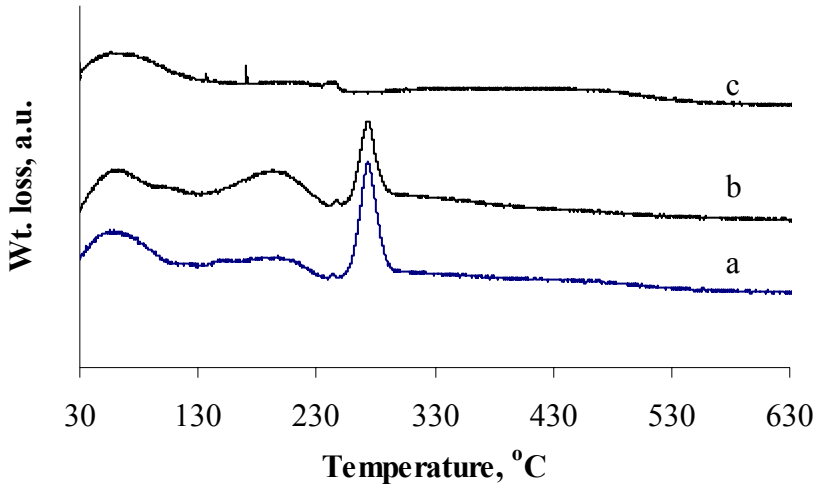

Figure 4.2a: Differential thermogravimetry plot for sonochemically prepared catalysts. (a) Sono 3/8; (b) Sono 1/10.7; (c) Sono 2.8/11.

b

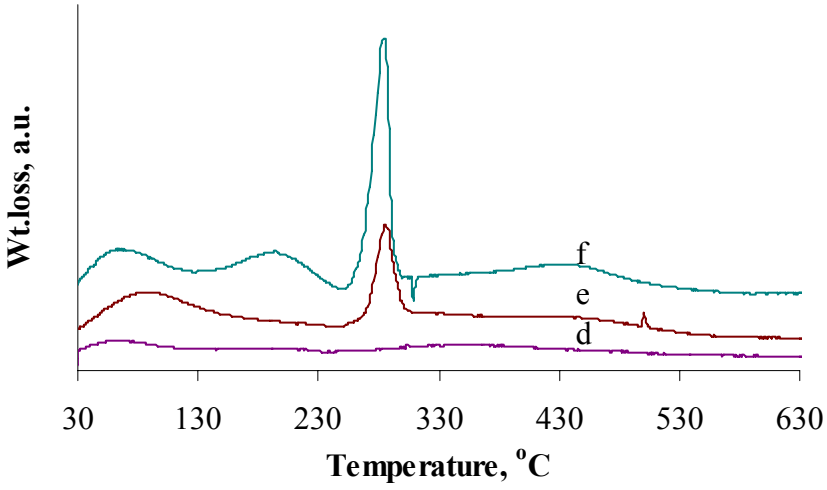

Figure 4.2b: Differential thermogravimetry plot for sonochemically prepared catalysts. (d) Sono 3/11.5; (e) Sono 2/12.2; (f) Sono 4/18.

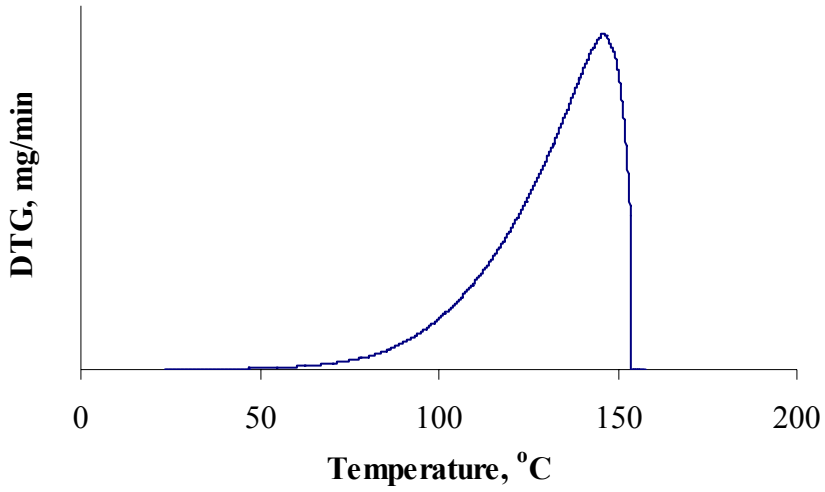

Figure 4.3: Differential thermogravimetry chart for tungsten carbonyl.

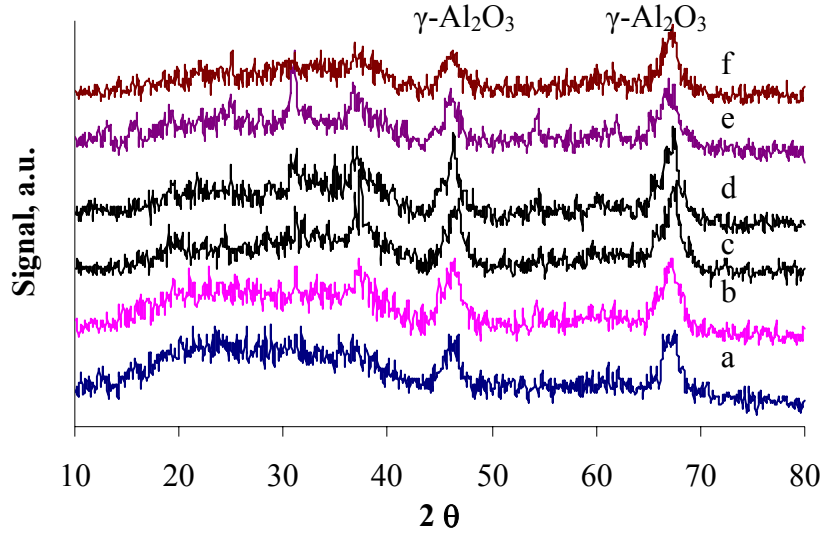

Figure 4.4: XRD patterns for sonochemically prepared catalysts. (a) Sonicated γ-Al_2O_3; (b) Sono 3/8; (c) Sono 1/10.7; (d) Sono 2.8/11; (e) Sono 2/12.3; (f) Sono 3/11.5.

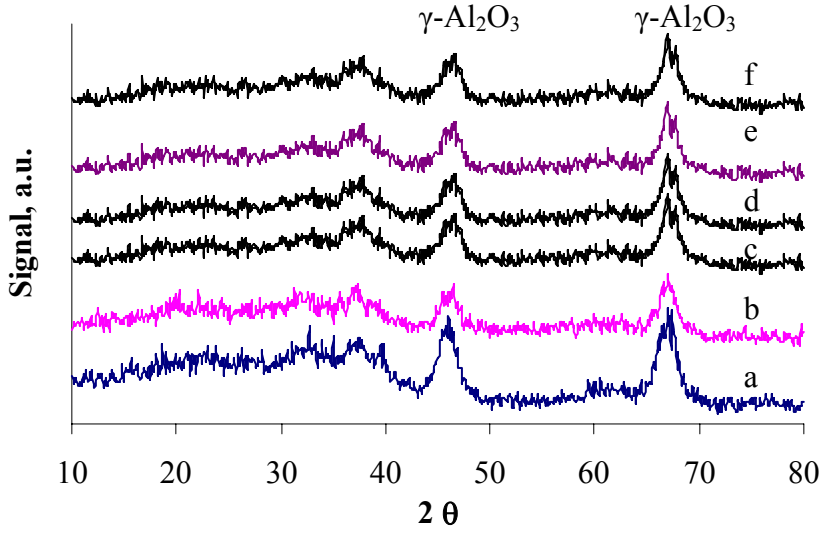

Figure 4.5: XRD pattern for impregnated catalysts. (a) γ-Al_2O_3; (b) Imp 1/13; (c) Imp 2/13; (d) Imp 3/7; (e) Imp 3/7; (f) Imp 3.1/12.2.

respectively. Similar patterns are observed for impregnated and sonochemically synthesized catalysts. It can be seen that none of the XRD patterns indicate any peak other than for γ-Al_2O_3 indicating that the metals are highly dispersed over the support and their particle sizes are below the detection limit of XRD technique (~5 nm). These results are in agreement with those reported by Brito et al. (1993). The patterns also indicate that the intensity of characteristic peaks for alumina (at 2θ values of 46.5° and 67.2°) decrease with the deposition of cobalt and tungsten metals which may be the results of the deposition of metals on the support. Figure 4.6 shows a comparison of XRD patterns for γ-Al_2O_3 with impregnated and sonochemically prepared catalysts with comparable metal loadings. It is observed from the chart that sonochemically prepared catalysts show lower intensities of characteristic peaks of γ-Al_2O_3 than those shown by impregnated catalysts, which leads to a conclusion that the crystallinity of the support in sonochemically prepared catalysts is lowered by the this method of catalyst synthesis (Dhas et al., 2001).

4.1.5 Temperature Programmed Desorption

The ammonia TPD analysis of synthesized catalysts was conducted to measure their acidic properties. Ammonia being a basic molecule adsorbs on the acid centres of the catalysts. The temperature of desorption of ammonia indicates the strength of acid centres, higher temperature indicates the strong acidity and vice versa. Three temperature ranges have been indicated in literature for strength of acid centres. These are 20-200, 200-350 and 350-550 °C, which correspond to weak, intermediate and strong acid centres

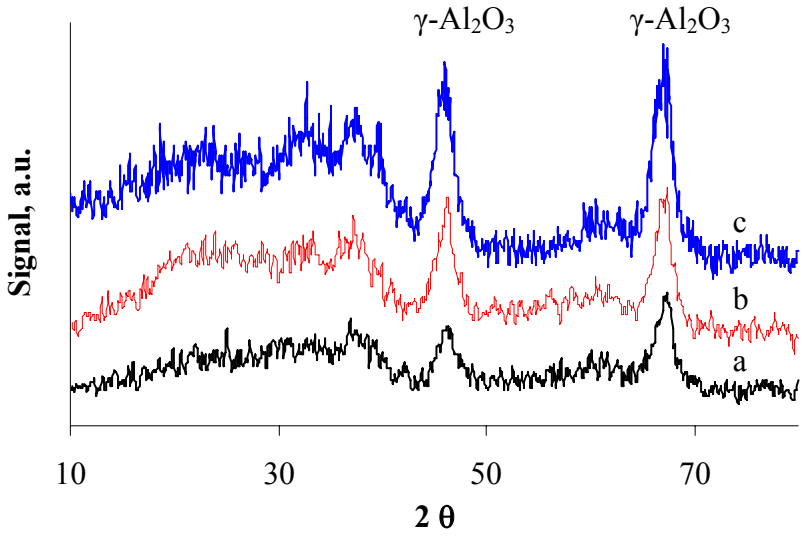

Figure 4.6: XRD patterns for prepared catalysts. (a) Sono 3/11.5; (b) Imp 3.1/12.2; (c) γ-Al_2O_3.

(Lewandowski and Sarbak, 2000). The desorption peak intensity indicates the number of acid sites; higher intensity indicates higher number of acid sites.

Figures 4.7a and 4.7b indicate the TPD profiles for sonochemically prepared catalysts. γ-Al_2O_3 (both sonicated and unsonicated) has strong acid centres in the temperature region of 400 – 500 °C and the deposition of metals on γ-Al_2O_3 leads to generation of additional intermediate and strong acid centres. It can be observed from the figures that Sono 3/8 and Sono 1/10.7 display the presence of intermediate and strong acid centres. The intermediate acid centres increase in strength and shift towards higher temperature as the total metal loading is increased from 11 wt % (for Sono 3/8) to 22 wt % (for Sono 4/18). For example, Sono 3/8 shows the intermediate acid centres at 345 °C which shifts to 452 °C for Sono 4/18. Figures 4.8a and 4.8b indicate the TPD profiles for impregnated catalysts. These profiles indicate a trend similar to the one shown by sonochemically synthesized catalysts. An increase in total metal loading from 10 wt % (for Imp 3/7) to 15.4 wt % (for Imp 3.1/12.3) leads to generation of intermediate acid centres which increase in strength with an increase in metal loading.

4.1.6 Temperature Programmed Reduction

All prepared catalysts were characterized with the temperature programmed reduction (TPR) to identify the phases formed as a result of synthesis and to study their reducibility. It has been discussed in literature that W strongly interacts with γ-Al_2O_3 and shows very low reducibility (Martin et al., 2003). It has also been reported that γ-Al_2O_3 supported tungsten oxide shows two main reduction peaks at 750 °C and 1050 °C and

a

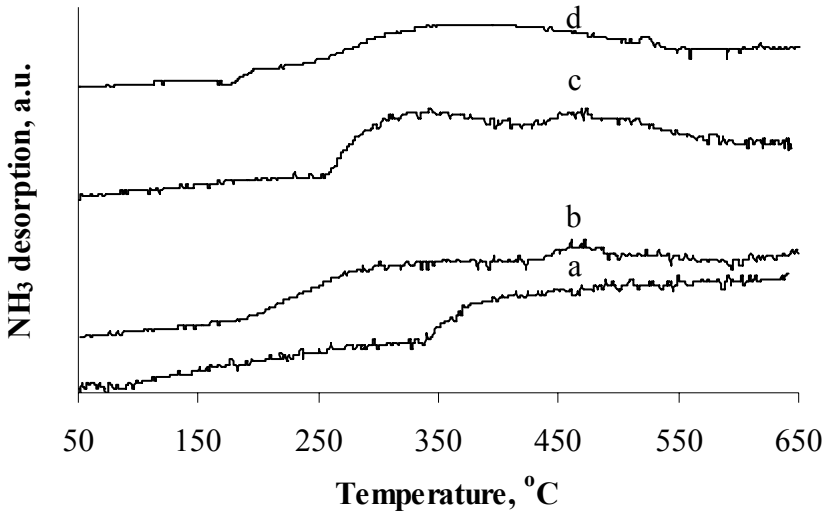

Figure 4.7a: NH_3 TPD profiles for sonochemically prepared catalysts. (a) Sonicated gamma alumina; (b) Sono 3/8; (c) Sono 1/10.7; (d) Sono 2.8/11.

b

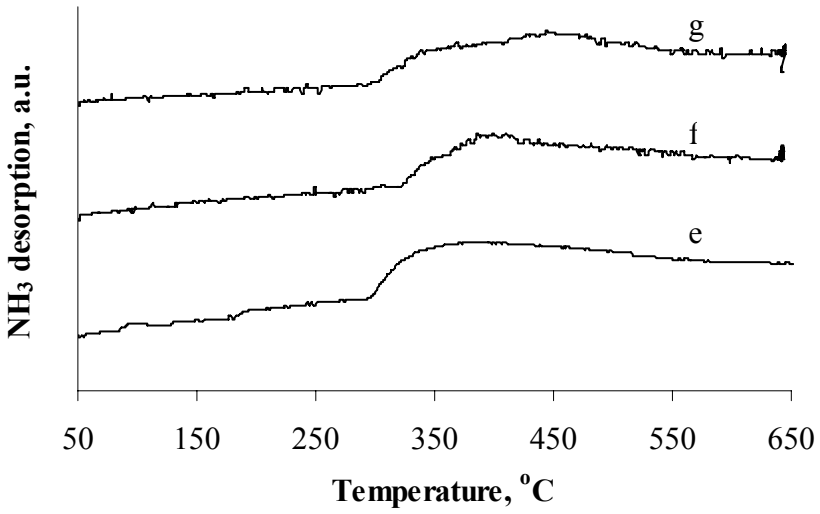

Figure 4.7b: NH_3 TPD profiles for sonochemically prepared catalysts. (e) Sono 2/12.2; (f) Sono 3/11.5; (g) Sono 4/18.

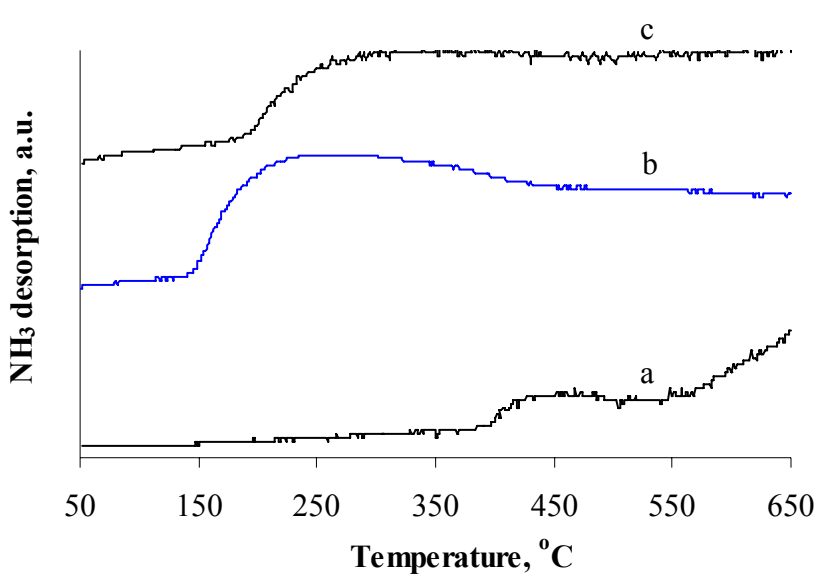

Figure 4.8a: NH_3 TPD profiles for impregnated catalysts. (a) Gamma alumina; (b) Imp 3/7; (c) Imp 3/10.

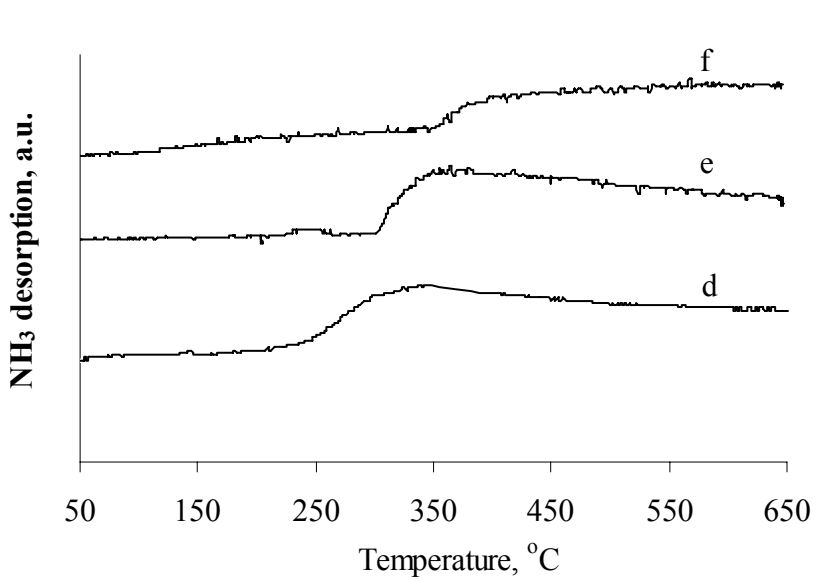

Figure 4.8b: NH_3 TPD profiles for impregnated catalysts. (d) Imp 1/13; (e) Imp 2/13; (f) Imp 3.1/12.3.

shows an additional peak at 300 °C as the loading is increased (Kadkhodayan and Brenner, 1989). The peak at 750 °C is assigned to the presence of W^{+6} and the peak at 1050 °C is assigned to W^{+4} species (Martin et al., 2003). Figure 4.9 shows the TPR profile for sonochemically prepared catalysts. The profiles indicate peaks in the temperature ranges of 200 – 450 °C and 730 – 800 °C. The peaks in low temperature region can be assigned to two stage reduction of larger sized and less support interacting Co_3O_4 species to Co^0 through an intermediate phase CoO (Herrera and Resasco, 2003).

$$Co_3O_4 + H_2 \rightarrow 3CoO + H_2O$$

$$3CoO + 3H_2 \rightarrow 3Co^0 + 3H_2O$$

The peak at higher temperature (> 700 °C) can be either due to the reduction of small sized, finely distributed and highly support interacting CoO phase (Herrera and Resasco, 2003) or due to the reduction of W^{+6} phase (Kadkhodayan and Brenner, 1989). It can also be seen that an increase in Co loading from 1 to 3 wt % causes a shifting of low temperature peak from 424 °C to 400 °C. This indicates an increase in the reducibility of the catalysts and formation of larger sized Co_3O_4 crystallites. Figure 4.9 further indicates that an increase in W loading from 8 to 11.5 wt % leads to a reduction in low temperature peak intensity and the catalyst with 3 wt % Co and 11.5 wt % W shows no or minimum peaks indicating fine distribution of metals on support with very little formation of bulk Co_3O_4 species. A further increase in loading of Co to 4 wt % and W to 18 wt % leads to the formation of bulk type larger Co_3O_4 crystallites and decrease in dispersion. This indicates that except for a very narrow range of metal loadings (Co ~ 3 wt % and W ~ 11.5 wt %) formation of less distributed bulk Co_3O_4 takes place. Figure 4.10 shows that impregnated cobalt oxide on γ-Al_2O_3 displays peaks at553 and 682 °C

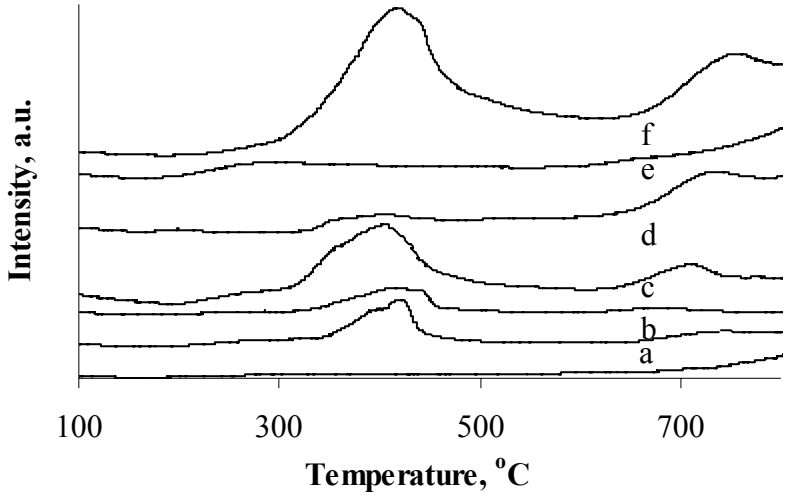

Figure 4.9: TPR profiles of sonochemically synthesized catalysts. (a) Sono 0/10; (b) Sono 1/10.7; (c) Sono 2/12.3; (d) Sono 3/8; (e) Sono 2.8/11; (f) Sono 3/11.5.

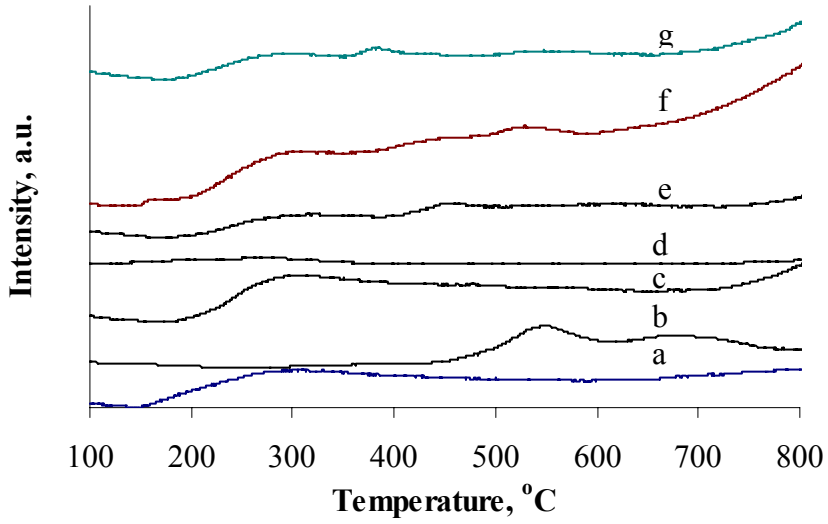

Figure 4.10: TPR profiles of impregnated catalysts. (a) Imp 0/10; (b) Imp 3/0; (c) Imp 1/13; (d) Imp 2/13; (e) Imp 3/7; (f) Imp 3/10; (g) Imp 3.1/12.2 .

and indicates that an increase in W loading from 0 to 12.2 wt % leads to the shifting of low temperature peaks from 553 to 387 °C. This change in reducibility by increase in tungsten loading may be due to the interaction between Co and W metals. It can also be seen that all the impregnated catalysts show very small peaks as compared with the sonochemically prepared catalysts indicating lower formation of bulk type Co_3O_4 crystallites thus indicating that most of the cobalt is present as strong support interacting species. These catalysts do not show any peak in 750 °C region which indicates the absence of W^{+6} species in all impregnated catalysts.

4.1.7 X-Ray Photoelectron Spectroscopy Studies

Selected catalysts were analyzed with XPS to determine the surface atomic composition. The atomic compositions results from this study were converted to weight percentage compositions for a direct comparison with the results from ICP analysis which gave bulk analysis. Table 4.3 indicates the theoretical, bulk and surface compositions of cobalt and tungsten metals. It can be seen from the table that all the impregnated catalysts display very close values of bulk and surface concentrations of deposited metals. For example, Imp 0/10 shows a bulk concentration of tungsten as 10.1 wt % and a surface concentration of it as 9.8 wt %. A similar observation can be made for Imp 3/11.5 for which shows the bulk concentrations of 3.1 (Co)/12.2 (W) wt % were very similar to the surface concentrations of 2.1 (Co)/12.5(W) wt %. On the other hand, all the sonochemically synthesized catalysts show a big difference between bulk and surface concentrations. For example, Sono 0/10 indicates a bulk concentration of tungsten as 9.9 wt % and a surface concentration of it as 21.5 wt %. Sono 3/11.5 also displays a trend

Table 4.3: Theoretical, bulk and surface loadings of cobalt and tungsten metals in synthesized catalysts.

Catalyst	Cobalt wt %			Tungsten wt %		
	Theor.	Bulk	Surface	Theor.	Bulk	Surface
Imp 0/10	0	0.0	0.0	10	10.1	9.8
Imp 3/7	3	2.8	2.3	7	6.8	6.9
Imp 3/10	3	2.9	2.6	10	9.7	10.3
Imp 3/11.5	3	3.1	2.1	13	12.2	12.5
Sono 0/10	0	0.0	0.0	12	10.0	21.5
Sono 3/8	3	3.0	1.5	10	8.0	17.0
Sono 2.8/11	3	2.8	2.1	13	11.0	19.0
Sono 3/11.5	3	3.0	3.8	13	11.5	20.5
Sono 4/18	4	4.0	0.1	18	15.4	21.9

similar to the one shown by Sono 0/10 and shows the bulk concentrations of 3.0 (Co)/11.5 (W) wt % and surface concentrations of 3.0 (Co)/20.5 (W) wt %. This indicates that most of the deposited cobalt and tungsten metals are within the 10 Å from the surface in sonochemically synthesized catalysts which is in stark contrast with the impregnated catalysts in which most of these metals are uniformly dispersed throughout the support.

Table 4.4 summarizes the results from characterization studies of all the synthesized catalysts.

4.1.8 Implication of Characterization results on HDS and HDN Activity

From BET surface area analysis, it was observed that the sonochemical method produces catalysts with a lower surface area than those produced using the impregnation method. Sono 3/11.5 and Imp 3.1/12.2 indicate a surface area of 177 and 183 m^2/g, respectively. It can also be seen that the sonochemical method leads to larger reduction in the mesopore volume of the support. In general, catalysts with a high surface area are desired as higher dispersion of the catalyst metals can be achieved. But it is difficult to correlate the HDS and HDN activity of catalyst with surface area as it depends not only on metal loadings but also on other physicochemical properties. In the literature the HDN activity has been associated with an increase in the number of weak and intermediate acid centres (Lewandowski and Sarbak, 2000). It can be seen from TPD analysis that an increase in total metal loading on the support leads to generation of intermediate temperature acid sites. Sono 1/10.7, Sono 4/18 and Imp 3/7 show a generation of larger number of intermediate acid sites so higher HDN activity can be expected from them. The HDS has not been particularly correlated with acidity (Van Veen et al., 1993) so no

Table 4.4: Summary of properties of impregnated and sonochemically synthesized catalysts.

Characterization technique	Impregnated Catalysts	Sonochemical Catalysts
BET surface are, pore volume and pore size distribution	Lower surface area and pore volumes than the one shown by γ-Al_2O_3 support.	Lower surface area and pore volumes than the ones shown by impreganted catalysts.
	Macropore volumes similar to the one shown by γ-Al_2O_3 support.	Higher macropore volumes than the ones shown by impregnated catalysts.
X-ray diffraction	Catalysts metal crystallites smaller than the detection limit of the machine.	Same as with impregnated catalysts.
	Lower crystallinity of γ-Al_2O_3 support in all the synthesized catalysts.	Lower crystallinity of γ-Al_2O_3 support in all the synthesized catalysts as compared with the impregnated catalysts.
Temperature programmed desorption	Generation of intermediate acid centres with the incorporation of metals in all the catalysts.	Same as with impregnated catalysts.
	Increase in the intensity of	Same as with impregnated

	acid centres with an increase in total metal loading.	catalysts.
Temperature programmed reduction	Generation of finely distributed and highly support interacting cobalt oxide species.	Generation of bulk type and less support interacting cobalt oxide species.
	No peaks corresponding to the presence of tungsten oxide species in the temperature range investigated.	Same as with impregnated catalysts.
X-ray photoelectron Studies	Metal oxides distributed uniformly over the γ-Al_2O_3 support.	Metal oxides present mostly on the surface of the γ-Al_2O_3 support.

particular activity can be predicted from TPD analysis. Attempts have been made to correlate the reducibility of oxide catalysts and their conversions to sulfide state with the HDS and HDN activities. It is observed from TPR profiles of sonochemically prepared catalysts that an increase in tungsten loading from 8 to 11.5 wt % leads to a reduction in low temperature peak (at ~ 420 °C) intensity and a catalyst with 11.5 wt % tungsten shows no low temperature peak. With impregnated catalyst, it can be seen that an increase in tungsten loading leads to the shifting of 530 °C (with Imp 3/0 catalyst) peak to lower temperature region. These peaks correspond to the presence of cobalt species and don't describe the reducibility of tungsten species which is present in larger proportion and is the main metal for catalytic activity. Consequently, no particular activity can be predicted from the TPR profiles of synthesized catalysts.

4.2 Catalyst Performance Evaluation and Screening

The performance tests for all synthesized catalysts were carried out using LGO as the feed in a trickle bed reactor at reaction temperatures of 340, 350 and 360 °C, pressure of 8.9 MPa, LHSV of 2 h^{-1} and hydrogen gas /gas oil ratio (G/L) of 600 mL/mL. Table A.1 in Appendix A shows the data obtained from screening tests. The detailed discussion on catalyst performance is given below.

4.2.1 Studies on HDS and HDN Activities

The effects of metal loading and the preparation methods on sulfur and nitrogen conversions of LGO are discussed using HDS and HDN conversions X_i and selectivity S_{SN} at different reaction conditions for synthesized catalysts. The conversion is defined by Equation (4.1).

$$X_i = \frac{C_{iF} - C_{iP}}{C_{iF}} * 100 \qquad (4.1)$$

Where C_{iF} and C_{iP} are the concentrations of sulfur and nitrogen species in feed and in the reaction product.

The selectivity is defined by Equation (4.2).

$$S_{SN} = \frac{r_{hds}}{r_{hdn}} \tag{4.2}$$

The selectivity used here is the selectivity of sulfur (S) removal with respect to nitrogen (N) removal. r_{hds} and r_{hdn} are the rates of hydrodesulphurization and hydrodenitrogenation reactions calculated using the concentrations of S and N species measured in feed and reaction product. The rates of HDS and HDN are calculated using Equation b.3 and b.4 (See Appendix B).

Table 4.5 indicates that the impregnated catalysts show a maximum in S and N conversions for Imp 3/10. A further increase in metal loading leads to a slight reduction in the conversion values. This can be explained that an increase in metal loadings from Imp 3/7 to Imp 3/10 leads to increase in the amount of monolayer of the metals on the support and increase in the catalytic activity. A further increase in metal loadings leads to the formation of multilayers and leads to slight drop in activity (Clausen et al., 1996). Figures 4.11 through 4.14 indicate that the S conversions are much higher than N conversions within the temperature range studied, indicating the ease in conversion of sulfur compounds compared to that of nitrogen compounds present in light gas oil derived from oil sands. Figures 4.11 to 4.14 also indicate that impregnated catalysts perform better than sonochemically prepared catalysts for HDS and HDN of LGO. For example, Imp 3/7 shows a S conversion of 72.3 wt % at 340 °C which increases to 85.7 wt % with an increase in temperature to 360 °C, whereas Sono 3/8 shows a S conversion of 30.8 wt % which increases to 53.4 wt % within the same temperature range.

Table 4.5: Effect of metal loading, preparation procedure and temperature on sulfur and nitrogen conversions.

Catalyst / Temperature°C	S Conversion, wt %			N Conversion, wt %			Selectivities, $Rate_{hds}/Rate_{hdn}$		
	340	350	360	340	350	360	340	350	360
Imp 3/7	72.3	80.0	85.7	19.4	25.6	35.2	121.1	102.4	79.9
Imp 3/10	82.7	89.0	93.0	29.2	45.1	56.8	92.9	64.6	54.1
Imp 3.1/12.2	75.9	86.2	91.7	26.8	42.8	57.1	92.7	66.3	53.0
Imp 1/13	58.9	65.0	78.3	21.4	26.3	36.7	89.6	80.9	70.2
Imp 2/13	73.7	83.2	89.7	22.5	35.7	45.9	106.9	76.6	64.4
Sono 3/8	30.8	41.3	53.4	14.1	18.5	26.0	70.1	72.4	67.1
Sono 2.8/11	64.9	70.2	77.6	13.3	23.1	33.4	157.1	99.4	76.3
Sono 3/11.5	73.2	80.8	87.9	20.0	29.1	42.5	119.1	91.1	68.2
Sono 1/10.7	24.7	35.5	46.4	18.2	23.2	30.8	44.0	49.9	49.5
Sono 2/12.3	28.8	40.2	53.2	21.2	24.4	33.2	44.3	53.9	52.6
Sono 4/18	33.4	45.2	57.9	23.2	30.3	40.5	47.0	49.0	47.1

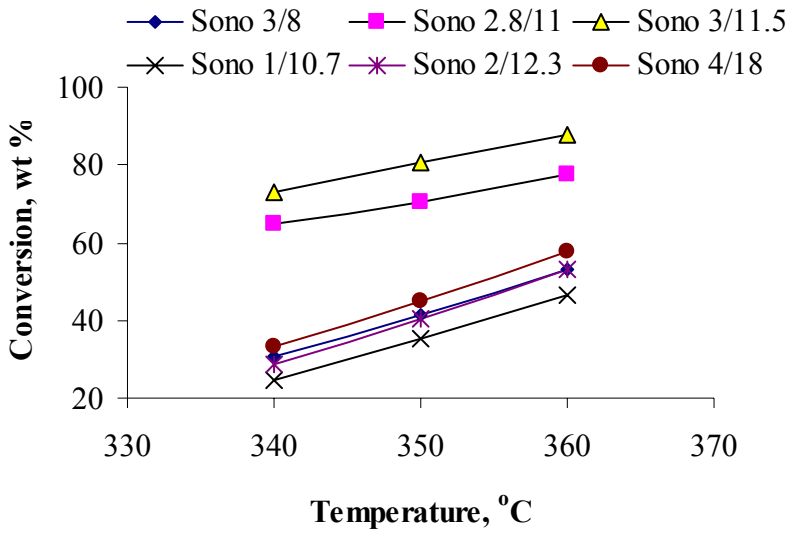

Figure 4.11: Effect of temperature on S Conversions of LGO at Pressure = 8.9 MPa, G/L = 600 mL/mL and LHSV ~ 2.0 h^{-1} with sonochemically synthesized catalysts.

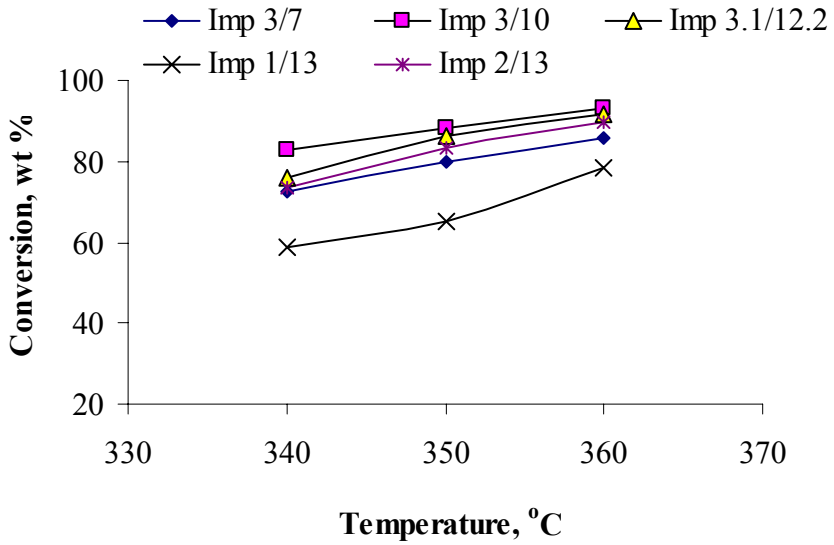

Figure 4.12: Effect of temperature on S Conversions of LGO at Pressure = 8.9 MPa, G/L = 600 mL/mL and LHSV ~ 2.0 h^{-1} with impregnated catalysts.

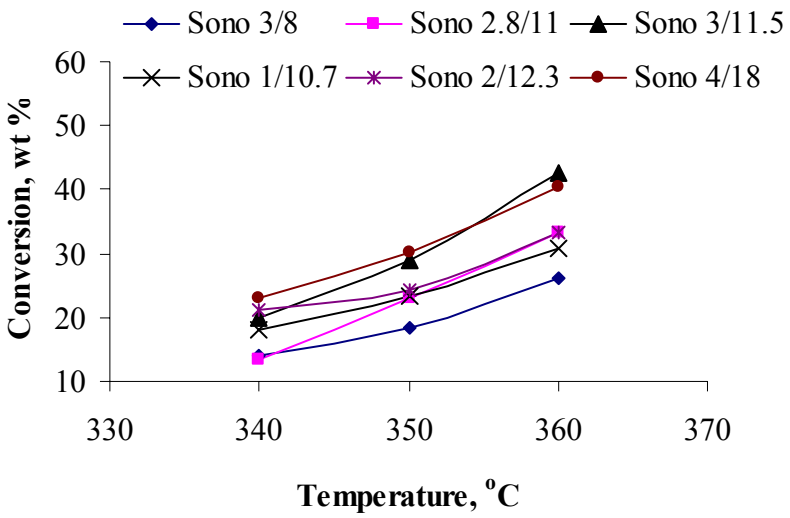

Figure 4.13 Effect of temperature on N Conversions of LGO at Pressure = 8.9 MPa, G/L = 600 mL/mL and LHSV ~ 2.0 h^{-1} with sonochemically synthesized catalysts.

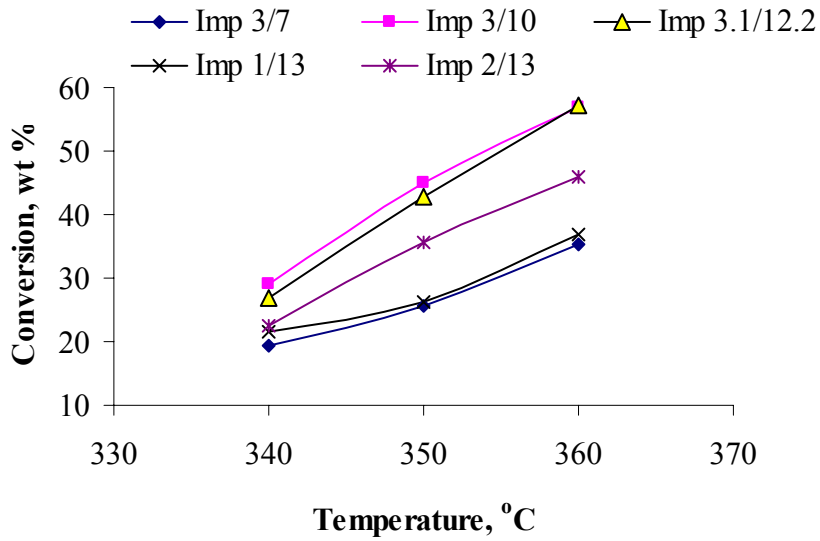

Figure 4.14: Effect of temperature on N Conversions of LGO at Pressure = 8.9 MPa, G/L = 600 mL/mL and LHSV ~ 2.0 h^{-1} with impregnated catalysts.

A similar observation can be made for S conversions also. This can be explained on the basis of TPR profiles. TPR plots of the sonochemically prepared catalysts indicate the formation of bulk type of species for all catalysts except for Sono 2.8/11 and Sono 3/11.5. In literature, these bulk species have been indicated to form at a metal loading typically higher than 12 wt %, where the multilayer formation starts to take place and are not as catalytically active as the monolayered species upon sulfiding (Clausen et al., 1996). The TPR profiles for impregnated catalysts show relatively much lesser formation of bulk species. This might be the reason for better conversion results as indicated in figures.

Selectivity has been defined as the ratio of rate for HDS to the rate for HDN reactions for light gas oil (Equation 4.2). Figure 4.15 indicates the selectivities for impregnated catalyst. It can be seen that all impregnated catalysts show a decrease in selectivity with an increase in reaction temperature. For example, Imp 3/10 shows a selectivity of 92.9 at 340 °C which decreases to 54.1 as the temperature is increased to 360 °C. This means that with impregnated catalysts, the rate of HDN increases at a faster rate than the rate of HDS as the reaction temperature is increased. Figure 4.16 shows the selectivities for sonochemically prepared catalysts. It can be seen that Sono 3/11.5 and Sono 2.8/11 indicate a trend of decrease in selectivity with an increase in reaction temperature which is similar to the trend shown by impregnated catalysts. Other sonochemically synthesized catalysts indicate a very small variation in selectivity with an increase in reaction temperature from 340 to 360 °C. This trend can be seen similar to the trend shown by TPR profiles of studied catalysts. TPR studies indicate the formation of easily reduced bulk type species for all the sonochemically prepared catalysts except for

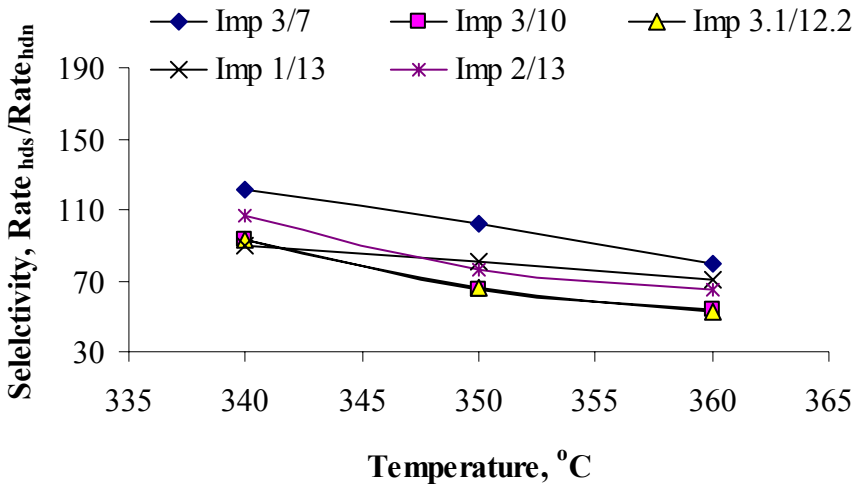

Figure 4.15: Effect of temperature on selectivities of LGO at Pressure = 8.9 MPa, G/L = 600 mL/mL and LHSV ~ 2.0 h^{-1} with sonochemically synthesized catalysts.

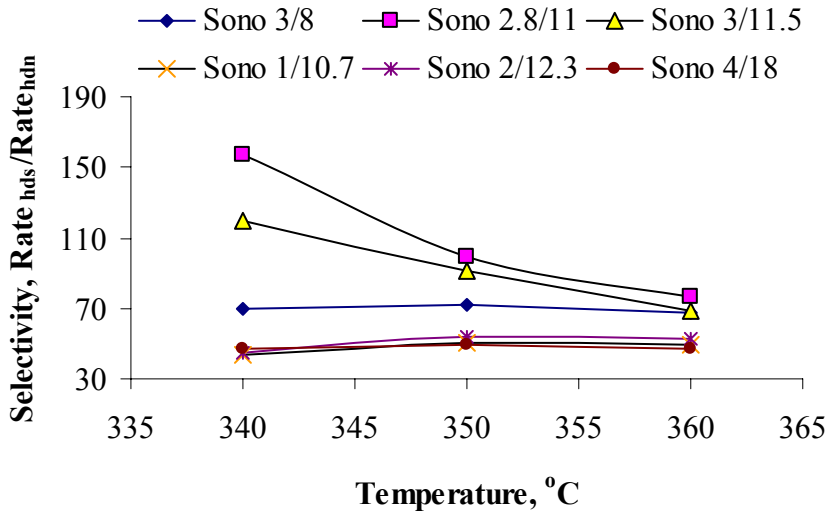

Figure 4.16: Effect of temperature on selectivities of LGO at Pressure = 8.9 MPa, G/L = 600 mL/mL and LHSV ~ 2.0 h^{-1} with impregnated catalysts.

Sono 3/11.5 and Sono 2.8/11. It can be seen that sonochemical catalysts indicating the presence of bulk type of species show very little change in selectivity with temperature in addition to lower sulfur and nitrogen conversions. So, the presence of bulk type of species may be responsible for the poor performances.

4.3 Comparison of Performances of Sono 3/11.5 and Imp 3/10

Imp 3/10 and Sono 3/11.5 catalysts showed the best activity for HDS and HDN of LGO amongst all the screened catalysts. So, these catalysts were selected for performance and optimization studies. A kinetic study on HDS and HDN was also performed with them. The studies were carried out at three different values of each of the parameters including reaction pressure, reaction temperature, LHSV and G/L. This section discusses the effects of reaction conditions (pressure: 8.9-10.3 MPa, temperature: 340-380 °C, LHSV: 1.5-2.5 h^{-1}) on HDS and HDN. The two selected catalysts were examined for 23 days each at above mentioned reactions. To ascertain that the deactivation of catalysts was not dominant, experimental run at a reaction temperature of 370 °C, LHSV ~ 2 h^{-1}, pressure of 8.9 MPa and G/L of 600 mL/mL was repeated and results were compared with those from previous runs. Results of error analysis are presented in Figures 4.17 and 4.18. The standard deviation for Sono 3/11.5 is 0.77 for sulfur conversions and 0.1 for nitrogen conversions. Similarly for Imp 3/10, standard deviations are 0.53 and 2.1 for S and N conversions, respectively. It is evident that results are repeatable in nature and the effect of deactivation can be neglected within the three weeks of time-on-stream.

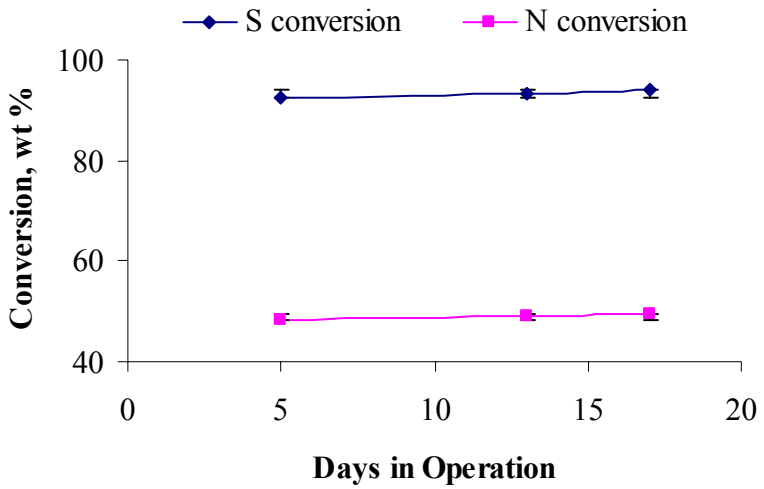

Figure 4.17: S and N conversions with Sono 3/11.5 at Temperature = 370 °C, Pressure = 8.9 MPa, LHSV ~ 2.0 h^{-1} and G/L = 600 mL/mL

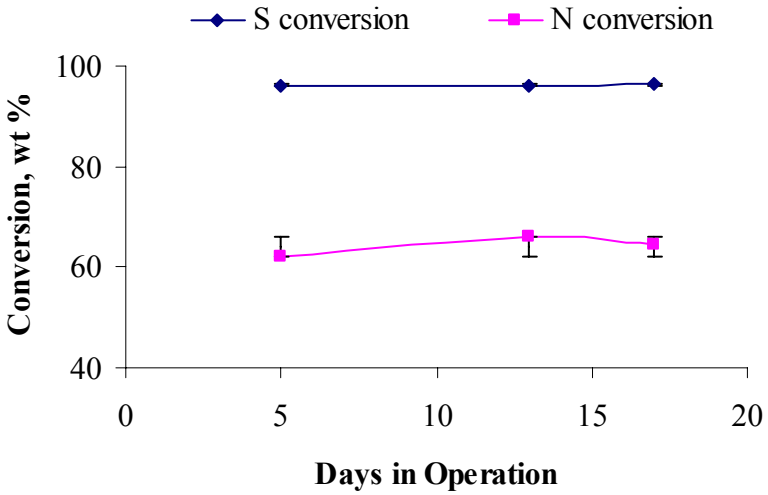

Figure 4.18: S and N conversions with Imp 3/10 at Temperature = 370 °C, Pressure = 8.9 MPa, LHSV ~ 2.0 h^{-1} and G/L = 600 mL/mL.

4.3.1 Effects of Reaction Conditions on HDS and HDN over Selected Catalysts

4.3.1.1 Effects of Temperature and LHSV

Figures 4.19 through 4.22 indicate the effects of temperature and LHSV on S and N conversions on Sono 3/11.5 and Imp 3/10. The effect of LHSVs (1.5, 2.0 and 2.5 h^{-1}) on HDS and HDN activities of selected catalysts at three different temperatures (340, 360 and 380 °C) was studied. Other parameters including reaction pressure and G/L were kept constant at 8.9 MPa and 600 ml/mL, respectively. It can be observed from the figures that Imp 3/10 shows better S and N conversions than Sono3/11.5 at all the temperatures and LHSVs investigated. It can be seen that a similar observation was made during the screening studies also. For example, at 380 °C and 2.5 h^{-1}, the S conversions are 96.8 and 94 wt % for Imp 3/10 and Sono 3/11.5, respectively. It can also be observed from the figures that all the values of S conversions fall in very small range at 380 °C. For example, these vary from 94 to 97.9 wt % for Sono 3/11.5 and 96.8 to 98.8 wt % for Imp 3/10 for a decrease in LHSV from 2.5 to 1.5 h^{-1}. This indicates that rate of HDS is fast enough to mask the effects of increase in LHSV. It can be observed from Figure 4.19 that Sono 3/11.5 doesn't show any change in S conversions with an increase in LHSV from 2.0 to 2.5 h^{-1} in the temperature range of 340-360 °C. A similar observation can be made about N conversion at 340 °C (see Figure 4.21). Figures 4.19 and 4.22 indicate that the Imp 3/10 shows higher values of S and N conversions at similar reaction conditions. This implies that the HDS activity of Sono 3/11.5 is much lower than the HDS activity of Imp 3/10 in a temperature range of 340-360 °C. Figures 4.19 through 4.22 also reveal that an increase in temperature from 340 to 360 °C leads to a continuous increase in S and N conversions thus indicating reactions in kinetically driven zone. Figures also

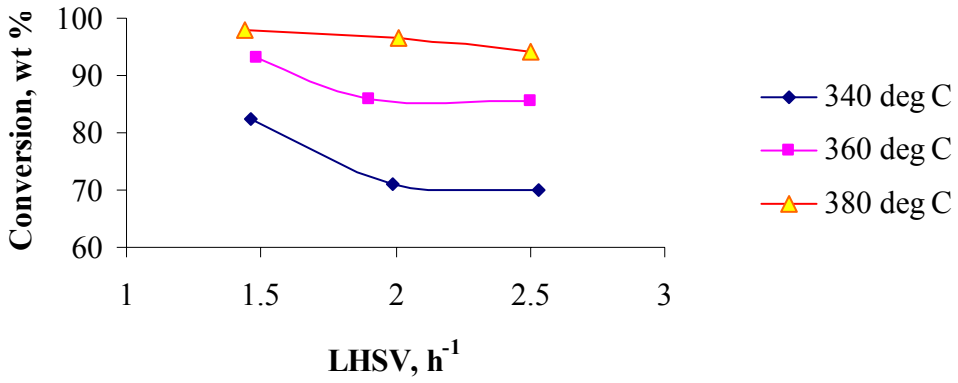

Figure 4.19: Effects of LHSV on the conversion of sulfur species present in LGO at Pressure = 8.9 MPa, G/L = 600 mL/mL with sonochemically prepared Co (3 wt %)-W (11.5 wt %) /γ-Al_2O_3 (Sono 3/11.5) catalyst.

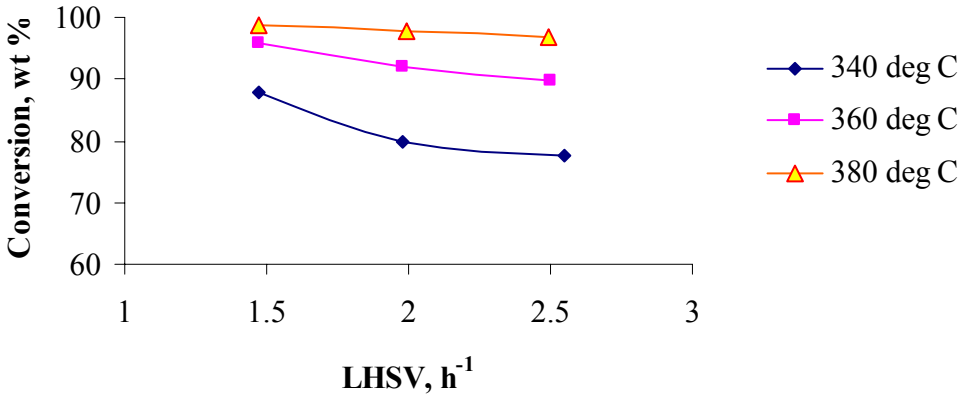

Figure 4.20: Effects of LHSV on the conversion of sulfur species present in LGO at Pressure = 8.9 MPa, G/L = 600 mL/mL with impregnated Co (3 wt %)-W(10 wt %)/γ-Al_2O_3 (Imp 3/10) catalyst.

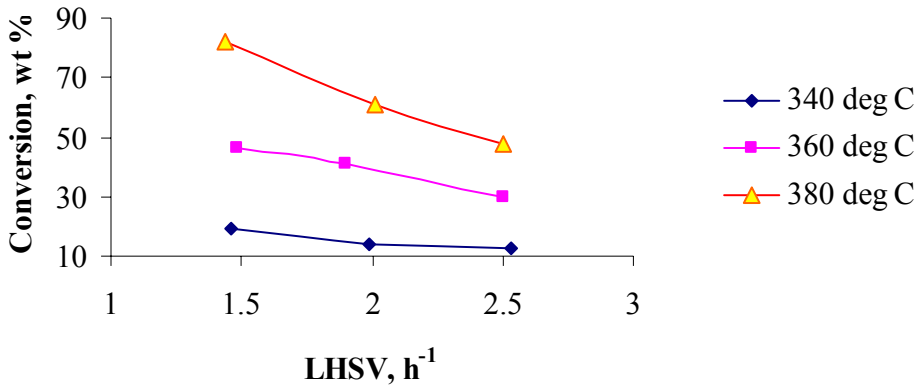

Figure 4.21: Effects of LHSV on the conversion of nitrogen species present in LGO at Pressure = 8.9 MPa, G/L = 600 mL/mL with sonochemically prepared Co (3 wt %)-W (11.5 wt %) /γ-Al_2O_3 (Sono 3/11.5) catalyst.

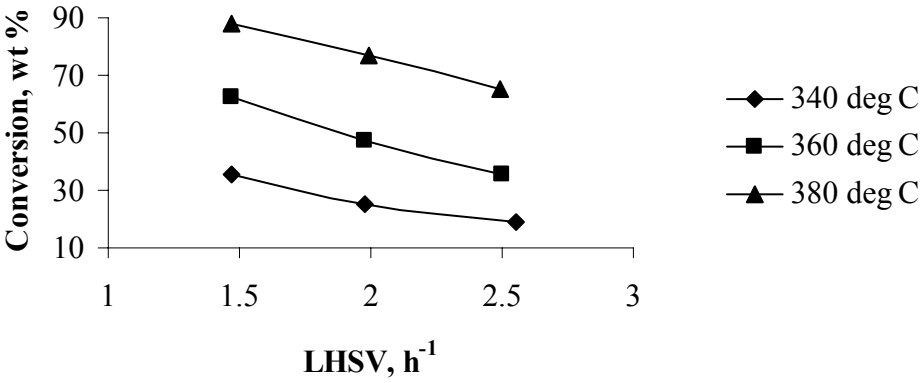

Figure 4.22: Effects of LHSV on the conversion of nitrogen species present in LGO at Pressure = 8.9 MPa, G/L = 600 mL/mL with impregnated Co (3 wt %)-W(10 wt %)/γ-Al_2O_3 (Imp 3/10) catalyst.

indicate that a further increase in temperature from 360 to 380 °C leads to an increase in the rate of S conversions, however, at a lower rate. This may be because of the equilibrium limitation at higher reaction temperatures for reversible HDS reaction (Steiner and Blekkan, 2002). It is interesting to see that Figures 4.21 and 4.22 show continuous increase in the rate of N conversion with an increase in temperature from 340 to 380 °C, which indicates that HDN occurs in the regime away from the equilibrium limitation.

4.3.1.2 Effect of Pressure

The effects of reaction pressure on the HDS and HDN activities of both impregnated and sonochemically synthesized catalysts were studied in a range of 7.6–10.3 MPa at a temperature of 380 °C and LHSV of 1.5 h^{-1} as both the catalysts showed maximum activities for above mentioned reactions at these conditions. The effects of pressure on S and N conversions are shown in Figures 4.23 through 4.26. It can be observed from the figures that effect of pressure on HDS of LGO was marginal for both the catalysts. For example, Sono 3/11.5 shows a value of S conversion as 97.7 wt % at 7.6 MPa which increases to 97.9 at 10.3 MPa whereas Imp 3/10 shows S conversion as 98.2 % at 7.6 MPa which increases to 99.0 wt % at 10.3 MPa. The figures also indicate that most of the values for S conversions are very high (>97 wt %) and are a very weak function of pressure in the range investigated. This might be because of the prominence of direct sulfur extraction pathway over pre-hydrogenation pathway which is a stronger function of pressure at these process conditions. It can also be observed that an increase in pressure from 8.9 to 10.3 MPa shows comparatively much lesser increase in S conversions than that with the increase in pressure from 7.6 MPa to 8.9 MPa. This might

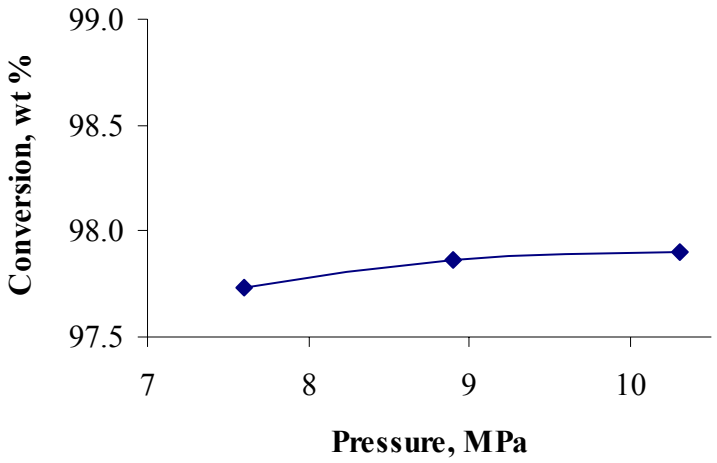

Figure 4.23: Effects of pressure on the conversion of sulfur species present in LGO at Temperature = 380 °C, G/L = 600 mL/mL and LHSV ~ 1.5 with sonochemically prepared Co (3 wt %)-W (11.5 wt %) /γ-Al_2O_3 (Sono 3/11.5) catalyst.

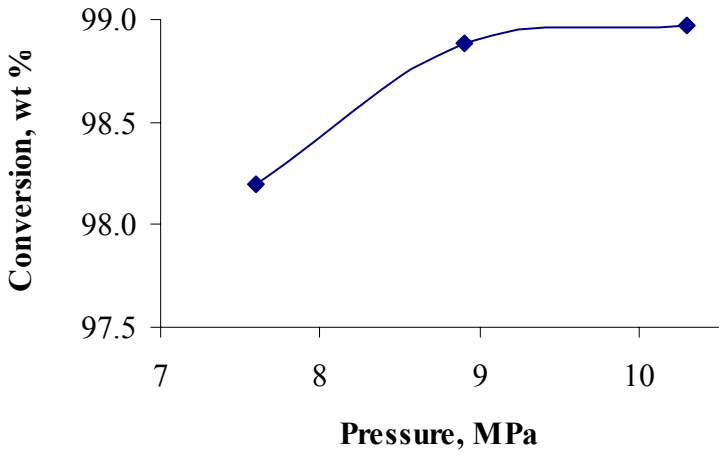

Figure 4.24: Effects of pressure on the conversion of sulfur species present in LGO at Temperature = 380 °C, G/L = 600 mL/mL and LHSV ~ 1.5 with impregnated Co (3 wt %)-W (10 wt %) /γ-Al_2O_3 (Imp 3/10) catalyst.

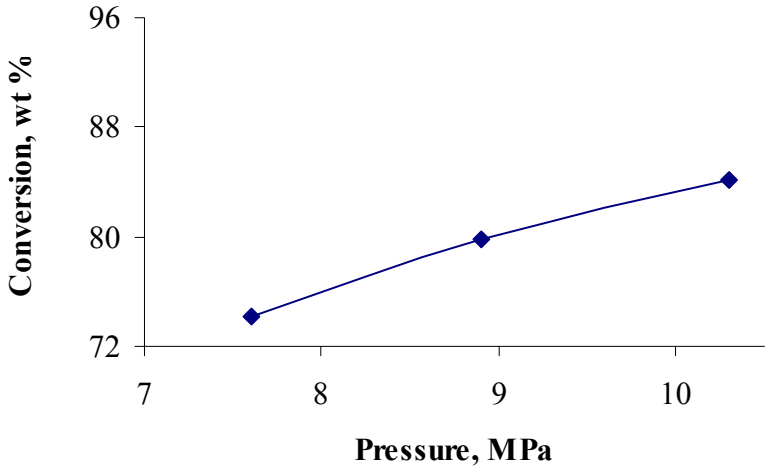

Figure 4.25: Effects of pressure on the conversion of nitrogen species present in LGO at Temperature = 380 °C, G/L = 600 mL/mL and LHSV ~ 1.5 with sonochemically prepared Co (3 wt %)-W (11.5 wt %) /γ-Al_2O_3 (Sono 3/11.5) catalyst.

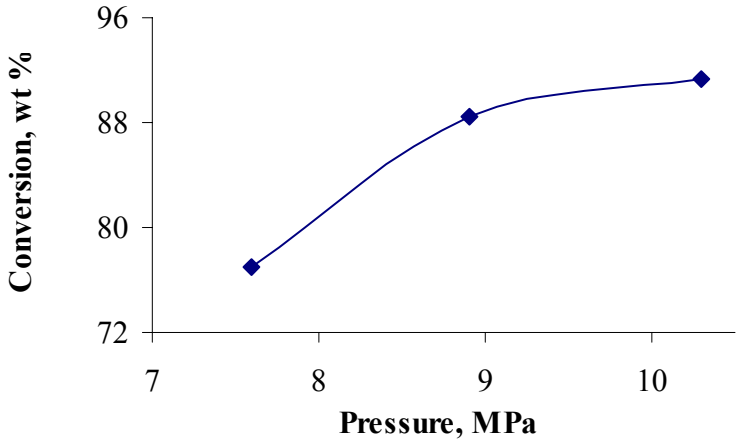

Figure 4.26: Effects of pressure on the conversion of nitrogen species present in LGO at Temperature = 380 °C, G/L = 600 mL/mL and LHSV ~ 1.5 with impregnated Co (3 wt %)-W (10 wt %) /γ-Al_2O_3 (Imp 3/10) catalyst.

be the effect of competitive adsorption of N compounds (Clausen et al., 1996) or due to reversibility of conversion of refractory sulfur compounds such 4,6 DMDBT. It can also be due to the reduction in effectiveness factor with an increase in reaction temperature (see Appendix G). Figures 4.25 and 4.26 depict the N conversions in the pressure range investigated. Both figures indicate that N conversion is a much stronger function of pressure than S conversion. It can be seen that both catalysts indicate a significant increase in N conversion with an increase in pressure. For example, Sono 3/11.5 shows a N conversion of 74.2 wt % at 7.6 MPa which increases to 84.1 wt % at 10.3 MPa whereas Imp 3/10 shows a N conversion of 77.0 wt % at 7.6 MPa which increases to 91.3 wt % at 10.3 MPa. This might be because HDN proceeds through hydrogenation of the aromatic ring which is strong function of hydrogen partial pressure (Clausen et al., 1996).

4.3.1.3 Effect of Hydrogen gas/Gas oil Ratio

Figures 4.27 through 4.30 show the effects of G/L on HDS and HDN of LGO. It can be seen from the figures that Sono 3/11.5 and Imp 3/10 display different trends for S and N conversions with G/L. Sono 3/11.5 shows no increase in S conversion with an increase in G/L from 400 to 600 mL/mL but shows a marginal increase in it from 97.7 to 98.4 wt % as G/L is increased further to 800 mL/mL. On the other hand, Imp 3/10 shows a marginal increase in S conversion from 97.6 to 98.2 wt % with an increase in G/L from 400 to 600 mL/mL but shows no increase in it with a further increase in G/L to 800 mL/mL. A similar observation can be made for N conversions also. This can be explained on the basis of inhibition effect caused by H_2S formed during HDS (Botchway et al., 2004). It indicates towards the possibility that with Sono 3/11.5, HDS and HDN are

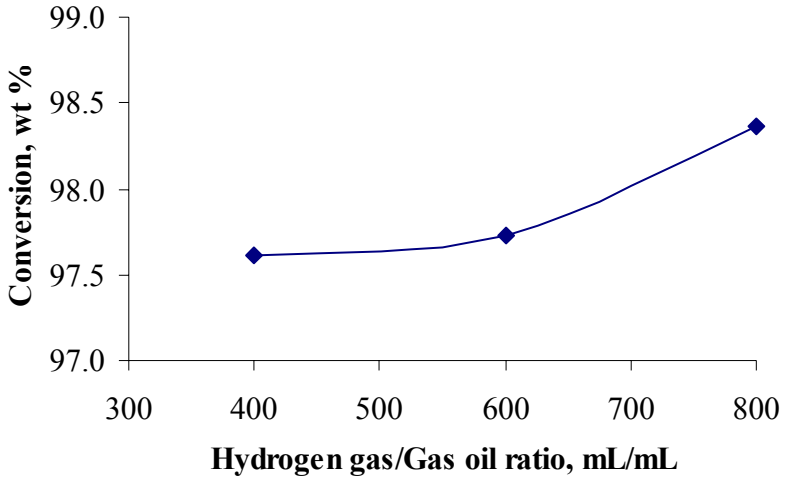

Figure 4.27: Effects of G/L on the conversion of sulfur species present in LGO at Pressure = 10.3 MPa, Temperature = 380 °C and LHSV ~ 1.5 with sonochemically prepared Co (3 wt %)-W (11.5 wt %) /γ-Al_2O_3 (Sono 3/11.5) catalyst.

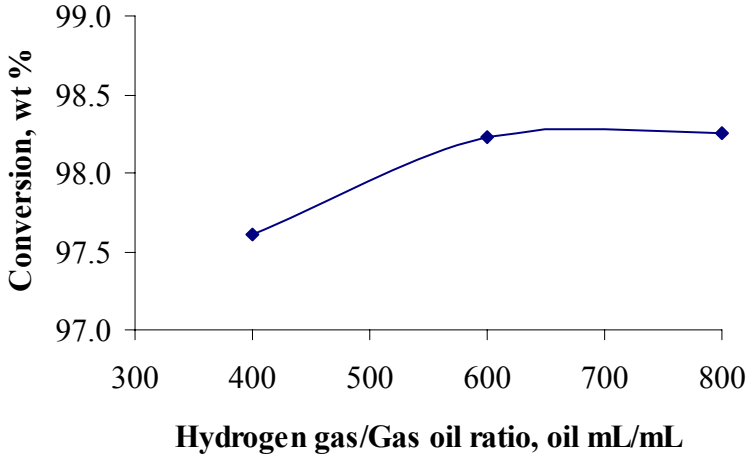

Figure 4.28: Effects of G/L on the conversion of sulfur species present in LGO at Pressure = 10.3 MPa, Temperature = 380 °C and LHSV ~ 1.5 with impregnated Co (3 wt %)-W (10 wt %) /γ-Al_2O_3 (Imp 3/10) catalyst.

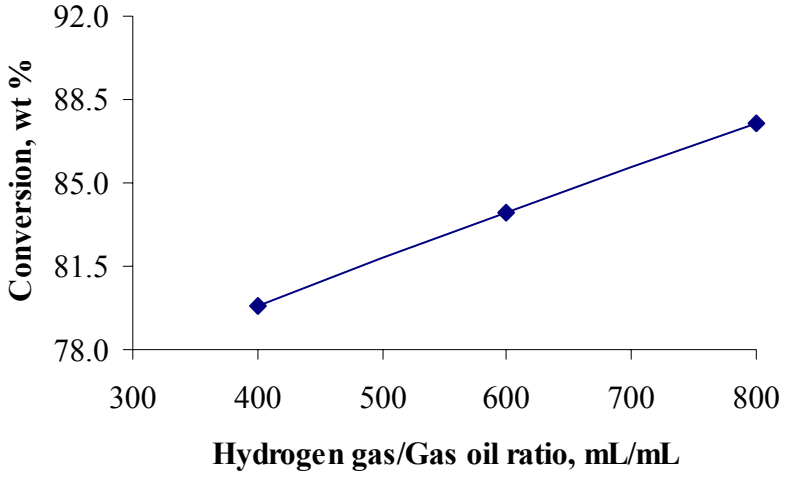

Figure 4.29: Effects of G/L on the conversion of nitrogen species present in LGO at Pressure = 10.3 MPa, Temperature = 380 °C and LHSV ~ 1.5 with sonochemically prepared Co (3 wt %)-W (11.5 wt %) /γ-Al_2O_3 (Sono 3/11.5) catalyst.

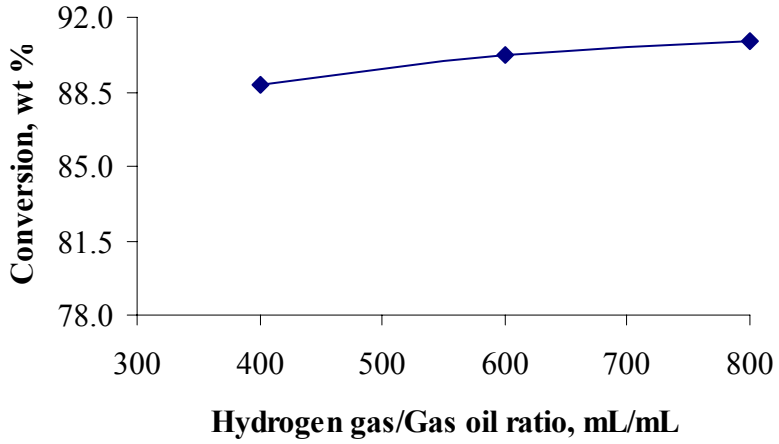

Figure 4.30: Effects of G/L on the conversion of nitrogen species present in LGO at Pressure = 10.3 MPa, Temperature = 380 °C and LHSV ~ 1.5 with impregnated Co (3 wt %)-W (10 wt %) /γ-Al_2O_3 (Imp 3/10) catalyst.

strongly inhibited by H_2S in the range of G/L from 400 to 600 mL/mL and don't show any appreciable increase in S and N conversions. But an increase in G/L from 600 to 800 mL/mL causes its' dilution and leads to increase in the rates of reactions and consequently in S and N conversions. On the other hand, HDS and HDN with Imp 3/10 appear to operate in moderately H_2S inhibited zone thus an increase in G/L from 400 to 600mL/mL leads to increase in dilution of hydrogen sulfide and ammonia and consequently leads to increase in the rates of HDS and HDN. A further increase in G/L to 800 mL/mL leads to further dilution of H_2S but no further increase in conversion as the effect of its' dilution on rate of S and N conversions decreases below observable limits.

4.3.1.4 Summary of the Effects of Reaction Conditions on HDS and HDN over Sono 3/11.5 and Imp 3/10

Tables 4.6 and 4.7 show the conversions with Sono 3/11.5 and Imp 3/10 at different operating conditions. It can be seen that both the catalysts show similar trends for S and N conversions as the reaction conditions are varied. Both the catalysts indicate increase in S and N conversions with a decrease in LHSV from 2.5 to 1.5 h^{-1} and an increase in temperature from 340 to 380 °C. The two catalysts indicate maximum conversions at 1.5 h^{-1} and 380 °C. The reaction pressure is varied from 7.6 to 10.3 MPa at these LHSV and temperature. Tables 4.6 and 4.7 also indicate that an increase in pressure leads to increase in S and N conversions for both the catalysts up until 10.3 MPa. For example, Sono 3/11.5 shows the S and N conversions at 97.7 and 74.3 wt % at 7.6 MPa which increase to 97.9 and 84.1 wt % as the pressure is increased to 10.3 MPa. Similarly, Imp 3/10 shows the S and N conversions at 98.2 and 77 wt % at 7.6 MPa which increase to 98.9 and 91.0 wt % as the pressure is increased to 10.3 MPa. This implies that both the

Table 4.6: Effect of temperature, pressure, LHSV and hydrogen gas/ gas oil ratio on S and N conversions of LGO with Sono 3/11.5.

LHSV, h^{-1}	Hydrogen gas/Gas oil, mL/mL	Pressure, MPa	Temperature, ^{o}C	S Conversion, wt %	N Conversion, wt %
1.5	600	8.9	340	82.5	14.4
2.0	600	8.9	340	70.2	19.7
2.5	600	8.9	340	71.0	13.2
1.5	600	8.9	360	93.1	46.5
1.9	600	8.9	360	85.8	41.0
2.5	600	8.9	360	85.6	30.0
1.4	600	8.9	380	97.9	82.5
2.0	600	8.9	380	96.6	60.9
2.5	600	8.9	380	94.0	48.0
1.5	600	7.6	380	97.9	74.3
1.5	600	8.9	380	97.7	79.9
1.5	600	10.3	380	97.9	84.2
1.5	400	10.3	380	97.6	83.9
1.5	600	10.3	380	97.7	79.9
1.5	800	10.3	380	98.4	87.6

Table 4.7: Effect of temperature, pressure, LHSV and hydrogen gas/ gas oil ratio on S and N conversions of LGO with Imp 3/10.

LHSV, h^{-1}	Hydrogen gas/Gas oil, mL/mL	Pressure, MPa	Temperature, ^{o}C	S Conversion, wt %	N Conversion, wt %
1.5	600	8.9	340	87.7	35.5
2.0	600	8.9	340	79.9	25.2
2.6	600	8.9	340	77.5	19.0
1.5	600	8.9	360	95.7	62.7
2.0	600	8.9	360	92.1	47.0
2.5	600	8.9	360	89.8	35.9
1.5	600	8.9	380	98.8	87.8
2.0	600	8.9	380	97.6	76.8
2.5	600	8.9	380	96.8	65.5
1.4	600	7.6	380	98.2	77.0
1.5	600	8.9	380	98.9	88.5
1.5	600	10.3	380	99.0	91.0
1.4	400	10.3	380	97.0	88.8
1.5	600	10.3	380	98.9	90.2
1.6	800	10.3	380	99.0	90.9

catalysts show maximum conversions at 10.3 MPa within the range investigated. Table 4.6 further shows that, with Sono 3/11.5, an increase in G/L from 400 to 800 mL/mL does not lead to a significant increase in S conversion (97.6 to 98.4 wt %) but does result in an appreciable increase in N conversion (83.9 to 87.6 wt %). This indicates that this catalyst shows maximum conversion for G/L at 800 mL/mL. So, the best reaction conditions within the range studied for Sono 3/11.5 are: Temperature = 380 °C, Pressure = 10.3 MPa, LHSV ~ 1.5 h^{-1} and G/L = 800 mL/mL. It can be seen that Imp 3/10 shows S and N conversion (98.9 and 90.9 wt %, respectively) at these reaction conditions, which are the maximum conversions shown by this catalyst. So, it can be seen that Imp 3/10 shows better performances than Sono 3/11.5 within the range of studied reaction parameters.

4.4 Kinetic Studies

The two catalysts were investigated in detail for kinetic analysis. The data obtained from performance studies with Sono 3/11.5 (see Table C.1, Appendix C) and Imp 3/10 (see Table D.1, Appendix D) were used to examine the external and internal mass transfer resistances.

4.4.1 External Resistances for HDS and HDN Reactions

The influence of external mass transfer was evaluated on HDS and HDN of LGO. The Satterfield's criterion (1969) (see Equation e.1, Appendix E), which compares the rate of diffusion of hydrogen from bulk phase to the catalyst surface with its rate of reaction in the catalyst pellet, was used for checking whether the mass transfer of hydrogen was the limiting factor in the reaction set up (see Appendix E for detail calculation procedure). As per the literature (Hoffman et al. 1996), the value of left side

of the criterion should be at least 10 times larger than the value of right side for it to conclude that the mass transfer is dominant in the reaction set up. However, the calculated value of left side of the criterion was only 4 times of that of the right side. This indicates that the HDS reaction may not be limited by mass transfer of hydrogen from bulk gas phase to the catalyst pellet external surface (see Table E.1, Appendix E). It can also be seen from the table E.1 that the value of right hand side of the criterion is 25 times larger than the left hand side for HDN and thus clearly indicates that HDN is not limited by mass transfer of hydrogen from bulk gas phase to the catalyst pellet external surface.

4.4.2 Internal Resistances for HDS and HDN Reactions

Pore diffusion resistances were evaluated for HDS and HDN reactions at different reaction conditions. A calculation for β (defined as the ratio of maximum temperature difference that could exist between the catalyst pellet core and the catalyst pellet surface temperature: Fogler, 1998) was done to estimate the temperature increase in the catalyst pellet due to the reaction. A value of zero for β indicates that the pellet core temperature is equal to the surface temperature and no temperature gradient exists in the catalyst pellet. The calculation showed a value of β as 0.00009 which indicated that catalyst pellet core was 0.06 °C hotter than its external surface (see Table F.1, Appendix F). This implied that the catalyst pellet could be assumed isothermal.

For further ensuring the isothermality of catalyst pellet, Anderson's criterion (1963), which compares the rate of heat generation from the reaction inside the catalyst pellet with the rate of heat removal by conduction and convection, was also used (see Equation f.8, Appendix F). This criterion also indicated that catalyst pellet could be assumed isothermal for pore diffusion resistance analysis. The calculations for β and

Anderson's criterion were done for HDS only as the concentration of sulfur species in LGO feed was much higher (15950 ppmw) than the concentration of nitrogen species (209 ppmw) and bulk of the heat of reaction was expected to be contributed from HDS.

Thiele modulus couldn't be used in the pore diffusion resistance analysis as it required the information about intrinsic rates of reactions and the values of reaction rates obtained from the S and N conversion data were overall in nature. So, from the literature, another dimensionless modulus (Φ) was used which was based on global rate of reaction (Satterfield, 1970). The values of Φ's were calculated using the rates for conversion of sulfur and nitrogen species as their calculated bulk diffusivities (see Table E.1 in Appendix E) were found to an order of magnitude lower than the diffusivity of hydrogen in gas oil. Tables 4.8 and 4.9 show the calculated values of dimensionless modulus (Φs) for HDS reactions with Sono 3/11.5 and Imp 3/10 (see Equation f.9, Appendix F). These values have been calculated assuming that the values of effective diffusivity of sulfur species present in LGO are the same for both the catalysts and are equal to the diffusivity of average gas oil molecules. Both the tables indicate lower values of Φs at lower reaction temperatures and show increased values with an increase in reaction temperature. For example, Sono 3/11.5 shows a value of Φs as 3.4 at 340 °C which increases to 37.9 as the temperature is increased to 380 °C. Similarly, Imp 3/10 shows a value of Φs as 5.6 at 340 °C which increases to 71.7 with an increase in reaction temperature to 380 °C. Since the values of effectiveness factors are inversely related to Φs in higher modulus zone, it indicates a decrease in effectiveness factor with an increase in reaction temperature. For a first order isothermal reaction in spherical particles, the value of effectiveness factor ranges from 0.7 (for Φs ~ 5) to 0.2 (for Φs ~ 45) (Satterfield,

Table 4.8: Calculated dimensionless moduli for HDS of LGO with Sono 3/11.5.

LHSV, h^{-1}	Hydrogen gas/Gas oil, mL/mL	Pressure, MPa	Temperature, °C	Effective diffusivity of S compounds, cm^2/s	S Concentration, gmol/cc	Rate S conversion, gmol S/s-cc Cat.	Dimensionless modulus, Φs
1.5	600	8.9	340	4.11E-06	6.16E-05	1.76E-07	5.0
2.0	600	8.9	340	4.11E-06	1.05E-04	2.04E-07	3.4
2.5	600	8.9	340	4.11E-06	1.02E-04	2.62E-07	4.5
1.5	600	8.9	360	4.65E-06	2.44E-05	2.01E-07	12.8
1.9	600	8.9	360	4.65E-06	4.99E-05	2.38E-07	7.4
2.5	600	8.9	360	4.65E-06	5.06E-05	3.12E-07	9.6
1.4	600	8.9	380	5.22E-06	7.49E-06	2.05E-07	37.9
2.0	600	8.9	380	5.22E-06	1.19E-05	2.83E-07	32.9
2.5	600	8.9	380	5.22E-06	2.10E-05	3.43E-07	22.6
1.5	800	10.3	380	5.22E-06	5.75E-06	2.14E-07	51.4

Table 4.9: Calculated dimensionless moduli for HDS of LGO with Imp 3/10.

LHSV, h^{-1}	Hydrogen gas/Gas oil, mL/mL	Pressure, MPa	Temperature, °C	Effective diffusivity of gas oil, cm^2/s	S Concentration, gmol/cc	Rate S conversion, gmol S/s-cc Cat.	Dimensionless modulus, Φs
1.5	600	8.9	340	4.11E-06	4.38E-05	1.88E-07	7.5
2.0	600	8.9	340	4.11E-06	7.18E-05	2.30E-07	5.6
2.6	600	8.9	340	4.11E-06	8.02E-05	2.88E-07	6.3
1.5	600	8.9	360	4.65E-06	1.51E-05	2.05E-07	21.1
2.0	600	8.9	360	4.65E-06	2.79E-05	2.66E-07	14.8
2.5	600	8.9	360	4.65E-06	3.60E-05	3.27E-07	14.1
1.5	600	8.9	380	5.22E-06	4.09E-06	2.12E-07	71.7
2.0	600	8.9	380	5.22E-06	8.25E-06	2.83E-07	47.5
2.5	600	8.9	380	5.22E-06	1.11E-05	3.51E-07	43.9

1970). This indicates that at lower reaction temperatures (from 340 to 360 °C) the global rate of reaction is governed by both diffusional resistance and surface reaction (Satterfield, 1970), but as the reaction temperature is increased, the rate of surface reaction increases faster (following the Arrhenius rate law) than the rate of diffusion (following linear behavior with temperature, as shown by Wilke Chang equation, 1955) and the overall rate of HDS of LGO becomes more controlled by pore diffusion resistance. This also shows that the rate expression derived for HDS is apparent rate and represents the overall rate of reaction.

Tables 4.10 and 4.11 show the values of dimensional modulus (Φ_N) for HDN of LGO with Sono 3/11.5 and Imp 3/10. These values have been calculated assuming the effective diffusivity being same for sulfur and nitrogen compounds present in gas oil. It is interesting to see that the values of Φ_N are much lower for HDN than those for HDS. For example, Sono 3/11.5 shows a value of Φ_N as 0.2 at 340 °C which increases to 3.9 as the temperature is increased to 380 °C. Similarly, Imp 3/10 shows a value of Φ_N as 0.4 at 340 °C which increases to 6.1 as the temperature is increased to 380 °C. Based on the values of dimensionless modulii, it can be said that the HDN of LGO is not limited by pore diffusion resistance and the rate expression for HDN can be assumed to be intrinsic as against with HDS. A similar result was obtained by Van Zoonen and Douwes (1963), who studied the HDS and HDN of straight run gas oil on 3x3 mm pellets of Co (3 wt %) –Mo (10.4 wt %)/γ-Al_2O_3 catalyst at 3.4 MPa pressure and 375 °C.

It is interesting to observe that though both the catalysts show similar trends for dimensionless moduli for HDS and HDN of LGO but Sono 3/11.5 always displays lower values of the same than Imp 3/10. It indicates that Imp 3/10, despite being more limited

Table 4.10: Calculated dimensionless moduli for HDN of LGO with Sono 3/11.5.

LHSV, h^{-1}	Hydrogen gas/Gas oil, mL/mL	Pressure, MPa	Temperature, °C	Effective diffusivity of N compounds, cm^2/s	N Concentration, gmol/cc	Rate N conversion, gmol S/s-cc Cat.	Dimensionless modulus, Φ_N
1.5	600	8.9	340	4.11E-06	9.08E-06	8.90E-10	0.2
2.0	600	8.9	340	4.11E-06	8.51E-06	1.68E-09	0.3
2.5	600	8.9	340	4.11E-06	9.21E-06	1.41E-09	0.3
1.5	600	8.9	360	4.65E-06	5.67E-06	2.99E-09	0.8
1.9	600	8.9	360	4.65E-06	6.25E-06	3.39E-09	0.8
2.5	600	8.9	360	4.65E-06	7.42E-06	3.24E-09	0.7
1.4	600	8.9	380	5.22E-06	1.86E-06	5.19E-09	3.9
2.0	600	8.9	380	5.22E-06	4.15E-06	5.34E-09	1.8
2.5	600	8.9	380	5.22E-06	5.51E-06	5.23E-09	1.3
1.5	800	10.3	380	5.22E-06	2.72E-06	4.96E-09	2.5

Table 4.11: Calculated dimensionless moduli for HDN of LGO with Imp 3/10.

LHSV, h^{-1}	Hydrogen gas/Gas oil, mL/mL	Pressure, MPa	Temperature, °C	Effective diffusivity of N compounds, cm^2/s	N Concentration, gmol/cc	Rate N conversion, gmol S/s-cc Cat.	Dimensionless modulus, Φ_N
1.5	600	8.9	340	4.11E-06	6.93E-06	2.30E-09	0.6
2.0	600	8.9	340	4.11E-06	8.04E-06	2.20E-09	0.5
2.6	600	8.9	340	4.11E-06	8.72E-06	2.12E-09	0.4
1.5	600	8.9	360	4.65E-06	3.98E-06	4.05E-09	1.6
2.0	600	8.9	360	4.65E-06	5.64E-06	4.09E-09	1.1
2.5	600	8.9	360	4.65E-06	6.83E-06	3.94E-09	0.9
1.5	600	8.9	380	5.22E-06	1.29E-06	5.67E-09	6.1
2.0	600	8.9	380	5.22E-06	2.45E-06	6.71E-09	3.8
2.5	600	8.9	380	5.22E-06	3.64E-06	7.17E-09	2.7

by pore diffusion resistance than Sono 3/11.5, shows higher sulfur and nitrogen conversions.

4.4.3 Hydrodesulphurization and Hydrodenitrogenation Rate Kinetics

The rate models were developed based on following assumptions:

1. The HDS and HDN are irreversible.
2. The rate equations follow the Power Law and the Langmuir – Hinshelwood model.
3. The effect of hydrocracking on HDS and HDN reactions is negligible.

The rate expressions for HDS and HDN were fitted using non linear regression analysis. The values of activation energy and pre-exponential constant for HDS and HDN reactions with the two catalysts were evaluated using linear regression analysis. All the regression analyses were done using POLYMATH™ software. Different models were tested for HDS and HDN reactions (see Appendix G and H). The best fit for HDS rate expression was obtained with Power Law model ($0.9<R^2<0.95$). None of the tested Langmuir – Hinshelwood models gave a fit with reasonable accuracy for HDS (As shown in Tables G.1 and H.1 in Appendices G and H, respectively). The best fit for HDN model was obtained with a Langmuir-Hinshelwood type model ($0.9<R^2<0.95$). A power law model for HDN gave negative values of order of reaction at 340 °C and was thus discarded (As shown in Figures G.2 and H.2 in Appendices G and H, respectively).

4.4.3.1 Hydrodesulphurization Reaction kinetics

The HDS process was fitted with a Power Law model and the reaction was proposed to follow the form:

$$\text{R-S} \xrightarrow{k_{hds}} \text{Product}$$

The rate expression for Power Law model can be written as:

$$r_{hds} = -\frac{dC_S}{dt} = k_{hds}.C_S^n \qquad (4.3)$$

Where r_{hds} is the rate of HDS reaction, k_{hds} is the apparent reaction rate constant for HDS and C_s is the concentration of sulfur species. The values of r_{hds} are calculated using Equation b.3 in Appendix B. The values of k_{hds} and n were evaluated using non-linear regression analysis. The analyses show that n = 0.57 gives the best fit for the experimental data and consequently the best order of reaction. Data with both the catalysts could be fitted with reasonable accuracy ($0.9<R^2<0.95$). Table 4.12 along with Figures 4.31 and 4.32 shows the kinetic data for the parameters obtained from the analysis. It can be seen that the rate constant with Sono 3/11.5 are lower than the rate constants with Imp 3/10 indicating lower activity for HDS of LGO. A similar trend can be observed with apparent activation energy as well.

4.4.3.2 Hydrodenitrogenation Reation Kinetics

The HDN process was fitted with a Langmuir - Hinshelwood model with an inhibition term for sulfur species. The HDN reaction can be assumed to follow the form:

$$\text{R-N} \xrightarrow{k_{hdn}} \text{Product} + NH_3$$

The rate expression can be written as:

$$r_{hdn} = -\frac{dC_N}{dt} = \frac{k_{hdn}.C_N^n}{(1 + K_{hds}.C_S)^m} \qquad (4.5)$$

Table 4.12: Apparent kinetic parameters for hydrodesulphurization process using power law model.

Temperature, °C	Apparent rate constant, k_{hds} $(gmol^{0.43}\text{-}m^{1.71})/s\text{-}kg$ cat.	
	Imp 3/10	Sono 3/11.5
340	$(2.32 \pm 0.136)x10^{-5}$	$(2.00 \pm 0.137)x10^{-5}$
360	$(4.67 \pm 0.249)x10^{-5}$	$(3.70 \pm 0.249)x10^{-5}$
380	$(9.48 \pm 0.929)x10^{-5}$	$(7.04 \pm 0.549)x10^{-5}$
HDS Apparent Energy of Activation, kJ/kmol		
Sono 3/11.5	12.6	
Imp 3/10	14.1	

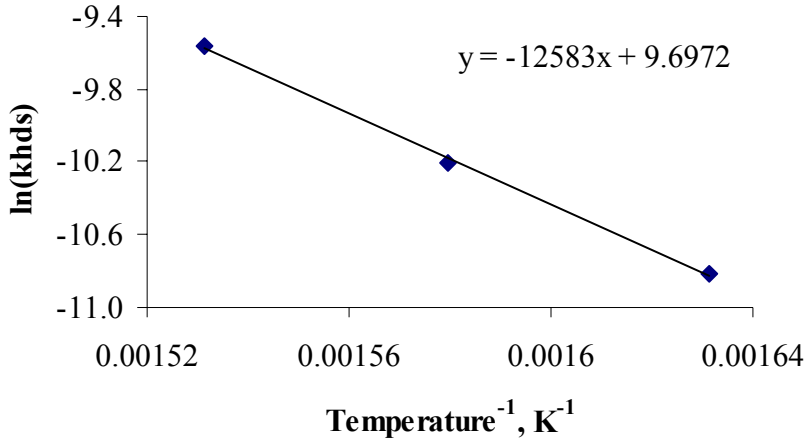

Figure 4.31: Arrhenius plot for HDS of LGO with Sono 3/11.5.

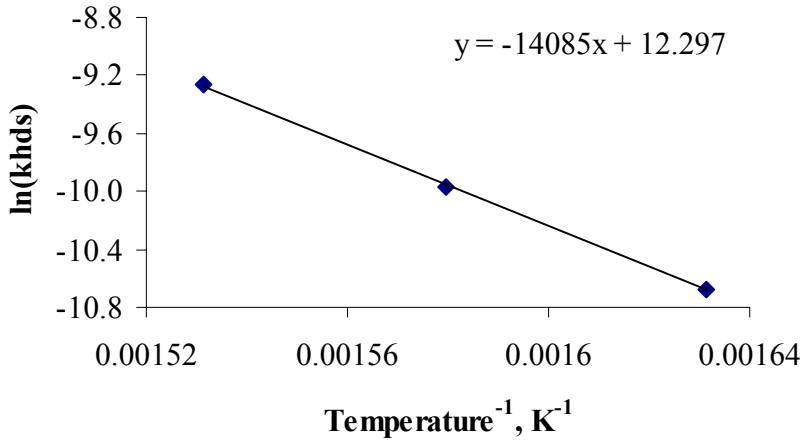

Figure 4.32: Arrhenius plot for HDS of LGO with imp 3/10.

Where, k_{hdn} is the rate constant and K_{hds} is the adsorption equilibrium constant for sulfur species in LGO. Above rate expression was fitted to the data obtained with Sono 3/11.5 and Imp 3/10 with reasonable accuracy ($0.9<R^2<0.95$).

Table 4.13 shows the values of the kinetic parameters obtained for Imp 3/10. Figures 4.33 and 4.34 show the Arrhenius and Van't Hoff plots for HDN with Imp 3/10, respectively. Table 4.14 shows the kinetic parameters from 340 to 380 °C for Sono3/11.5. Figures 4.35 and 4.36 show the Arrhenius and Van't Hoff plots for HDN with Sono 3/11.5. Tables 4.13 and 4.14 indicate that reaction kinetics for HDN of LGO over the two catalysts can be adequately explained using Langmuir-Hinshelwood model in the analyzed range of reaction temperature. It is noteworthy to recall that the analysis in section 4.4.2 indicated that pore diffusion resistance could be neglected for HDN with Imp 3/10 and Sono 3/11.5. This indicates that the fitted kinetic expressions can be assumed to be intrinsic and shows that the HDN of LGO within the existing reaction setup proceeds through a dual site mechanism and is inhibited by adsorption of sulfur species which compete for the same catalytic sites for conversion as HDN.

4.5 Characterization of Spent Catalysts

Selected spent catalysts were characterized with thermogravimetry and BET surface area analyses. Imp 3/7, Imp 3/10, Imp 3.1/12.2, Sono 3/8, Sono 2.8/10 and Sono 3/11.5 were selected for post reaction characterization.

4.5.1 Thermogravimetry Analysis

Selected spent catalysts were tested with thermogravimetry with air. Figures 4.37 and 4.38 indicate the TGA plots with sonochemically prepared and impregnated catalysts. It can be seen that both the figures indicate a broad peak at 450 °C which can

Table 4.13: Apparent kinetic parameters for Langmuir - Hinshelwood model for HDN of LGO with Imp 3/10.

Temperature, °C	Rate constant, k_{hdn}, $(gmol\text{-}m^3)^{0.5}/s\text{-}kg\ cat$	Adsorption equilibrium constant, K_{hds}, $m^3/gmol$
340	$(2.62 \pm 0.177)x10^{-6}$	0.09325 ± 0.007
360	$(3.80 \pm 0.294)x10^{-6}$	0.0734 ± 0.010
380	$(6.46 \pm 0.534)x10^{-6}$	0.0664 ± 0.018
	n	0.5
	m	2.0
HDN energy of activation, kJ/mol		9.0
HDS heat of adsorption, kJ/mol		3.4

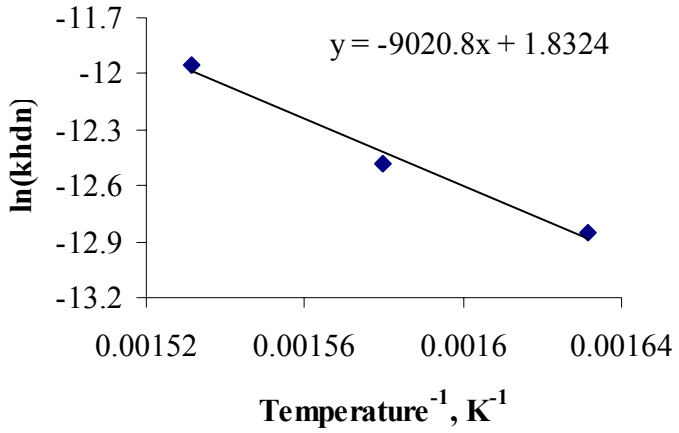

Figure 4.33: Arrhenius plot for HDN of LGO with Imp 3/10.

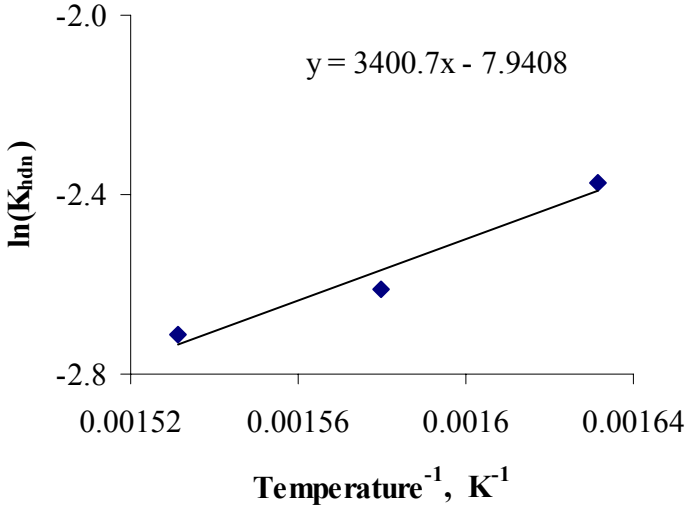

Figure 4.34: Van't Hoff plots for HDN of LGO with Imp 3/10.

Table 4.14: Apparent kinetic parameters for Langmuir-Hinshelwood model for HDN of LGO with Sono 3/11.5.

Temperature, °C	Rate constant, k_{hdn}, $(gmol)^{0.6}$-$m^{1.2}$/s-kg cat	Adsorption equilibrium constant, K_{hds}, m^3/gmol
340	$(1.37 \pm 0.941)x10^{-6}$	$(4.78 \pm 1.09)x10^{-3}$
360	$(1.70 \pm 0.240)x10^{-6}$	$(1.85 \pm 1.08)x10^{-3}$
380	$(6.21e \pm 0.0931)x10^{-6}$	$(1.00 \pm 0.10)x10^{-3}$
	n	0.4
	m	2.0
HDN energy of activation, kJ/mol		15.0
HDN heat of adsorption, kJ/mol		15.7

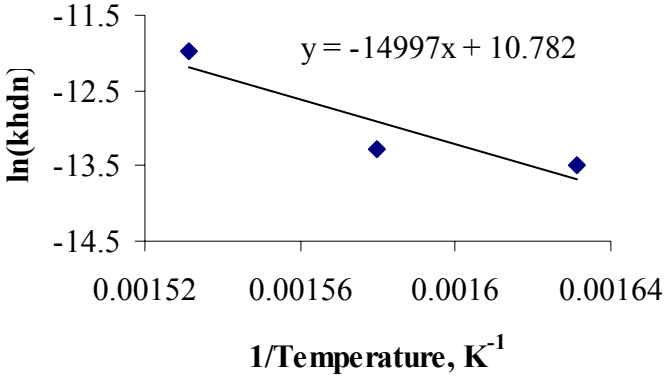

Figure 4.35: Arrhenius plot for HDN of LGO with Sono 3/11.5.

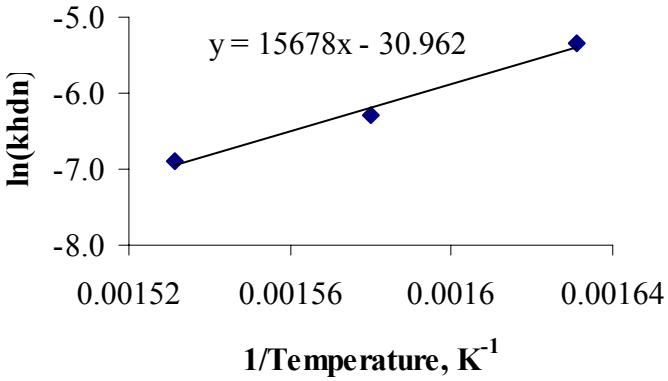

Figure 4.36: Van't Hoff plots for HDN of LGO with Sono 3/11.5.

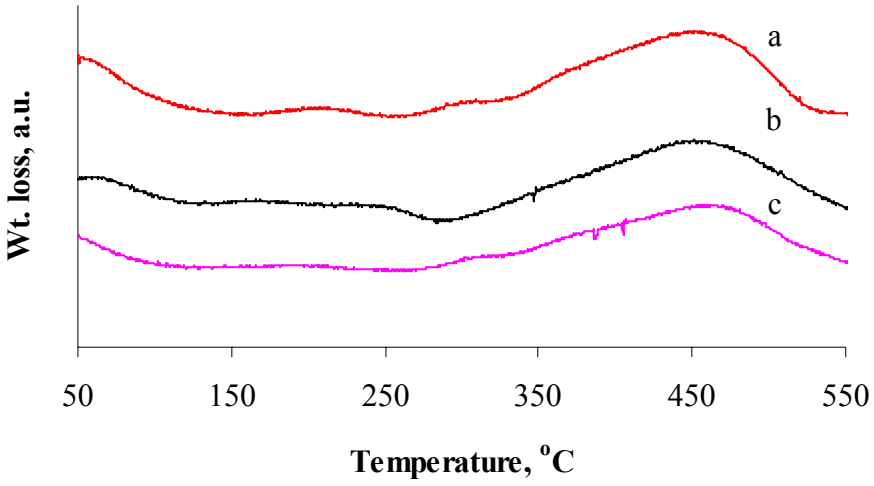

Figure 4.37: Thermogravimetry plots for spent sonochemical catalysts. (a) Sono 3/8; (b) Sono 2.8/11; (c) Sono 3/11.5.

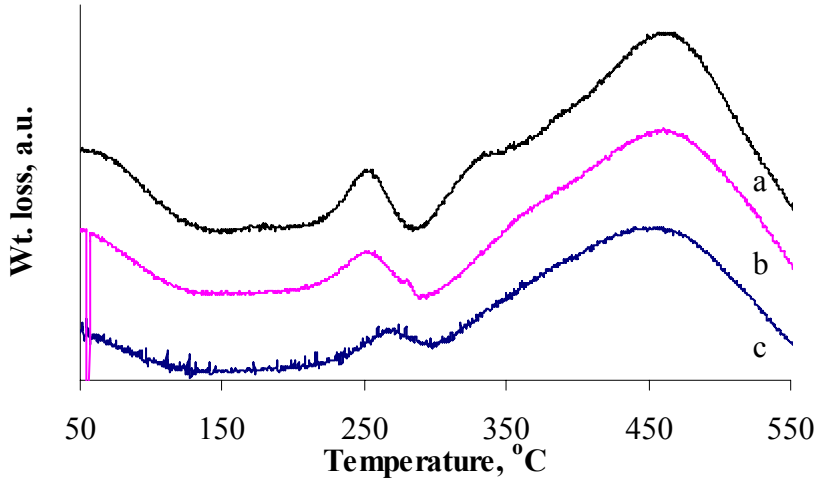

Figure 4.38: Thermogravimetry plots for spent impregnated catalysts. (a) Imp 3/7; (b) Imp 3/10; (c) Imp 3.1/12.2.

temperature range from 350 to 550 °C. It can be seen that impregnated catalysts show more weight loss in this temperature range indicating more deposition of carbonaceous be assigned to the presence of carbon species on the catalysts. The presence of these species can be responsible for reduction in surface area and pore volumes of the catalysts. Table 4.15 shows the weight losses displayed by different spent catalysts over the It is interesting to recall from screening studies that impregnated catalysts showed better S and N conversions than sonochemically preapared catalysts. This indicates that more deposition of carbonaceous material on impregnated catalysts may be due to higher HDS and HDN activities of these catalysts.

4.5.2 BET Surface Area Analysis

Table 4.16 shows the results of BET analysis done on spent catalysts. It can be seen from the table that all the spent catalysts indicate a reduction in BET surface area and total pore volume. This reduction in BET surface area and total pore volume can be attributed to the blockage of pores from carbonaceous deposits as indicated by thermogravimetry analysis and/or sintering of pores of catalysts from during the course of the reaction.

Table 4.15: Thermogravimetry with air - Weight losses shown by selected spent catalysts in the temperature range from 350 to 550 °C.

Catalyst	Initial weight, µg	Final weight, µg	% wt. loss
Sono 3/8	24529	22887	6.7
Sono 2.8/11	21262	19770	7.0
Sono 3.1/11.5	26327	24266	7.8
Imp 3/7	20994	19039	9.3
Imp 3/10	28447	25687	9.7
Imp 3/11.5	33267	30084	9.6

Table 4.16: BET surface area and adsorption pore volume analysis of selected spent catalysts.

Catalyst	BET surface area, m^2/g		Total pore volume, cc/g	
	Fresh	Spent	Fresh	Spent
Sono 3/8	188	156	0.51	0.39
Sono 2.8/11	185	150	0.53	0.36
Sono 3/11.5	177	146	0.54	0.36
Imp 3/7	183	154	0.52	0.34
Imp 3/10	186	158	0.53	0.37
Imp 3.1/12.2	183	151	0.50	0.33

5 CONCLUSIONS AND RECOMMENDATIONS

5.1 Conclusions

This study showed that impregnated catalyst outperformed sonochemically synthesized catalysts for HDS and HDN of LGO at all the reaction conditions. Various phases of work gave various conclusions as summarized below.

Phase 1: Catalysts Preparation and their Characterization

- Sonochemical method of synthesis of Co-W/γ-Al_2O_3 catalysts leads to relatively larger reduction in surface area (from 200 to 164 m^2/g) as compared to the impregnation method (from 200 to 183 m^2/g). The sonochemically prepared catalysts also show lower crystallinity of support than those prepared using impregnation method.
- Both impregnated and sonochemically prepared catalysts show generation of intermediate temperature acid centres which increase in intensity with an increase in total metal loading.
- Impregnated Co-W/γ-Al_2O_3 catalysts indicate a lesser formation of bulk type of cobalt oxide species than the corresponding sonochemically prepared catalysts.
- All sonochemically synthesized catalysts show that the tungsten metal is segregated near the surface of the catalyst whereas impregnated catalysts indicate that same is uniformly distributed throughout the bulk of the catalysts.

Phase 2: Catalyst Performance test with Light Gas Oil

- Impregnated Co(3 wt %)-W(10 wt %)/ γ-Al_2O_3 catalyst shows maximum activity for HDS (with conversion at 93.0 wt %) and HDN (with conversion at 57.1 wt %) of LGO at a pressure of 8.9 MPa, LHSV ~ 2 h^{-1}, hydrogen gas/gas oil =

600mL/mL and reaction temperature of 340-360 °C. A further increase in W loading to 12.2 wt % did not lead to any significant change in its activity.

- Sonochemically prepared catalysts indicate a maximum activity for HDS (with conversion at 87.9 wt %) and HDN (with conversion at 42.5 wt %) of LGO for Co(3 wt %)-W(11.5 wt %)/γ-Al_2O_3 and a further increase in Co loading to 4 wt % and W loading to 15.4 wt % leads to drastic reduction in its HDS activity (conversion at 57.9 wt %). However, this doesn't lead to any significant change in HDN activity.

Phase 3: Performance, Optimization and Kinetic Studies with Light Gas Oil

- The HDS of LGO over impregnated Co(3 wt %)-W(10 wt %)/γ-Al_2O_3 and sonochemical Co(3 wt %)-W(11.5 wt %)/γ-Al_2O_3 can be best represented using a Power Law model. Also, the HDS over the two catalysts is limited by pore diffusion resistances under the existing reaction conditions and the HDS energy of activation of over these catalysts are 14 and 12 kJ/kmol, respectively.
- The HDN of LGO over impregnated Co(3 wt %)-W(10 wt %)/ γ-Al_2O_3 and sonochemical Co(3 wt %)-W(11.5 wt %)/ γ-Al_2O_3 can be best represented using a Langmuir – Hinshelwood type model. Also, the HDN is not limited by pore diffusion resistance and the fitted model could be assumed to be representative of surface reaction indicating that HDN is inhibited by adsorption of sulfur species.

5.2 Recommendations:

From the experimental work and results obtained, the following recommendations are made.

- The HDS and HDN activity tests should be carried out using model compounds to investigate the effects of inhibition effects on the performance of tested catalysts.
- The sonochemically synthesized catalysts should be prepared using different metal precursors and their performances be compared for HDS and HDN.
- The sonochemical method of synthesis of catalysts should be tested with different catalytic metal combinations such as Ni-W and their performances be compared for HDS and HDN.
- The activity tests should be carried out with different sizes of catalyst particles to verify the calculated pore diffusion resistances and to indicate the catalyst pellet size required for their elimination.

6 LIST OF REFERENCES

Alvarez A., Escobar J., Toledo J.A., Perez V., Cortes M. A., Rivera E., "HDS of gas oil at different nitrogen content: comparison between different reaction systems", Fuel, Article in Press, 2006

Anderson J. B., "Criterion for isothermal behavior of a catalyst pellet", Chemical Engineering Science, 147-148, 18, 1963

Aoyagi K., McCaffrey W. C., Gray M.R., "Kinetics of hydrocracking and hydrotreating of coker and oilsands gas oils", Petroleum Science and Technology, 997-1015, 21(5 & 6), 2003

Arnoldy P., Van den H. J. A. M., De B.G.D., Moulijn J.A., "Temperature programmed sulfiding of molybdenum(VI) oxide/alumina catalysts", Journal of Catalysis, 35-40, 92, 1985

Bej S. K., Dalai A. K., Adjaye J., "Kinetics of hydrodesulfurization of heavy gas oil derived from oil-sands bitumen" Petroleum Science and Technology, 867-877, 20 (7 & 8), 2002.

Botchwey C., Dalai A.K., Adjaye J., "Two-stage hydrotreating of Athabasca heavy gas oil with interstage hydrogen sulfide removal: Effect of process conditions and kinetic analyses", Industrial and Engineering Chemistry Research, 5854-5861, 43(18), 2004

Breysse M., Djega M., Gerald P., Stephanie G., Christophe V., Michel P.G., Lemaire M., "Deep desulfurization: reactions, catalysts and technological challenges", Catalysis Today, 129-138, 84(3-4), 2003

Brito A., Arvelo R., Gonzalez. A.R., Borges M.E., Fierro J.L.G., "Variation in structural characteristics of a hydrotreatment catalyst with deactivation/regeneration cycles", Industrial and Engineering Chemistry Research, 374-380, 2, 1998

Callejas M.A., Martinez M.T., "Hydroprocessing of maya residue: intrinsic kinetics of sulfur nitrogen and vanadium removal reactions", Energy and Fuels, 629-636,13, 1999

Canada Gazette, Sulfur in Diesel Fuel Regulations, 2002

Chen J., Ring Z., "HDS reactivities of dibenzothiophenic compounds in a LC-finer LGO and H_2S/NH_3 inhibition effect", Fuel, 305-313, 83(3), 2004

Clausen B.S., Massoth F.E., Topsoe H., "Catalysis - Science and Technology", PRODUserv Springer Produktions – Gesellschaft, Berlin, 77, 1996

Daage M., Chianelli R.R., "Structure-function relations in Molybdenum sulfide catalysts: The rim edge model", Journal of Catalysis, 414-427, 149, 1994

Delmon B., "A new hypothesis explaining synergy between two phases in heterogeneous catalysis. The case of hydrodesulfurization catalysts", Bulletin des Societes Chimiques Belges, 979-987, 88(12), 1979

Dhas N.A., Ekhtiarzadeh A., Suslick K.S., "Sonochemical preparation of supported hydrodesulfurization catalysts", Journal of American chemical society, 8310-8316, 123 (34), 2001

Fogler S.H., "Elements of chemical reaction engineering", Prentice Hall PTR, 3rd edition, 752, 1998

Froment G. F., Van P., Ignace A., Hosten L. H., "1. Kinetics of the hydrodesulfurization on a cobalt-molybdenum/alumina catalyst. 2. Kinetics of the hydrogenolysis of

benzothiophene", Industrial & Engineering Chemistry Product Research and Development, 437-443, 25(3), 1986

Gates B.C., Katzar J.R., Schuit G.C.A., "Chemistry of catalytic processes", McGraw-Hill, New York, 1979

Girgis M.J., Gates B.C., "Reactivities, reaction networks and kinetics in high pressure catalytic hydroprocessing", Industrial and Engineering Chemistry Research, 2021-2058, 30, 1991

Gray M.R., Jokuty H., Yeniova L.,Nazarewycz, Wnke S.E., "The relationship between chemical structure and reactivity of Alberta bitumen and heavy oils", Canadian Journal of Chemical Engineering, 833-843, 69, 1994

Gusta E., Sundaramurthy V., Dalai A.K., Adjaye J., "Hydrotreating of heavy gas oil derived from Athabasca Bitumen over Co-Mo/ γ -Al2O3 catalyst prepared by sonochemical method", Topics in Catalysis, 147-153, 37(2-4), 2006

Herrera, J.E., Resasco D.E., "Role of Co-W interaction in the selective growth of single-salled carbon nanotubes from CO disproportionation", Journal of Physical Chemistry B, 3738-3746, 107(16), 2003

Ho T.C., "Hydrogenation Catalysis", 30(1), 1988

Kabe T., AoyamaY., Wang D., Ishiara A., Qian W., Hosoya M., Zhang Q., "Effects of H_2S on hydrodesulphurization of DBT and 4,6 DMDBT on alumina supported Ni-Mo and NiW catalysts", Applied Catalysis A, 237-247, 209, 2001

Kadkhodayan A., Brenner A., "Temperature programmed reduction and oxidation of metals supported on γ-Alumina", Journal of Catalysis, 311-321,117, 1989

Knudsen K.G., Cooper B. H., Topsoe H., "Catalyst and process technologies for ultra-low sulfur diesel fuel", Applied Catalysis, A: General, 205-215, 89(2), 1999

Landau M.V., Vradman L., Herkowitz M., Koltypin Y., Gedanken A., "Ultrasonically controlled deposition-precipitation", Journal of Catalysis, 22-36, 201(1), 2001

Lee J.J., Heeyeon K., Sang H.M., "Preparation of highly loaded, dispersed MoS_2/Al_2O_3 catalysts for the deep desulphurization for dibenzothiophenes", Applied Catalysis B: Environmental, 171-180, 41, 2003

Leglise J.,Gestel V., Duchet J.C., "Evidence of H_2S active species in the mechanism of thiophene hydrodesulphurization", Hydrotreating Technology for Pollution Control, Marcel Dekker, New York, 197-209, 1996

Lewandowski M., Sarbak Z., "The effect of boron addition of hydrodesulphurization and hydrodenitrogenation activity of $NiMo.Al_2O_3$ catalysts", Fuel, 487-495, 79(5), 2000

Lynch J., "Physico-Chemical Analysis of Industrial Catalysts, A practical Guide to Characterization", 7-8, Editions TECHNIP 27 rue Ginoux, 75737 PARIS Cedex 15, FRANCE, 2003

Ma X., Sakanishi K., Mochida I., "Hydrodesulphurization reactivities of various sulfur compounds in diesel fuels", Industrial and Engineering Chemistry Research, 218-222, 33, 1994c

Mahajan D., Marshall C.L., Castagnola N., Hanson J.C., "Sono synthesis and characterization of nano-phase molybdenum-based materials for catalytic hydrodesulfurization", Applied Catalysis, A: General, 83-91, 258(1), 2004

Marroquin G., Ancheyta J., Diaz J.A.I., "On the effect of reaction conditions on liquid phase sulfiding of a NiMo based catalysts", Catalysis Today, 75-81, 98, 2004

Martin C., Solana G., Malet P., Rives V., "Nb_2O_5-supported WO_3: a comparative study with WO_3/Al_2O_3", Catalysis Today, 365-376, 78(1-4), 2003

Mauchausse C., Kural E., Trimm D. L., Cant N. W., "Optimization of tungsten -based catalysts for the hydrotreatment of coal - derived liquids", Fuel, 203-209, 71(2), 1992

Satterfield C. N., Pelossof A. A., Sherwood T. K., "Mass transfer limitations in trickle bed reactor", AIChE Journal, 224-226, 15(2), 1969

Satterfield C. N., Modell M., Mayer J. F., "Interactions between catalytic hydrodesulfurization of thiophene and hydrodenitrogenation of pyridine", AIChE Journal, 1100-1107, 21(6), 1975

Satterfield C. N., Yang S. H., "Simultaneous hydrodenitrogenation and hydrodeoxygenation of model compounds in trickle bed reactor", Journal of Catalysis, 335-346, 81(2), 1983

Satterfield C. N., "Heterogeneous Catalysis in Industrial Practice, 2nd Ed.", 554, 1991

Schuit G.C.A., Gates B.C., "Chemistry and engineering of catalytic hydrodesulphurization of gas oils", AIChe Journal, 417-438, 19, 1973

Shi L., Tin K. C., Wong N. B., Li, C. L., "Hydrodesulfurization of petroleum" Petroleum Science and Technology, 519-533,17(5 & 6), 1999

Sie S.T., "Reaction order and role of H_2S sulfide in deep hydrodesulphurization of gas oils: consequence of industrial reactor configuration", Fuel processing Technology, 149-171, 61, 1999

Singhal G.H., Espino R.L., Sobel J.E., "Hydrodesulphurization of sulfur heterocyclic compounds, reaction mechanisms", Journal of Catalysis, 4460-4466, 67, 1981

Speight J.G., "The Desulfurization of Heavy Oils and Residua", Marcel Dekker Inc., New York, 2000

Steiner P., Blekkan E.A., "Catalytic hydrodesulphurization of light gas oil a over Ni-Mo catalyst", Fuel Processing Technology,1-12, 79, 2002

Sun M., Burgi T., Cattane R., Langeveld D.V., Prins R.,"TPS,XPS and QEXAFS investigation of the sulfidation of NiW/Al2O3-F catalysts", Journal of Catalysis, 258-269, 201(2), 2001

Suslick K. S., "Sonochemistry: a physical perspective", AIP Conference Proceedings, (Nonlinear Acoustics at the Turn of the Millennium), America Institute of Physics, New York, 95-104, 524 (1), 2000

Suvanto M., Raty J., Pakkanen A.T., "Catalytic activity of carbonyl precursor based CoW/Al2O3 catalysts in hydrodesulfurization of thiophene", Applied Catalysis A, 189-199, 181,1999

Texier S., Berhault G., Perot G., Diehl F., "Activation of alumina supported hydrotreating catalysts by organosulfide or H_2S: Effect of H_2S partial pressure used during the activation process", Applied catalysis A, 105-119, 293, 2005

Topsoe H., Candia R., Topsoe N.Y., Clausen B. S., "On the state of the cobalt-molybdenum-sulfur model", Bulletin des Societes Chimiques Belges, 783-806, 93(8-9), 1984

Trytten L. C., Gray M. R., Sanford E.C., "Hydroprocessing of narrow-boiling gas oil fractions: dependence of reaction kinetics on molecular weight", Industrial and Engineering Chemistry Research, 725-730, 29(5), 1990

Van Veen J.A.R., Coljin H.A., Hendriks P.A.J.M., Welsenes V.A.J.,"On the formation of type I and type II nickel molybdenum sulfide phases in nickel molybdenum/alumina hydrotreating catalysts and its catalytic implications", Fuel Processing Technology, 137-144, 35,1993

Voorhoeve R.J.H., "Electron spin resonance study of active centers in nickel tungsten sulfide hydrogenation catalyst", Journal of Catalysis, 236-242, 23, 1971

Whitehurst D.D., Takaaki I., Mochida I., "Present state of art and future challenges in hydrodesulphurization of polyaromatic sulfur compounds", Advances in Catalysis, 344-368, 42, 1998

Yang H., Chen J., Briker Y., Szynkarczuk, Ring Z., "Effect of nitrogen removal from light cycle oil on the hydrodesulphurization of DBT, 4, MDBT and 4, 6 DMDBT", Catalysis Today, 160-166, 109, 2005

Yu K., Nikitenko S.I., Gedanken A., "The sonochemical preparation of tungsten oxide nanoparticles", Journal of Materials Chemistry, 1107-1110, 12, 2002

Yui S.M., "Hydrotreating of coker derived gas oil: kinetics of HDS, HDN and mild hydrocracking, and correlations to the product yields and properties", AOSTRA Journal of Research, 211-224, 3, 1989

Van Z. D., Douwes C.T., "Effect of pellet pore structure on catalyst performance in the hydrodesulfurization of straight-run gas oil", Journal of Institute of Petroleum, 383-391, 49 (480), 1963

Zeuthen P., Knudsen K.G., Whitehurst D.D., “Organic nitrogen compounds in gas oil blends, their hydrotreated products and importance to hydrotreatment”, Catalysis Today, 307-314, 65, 2001

Zhang Q., Qian W.,”Effect of H_2S on HDS of DBT and 4, 6 DMDBT”, Sekiyu Gakkaishi 185-191, 40(3), 1997

APPENDICES

Appendix A: Product sulfur and nitrogen concentrations: Phase 2.

Table A.1: Sulfur and nitrogen concentrations in reaction products from catalysts screening tests. Pressure = 8.9 MPa, LHSV = 2 h^{-1} .

	Sulfur, ppm wt			Nitrogen, ppm wt		
Temperature °C / **Catalyst**	**340**	**350**	**360**	**340**	**350**	**360**
Imp 3/7	4415	3190	2287	168	156	135
Imp 3/10	2753	1855	1111	148	115	90
Imp 3.1/12.2	3836	2207	1330	153	120	90
Imp 1/13	6554	5582	3455	164	154	132
Imp 2/13	4195	2680	1643	162	134	113
Sono 3/8	11042	9366	7438	179	170	155
Sono 2.8/11	5604	4748	3570	181	161	139
Sono 3/11.5	4273	3069	1931	167	148	120
Sono 1/10.7	12017	10286	8544	171	160	145
Sono 2/12.3	11351	9537	7465	165	158	140
Sono 4/18	10623	8741	6715	161	146	124
Imp 3/7	4415	3190	2287	168	156	135

Appendix B: Calculation of sulfur & nitrogen molar concentrations and rates of reactions

Sulfur and nitrogen molar concentration in feed and reaction product were calculated using:

$$C_S = \frac{ppm_{wt} 10^{-6} d_{P,T}}{32.064} \quad \text{(b.1)}$$

And,

$$C_N = \frac{ppm_{wt} 10^{-6} d_{P,T}}{14.0067} \quad \text{(b.2)}$$

Where,

$d_{P,T}$ = Gas oil density at operating pressure and temperature, g/cc

C_S = Concentration of sulfur compounds in feed and reaction products, mol/cc

C_N = Concentration of nitrogen compounds in feed and reaction products, mol/cc

Rates of HDS and HDN reactions were calculated using:

$$r_{hds} = \frac{(C_{SF} - C_{SP})10^{-6} LHSV(4.5)}{(32.064)(3600)(3.84x10^{-3})} \quad \text{(b.3)}$$

$$r_{hdn} = \frac{(C_{NF} - C_{NP})10^{-6} LHSV(4.5)}{(14.0067)(3600)(3.84x10^{-3})} \quad \text{(b.4)}$$

Where,

r_{hds} and r_{hdn} = Rates of HDS and HDN reactions, mol/s-kg cat

C_{SF} and C_{SP} = Sulfur concentrations in feed and products, ppmw

C_{NF} and C_{NP} = Nitrogen concentrations in feed and products, ppmw

LHSV = Liquid hourly space velocity, h^{-1}

Appendix C: Product sulfur and nitrogen concentrations with Sono 3/11.5: Phase 3.

Table C.1: Sulfur and nitrogen concentrations in the reaction products from performance tests over sonochemically prepared catalyst.

LHSV, h^{-1}	Gas/Oil Ratio, mL/mL	Pressure, MPa	Temperature, ^{o}C	Sulphor, ppm wt.	Nitrogen, ppm wt.
2.0	600	8.9	370	1108	80
2.0	600	8.9	370	1176	83
2.0	600	8.9	370	1144	89
2.0	600	8.9	370	1193	88
2.0	600	8.9	370	1208	108
2.0	600	8.9	370	1214	102
2.0	600	8.9	340	4709	162
2.0	600	8.9	340	4752	169
2.0	600	8.9	360	2261	118
1.9	600	8.9	360	2265	124
2.0	600	8.9	380	541	82
2.0	600	8.9	380	598	107
1.4	600	8.9	380	354	38
1.4	600	8.9	380	340	37
1.5	600	8.9	360	1106	112
1.6	600	8.9	360	1076	115
1.5	600	8.9	340	2793	180
1.6	600	8.9	340	3002	161
2.0	600	8.9	370	1041	107
2.5	600	8.9	340	4539	187
2.5	600	8.9	340	4622	182
2.5	600	8.9	340	4689	182
2.5	600	8.9	360	2296	147
2.5	600	8.9	380	806	108
2.5	600	8.9	380	952	109
2.0	600	8.9	370	967	106
2.0	600	8.9	370	923	106
1.5	600	10.3	380	335	33
1.5	600	10.3	380	331	32

1.3	600	7.6	380	296	48
1.5	600	7.6	380	341	54
1.5	600	8.9	380	363	42
1.5	600	8.9	380	362	42
1.5	800	10.3	380	262	26
1.5	800	10.3	380	238	26
1.5	400	10.3	380	268	33
1.5	400	10.3	380	381	34

Appendix D: Product sulfur and nitrogen concentrations with Imp 3/10: Phase 3.

Table D.1: Sulfur and nitrogen concentrations in reaction products from performance tests with Imp 3/10.

LHSV, h^{-1}	Gas/Oil Ratio, mL/mL	Pressure, MPa	Temperature, ^{o}C	Sulphor, ppm wt.	Nitrogen, ppm wt.
1.8	600	8.9	370	404	30
2.0	600	8.9	370	576	54
2.0	600	8.9	370	619	61
2.0	600	8.9	370	591	63
2.0	600	8.9	370	597	79
2.0	600	8.9	370	637	78
2.0	600	8.9	370	621	81
2.0	600	8.9	370	621	80
2.0	600	8.9	340	3083	153
2.0	600	8.9	340	3213	157
1.9	600	8.9	360	1222	113
2.0	600	8.9	360	1259	111
1.5	600	8.9	380	253	29
1.5	600	8.9	380	186	26
1.5	600	8.9	380	164	24
1.5	600	8.9	360	658	76
1.5	600	8.9	360	683	78
1.5	600	8.9	340	1980	135
1.5	600	8.9	340	1959	135
2.1	600	8.9	380	470	53
2.0	600	8.9	380	376	49
2.0	600	8.9	370	582	69
2.0	600	8.9	370	603	71
2.6	600	8.9	340	3585	170
2.5	600	8.9	360	1625	135
2.5	600	8.9	360	1522	133
2.5	600	8.9	380	504	73
2.5	600	8.9	380	482	71
2.0	600	8.9	370	592	75

2.0	600	8.9	370	568	74
1.4	600	10.3	380	299	23
1.5	600	10.3	380	178	18
1.4	600	7.6	380	288	48
1.5	600	7.6	380	203	41
1.5	800	10.3	380	278	18
1.6	800	10.3	380	500	19
1.4	400	10.3	380	472	24
1.5	400	10.3	380	1082	28
1.6	400	10.3	380	381	26
1.5	600	10.3	380	318	21
1.6	600	10.3	380	283	21

Appendix E: Evaluation of external mass transfer resistance for HDS and HDN

Satterfield's criterion (1969) was used for examining whether the mass transfer of hydrogen in HDS and HDN of middle distillates was dominant or not:

$$\frac{10 d_p}{3 C_{LH_2}} \left(\frac{-1}{V_c} \frac{dn}{dt} \right) > k_{LS} \qquad \text{(e.1)}$$

Where,

k_{LS} = Overall mass transfer co-efficient for hydrogen, cm/s

C_{LH_2} = Hydrogen concentration in the liquid phase at equilibrium, mol/cc

$\left(\frac{-1}{V_c} \frac{dn}{dt} \right)$ = Rate of reaction for conversion of hydrogen, mol of H2/s-cc pellet

V_c = Catalyst volume = 4.26 cc (volume of the catalyst loaded in the reactor)

d_p = Average catalyst particle diameter = 0.17 cm

The validity of criterion indicated that mass transfer was dominant in the reaction setup.

Calculation of Overall Mass Transfer Co-efficient (k_{LS})

The overall mass transfer co-efficient was calculated using:

$$\frac{1}{k_{LS}} = \frac{1}{k_{iL}} + \frac{1}{k_{iS}} \qquad \text{(e.2)}$$

Where

k_{iL} = Liquid film side hydrogen – gas oil mass transfer co-efficient, cm/s

k_{iS} = Solid side hydrogen – gas oil mass transfer co-efficient, cm/s

Gotto–Smith's correlation (1975) was used for calculating the gas liquid mass transfer co-efficient (k_{iL}):

$$\frac{k_{iL} a_L}{D_{iL}} = \alpha_1 \left(\frac{G_L}{\mu_L} \right)^{\alpha_2} \left(\frac{\mu_L}{\rho_L D_{iL}} \right)^{(1/2)} \qquad \text{(e.3)}$$

Where,

k_{iL} = Liquid film side hydrogen – gas oil mass transfer co-efficient, cm/s

a_L = Interfacial surface area per unit volume = $(6/d_p)(1-\varepsilon)$ = 24.71 cm^{-1}

(Assuming the interfacial area is equal to the catalyst pellet outside area.)

d_p = Average particle diameter = 0.17 cm

(Average particle diameter between 10 and 12 mesh size.)

ε = Bed porosity = 0.3 (assumed, based on typical industrial values)

G_L = Liquid mass flow per unit area = 1.624e-3 g/cm^2-s

μ_L = Viscosity of gas oil at operating temperature, g/cm-s

D_{iL} = Diffusivity of hydrogen in gas oil, cm^2/s

ρ_L = Density of gas oil at operating temperature, g/c

$\acute{\alpha}_1$ = Constant based on the particle properties = 8.21

$\acute{\alpha}_2$ = Constant based on the particle properties = 0.39

(values of $\acute{\alpha}_1$ and $\acute{\alpha}_2$ calculated by extrapolating the data given by Gotto and smith, 1975)

Calculation of gas oil viscosity

Glasso's correlation (Published in Ahmed, 1989) was used for calculating the viscosity of gas oil at operating temperature:

$$\mu_L = 3.141x10^{10}\left(T-460\right)^{-3.444}\left(\log{}^{\circ}API\right)^{a} \qquad \text{(e.4)}$$

Where,

$$a = 10.313\log(T-460) - 36.447 \qquad \text{(e.5)}$$

And,

T = Operating temperature = 1175.7 °R

$$^{\circ}API = \frac{141.5}{SG} - 131.5$$

SG = Specific gravity of gas oil at 15.6 °R = 0.871

This gave,

°API = 30.96

The calculated values of a and μ_L were:

a = -7.006

μ_L = 0.282 cP

Calculation of gas oil molecular weight

Winn's correlation was used for calculating the average molecular weight of gas oil:

$$M = aT_b^{\alpha}\rho^{\beta} \qquad \text{(e.6)}$$

Where,

M = Average molecular weight of gas oil, g/mol

T_b = Average boiling point of gas oil = 568 °K

(Taken as the mid boiling point of distilation range of gas oil.)

ρ = Gas oil density at 15.6 °C, g/cc

a = Empirical constant = 5.805e-5

α = Empirical constant = 2.3776

β = -0.9371

(values of α and β are original values of the correlation, Trytten et al., 1990)

The calculated value of average molecular weight of gas oil was:

***M* = 233.5 g/mol**

Calculation of diffusivity of hydrogen in gas oil

Wilke-Chang correlation (1955) was used for calculating the effective diffusivity of hydrogen molecules:

$$\frac{D_{iL}\mu_L}{T} = 7.4x10^{-8}\frac{(XM)^{0.5}}{V_b^{0.6}} \quad \text{(e.7)}$$

Where,

D_{iL} = Bulk diffusivity of the hydrogen, cm^2/sec

μ_L = Gas oil viscosity, cP

T = operating temperature = 653.2 °K

X = Association parameter, (1 for mixture of hydrocarbons)

M = Gas oil molecular weight, g/mol

V_b= Hydrogen molar volume at normal boiling point

= 14.3 cc/mol (Wijngaarden, Industrial Catalysis, 1998)

The calculated value of bulk diffusivity of hydrogen in gas oil was:

D_{iL} = 5.3012e-4 cm^2/s

Calculation of density of gas oil at reaction pressure and temperature

Standing-Katz correlation (published in Ahmed, 1989) was used for calculating the density of the gas oil at reactor operating conditions:

$$\rho_L = \rho_0 - \Delta\rho_T + \Delta\rho_P \quad \text{(e.8)}$$

Where,

ρ_L = Density at operating temperature and pressure, lb/ft^3

ρ_0 = Density at 15.6 °C and atmospheric pressure = 54.375 lb/ft^3

(Value measured using densitymeter.)

$\Delta\rho_T$ = Temperature density correction, lb/ft^3

$\Delta\rho_P$ = Pressure density correction, lb/ft^3

Pressure and temperature corrections were calculated using:

$$\Delta\rho_P = \left[0.167 + 16.181x10^{-0.0425\rho_0}\right]\left(\frac{P}{1000}\right) - 0.01\left[0.299 + 263x10^{-0.603\rho_0}\right]\left(\frac{P}{1000}\right)^2 \quad \text{(e.9)}$$

$$\Delta\rho_T = \left(0.0133 + 152.4(\rho_0 + \Delta\rho_P)^{-2.45}\right)(T - 520) - \left(8.1x10^{-6} - 0.0622x10^{-0.764(\rho_0+\Delta\rho_P)}\right)(T - 520)^2 \quad \text{(e.10)}$$

Where,

P = 1300 psia

T = 1175.7 °R

The calculated values of pressure density correction, temperature density correction and density were:

$\Delta\rho_T$ = 10.763 lb/ft^3

$\Delta\rho_P$ = 0.302 lb/ft^3

ρ_L = 43.91 lb/ft^3 = 703.446 kg/

Using all the values calculated thus far give

k_{iL} = 1.74e-4 cm/s

Calculation of liquid – solid mass transfer co-efficient

Van Krevelen-Krekels equation (Published in Froment and Bishoff, 1990) was used for calculating liquid-solid mass transfer co-efficient in low interaction regime for:

$$\frac{k_{iS}}{D_{iL}a_S} = 1.8\left(\frac{G_L}{a_S\mu_L}\right)^{1/2}\left(\frac{\mu_L}{\rho_L D_{iL}}\right)^{1/3} \quad \text{(e.11)}$$

Where

a_S = Liquid solid interfacial surface area = a_L = 35.3 cm^{-1}

k_{iS} = Solid side hydrogen – gas oil mass transfer co-efficient., cm/s

Remaining terms are as defined before.

Using the values as calculated before:

k_{iS} = 8.83e-3 cm/s

Calculation of equilibrium concentration of hydrogen in gas oil

The concentration of hydrogen in gas oil phase was calculated using Henry's constant assuming it to be sparingly soluble in hydrocarbon mixtures.

The equilibrium concentration of hydrogen in bulk gas oil phase can be given by:

$$C_{LH_2} = \frac{P}{H_{H_2}} \qquad \text{(e.12)}$$

Where,

H_{H_2} = Henry's constant for hydrogen in gas oil, MPa-m^3/gmol

P = Reaction pressure, MPa

The Henry's constant can be calculated using the equation below:

$$H_{H_2} = \frac{v_n}{\lambda_{H_2}\rho_L} \qquad \text{(e.13)}$$

v_n = Hydrogen molar volume at standard conditions = 22400 cc/gmol

ρ_L = Density of gas oil at operating conditions = 703 kg/m^3

λ_{H_2} = Solubility of hydrogen in gas oil, cc/kg oil-MPa

Expression published by Hoffman et al. 1996 was used for calculating the solubility of hydrogen in gas oil fractions:

$$\lambda_{H_2} = a_0 + a_1 T + a_2 \frac{T}{\rho_{20}} + a_3 T^2 + a_4 \frac{1}{\rho_{20}^2} \qquad \text{(e.14)}$$

Where,

a_0 = -0.559729

a_1 = -0.42947e-3

a_2 = 3.07539e-3

a_3 = 1.94593e-6

a_4 = 0.835783

T = Reaction temperature, °C

ρ_{20} = Gas oil density at 20 °C, kg/m^3

λ_{H_2} = Hydrogen solubility in gas oil, Nl/kg oil-MPa

The calculated value of hydrogen solubility was:

λ_{H_2} = 2.00 Nl H_2/kg oil-MPa

The calculated value of Henry's constant for hydrogen in gas oil was:

H_{H_2} = 0.01616 MPa-m^3/gmol

The calculated value of hydrogen concentration in gas oil was:

C_{LH_2} = **5.57e-4 mol/cc of oil**

Calculation of rate of reaction for conversion of hydrogen

HDS rate equation was used for getting the rate of conversion of hydrogen:

$$\text{R-S} + \nu_i\ H_2 \rightarrow \text{R-(H)}_{2\text{vi-2}} + H_2S$$

The rate of conversion of S species was calculated using the data obtained from sulfur analysis of feed and product samples.

Rate of hydrogen was calculated from the relative rate of equation:

$$\frac{\text{Rate of conversion of S species}}{1} = \frac{\text{Rate of conversion of Hydrogen}}{\nu_i}$$

So in Satterfield's criterion, the rate was given by:

$$\left(-\frac{1}{V_c}\frac{dn}{dt}\right) = \frac{\nu_i \text{Rate of conversion of S species}}{\text{Volume of catalyst particles}} \qquad \text{(e.15)}$$

The stochiometric co-efficient for hydrogen in HDS reaction of LGO is ~3.0 mol/mol of sulfur converted.

$$v_i = 3.0$$

The rate of conversion of sulfur species was calculated using equation b.3 in Appendix B. The calculated conversion of hydrogen in Satterfield's criterion was:

For HDS

$$\left(-\frac{1}{V_c}\frac{dn}{dt}\right) = \textbf{8.49e-7}$$

For HDN

$$\left(-\frac{1}{V_c}\frac{dn}{dt}\right) = \textbf{6.71e-9}$$

For HDS

Left hand side of the Satterfield's criterion = 8.63e-4 cm/s

Right hand side of the Satterfield' criterion = 1.71e-4 cm/s

For HDN

The data used for calculation of values of Satterfield's criterion for HDN are same as those for HDS. The only difference is in the rate of HDN reaction.

Left hand side of the Satterfield's criterion = 6.75e-6 cm/s

Right hand side of the Satterfield' criterion = 1.71e-4 cm/s

Table E.1 summarizes the reaction conditions and calculated parameters for this section.

Table E.1: Mass transfer in laboratory trickle bed micro reactor – Summary of results.

Pressure, bar	90
Temperature, °C	380
LHSV, h^{-1}	2
Feed flow rate, g/h	9.0
Particle size , mm	1.7
Bed porosity	0.3
Mass flow, g/cm^2-sec	1.62e-3
Density of gas oil at operating conditions, kg/	693
Average molecular weight of gas oil, kg/mol	233.5
Viscosity of gas oil, cP	0.282
Henry's constant, MPa-m^3/gmol	0.01616
Hydrogen concentration in gas oil, gmol/cc	5.57e-4
Diffusivities	
Sulfur compounds,, cm^2/s	6.73e-5
Hydrogen, cm^2/s	5.20e-4
Mass transfer co-efficients	
Liquid film side hydrogen – gas oil mass transfer co-efficient, cm/s	1.74e-4
Solid side hydrogen – gas oil mass transfer co-efficient., cm/s	8.83e-3
Overall, cm/s	1.71e-4
HDN rate per unit volume of cat, gmol H_2/s-cc of cat.	6.75e-6
Left side of Satterfield's criterion for HDN	1.71e-4
HDS rate per unit volume of cat, gmol H_2/s-cc of cat.	8.49e-7
Left side of Satterfield's criterion for HDS	8.63e-4

Appendix F: Calculation of internal resistance for HDS and HDN.

Since HDS reaction is exothermic in nature, so non-isothermality of the catalyst particle was checked before calculating the effectiveness factor. It was checked by calculating the value of β which has been defined as the ratio of maximum possible temperature rise that could exist in a pellet relative to the surface temperature. For further ensuring the isothermality of catalyst pellet Anderson's criterion (1963) was used.

Calculation of β

$$\beta = \frac{\Delta T_{\max}}{Ts} = \frac{\Delta H_{Rx} D_e C_{AS}}{k_t T_S} \qquad \text{(f.1)}$$

Where ΔH_{Rx} = Heat of HDS reaction, kJ/mol

D_e = Effective diffusivity for sulfur containing molecules, cm^2/s

C_{AS} = Catalyst surface concentration of sulfur species, gmol/cc

(Assumed to be equal to the bulk concentration of sulfur species.)

k_t = Thermal conductivity of catalyst pellet = 5e-3 J/cm-°K (Wijngaarden, Industrial Catalysis, 1998)

T_S = Catalyst pellet surface temperature = 653.2 °K (Taken as equal to the bulk liquid temperature.)

Calculation of HDS heat of reaction

HDS heat of reaction for LGO derived from Athabasca bitumen ranges from 65 - 76 Btu/scf of hydrogen consumed.

The heat of reaction per unit volume of hydrogen consumed was converted to kJ/mol of sulfur by using the stoichiometric co-efficient for HDS reaction.

Heat of reaction for HDS = 76 Btu/scf (Taking upper value of the range)

= 2832.2 kJ/standard m^3 of hydrogen consumed

Now 1 mol of hydrogen = 22000 cc at STP

= 0.022 m^3 at STP

Or, 1 m^3 of hydrogen = 45.45 mol hydrogen

Which gives the heat of reaction = 62.31 kJ/mol of hydrogen consumed

Since the stoichiometric factor for hydrogen in HDS of LGO is 3.0 so the heat of the reaction per mol of S consumed will be = 187 kJ/mol of S converted

Or, ΔH_{Rx} **= 187000 J/mol sulfur**

Calculation of effective diffusivity of sulfur species in gas oil (*De*)

The effective diffusivity was calculated using:

$$D_e = \frac{\varepsilon_p D_{iL}}{\gamma_p} \qquad \text{(f.2)}$$

Where,

ε_p = Porosity of catalyst pellet

γ_p = Tortuosity of catalyst pellet

D_{iL} = Bulk diffusivity of sulfur containing molecules, cm^2/g

Since γ-Al_2O_3 is prepared using gels and then extruded to give the final shape. So the Probst and Wohlfahrt correlation (published in Wijngaarden, Industrial Catalysis, 1998) which gives the correlation between porosity and tortuosity of gel prepared catalysts was used.

$$\frac{\varepsilon_p}{\gamma_p} = e^{\left(m(1-1/\varepsilon_p)\right)} \qquad \text{(f.3)}$$

Where,

m = 1.8, (Range = 1.4 to 2.2, taken as the mid value of the range)

ε_p = 0.4, (Range = 0.35 to 0.7)

(Wijngaarden, Industrial Catalysis, 1998)

The calculated value of $\frac{\varepsilon_p}{\gamma_p}$ was:

$$\frac{\varepsilon_p}{\gamma_p} = 0.067$$

Calculation of bulk diffusivity of sulfur species (D_{iL})

It was assumed that the organic sulfur compounds had same density, average boiling point and molecular weight as that of light gas oil feed. These assumptions also indicated that the molar volume of average sulfur compounds were equal to that of the LGO. The diffusivity was calculated using Tyn-Calus correlation (Published by Reid et al., 1987).

$$D_{iL} = 8.93x10^{-8} \frac{v_L^{0.267}}{v_i^{0.433}} \frac{T}{\mu_L} \qquad \text{(f.4)}$$

Where,

T = Temperature of gas oil = 653 °K

μ_L = Viscosity of gas oil at reaction temperature

= 0.282 mPa.s (from Appendix C)

v_i = Molar volume of sulfur containing molecules at normal boiling conditions, cc/mol

v_L = Molar volume of gas oil molecule at normal boiling conditions, cc/mol

The molar volumes were calculated using equation d.3:

$$v = 0.285 v_c^{1.048} \qquad \text{(f.5)}$$

Where,

v_c = Critical specific volume of liquid, cc/mol

Where v_c is given by:

$$v_c = v_c^m M \qquad \text{(f.6)}$$

Where M = 233.5 g/mol (from Appendix C)

The critical molar volumes were calculated using Riazi-Daubert Correlation (Ahmed, 1989):

$$v_c^m = 7.5214 x 10^{-3} T_{MeABP}^{0.2896} d_{15.6}^{-0.7666} \qquad \text{(f.7)}$$

Where,

v_c^m = Critical specific volume, ft^3/lb

T_{MeABP} = Mean average boiling point = 1022.67 °R

$d_{15.6}$ = Spefic gravity at 15.6 °C = 0.871

The calculated values of critical specific volumes for sulfur compounds and solvent liquid were:

v_c^m = 0.0622 ft^3/lb = 3.887 cc/g

which gave

$v_c = M \,.\, v_c^m$ = 905.6 cc/mol

Using equation d.3 gives

v_i = 357.86 cc/mol

And the calculated value of diffusivity of sulfur compounds came out to be:

D_{iL} = 7.79e-5 cm^2/g

So, using equation d.2, the calculated value of effective diffusivity was:

$\boldsymbol{D_e}$ **= 5.22e-6 cm^2/g**

Using the values mentioned above, the calculated value of β was:

β = 9e-5

Anderson's criterion

$$\frac{\left|\Delta H_{Rx}\right|\left\langle R_A\right\rangle d_p^2}{4k_t T_S} < \frac{0.75 T_S R}{E_a} \qquad \text{(f.8)}$$

Where $\langle R_A \rangle$ = Global rate of reaction per unit volume of catalyst = 2.83e-7 gmol/s-cc cat

k_t = Thermal conductivity of the catalyst = 5e-3 J/cm-°K

R = Universal gas constant = 8.314 J/gmol-°K

E_a = Energy of activation = 82060 J/gmol (Taken from Gusta E., 2005)

Remaining parameters are already defined.

The two sides of Anderson's criterion are:

Left hand side of Anderson's criterion = 8.9e-5

Right hand side of Anderson's criterion = 0.05 (For E_{act} = 82060 J/mol)

= 0.10 (For E_{act} = 164120 J/mol)

Table F.1 summarizes the results of the isothermality of the catalyst pellet.

Calculation of Φ

The value of Thiele modulus could not be calculated from the data obtained from experiments as it required the information about intrinsic rate of reaction. A different dimensionless modulus was used to estimate the pore diffusion resistance (published in Satterfield, 142, 1970):

$$\Phi \equiv \frac{R^2}{D_e}\left(-\frac{1}{V_c}\frac{dn}{dt}\right)\frac{1}{C_{AS}} \qquad \text{(f.9)}$$

Table F.1: **Isothermality of the catalyst pellet – Summary of results**

Heat of reaction, J/gmol sulfur	187000
Effective diffusivity, cm^2/s	5.22e-6
Surface concentration of sulfur compounds (In LGO feed), mol s/cc	3.53e-4
Thermal conductivity of catalyst pellet, J/cm-°K	0.5e-3
Pellet surface temperature, °K	658
Energy of activation, J/mol	82060
Value of β	9e-5
Global rate of reaction, mol sulfur/s-cc cat.	2.83e-7
LHS of Anderson's equation	8.9e-5
RHS of Anderson's equation	0.05

Where,

$\left(-\frac{1}{V_c}\frac{dn}{dt}\right)$ = Global rate of reaction per unit volume of the catalyst, gmol/s-cc cat

C_{AS} = Surface concentration of sulfur compounds, gmol/cc (taken as the bulk concentration)

R = Average radius of catalyst pellet, cm

D_e = Effective diffusivity of sulfur containing molecules, cm^2/s

Concentration of sulfur compounds at the inlet of the reactor (same as in feed)

= 3.53e-4 gmol/cc

Concentration of sulfur compounds at the outlet of the reactor (in the product)

= 4.38e-5 gmol/cc

This gives the dimensionless modulus and first order effectiveness factors (particle shape approximated with the shape of a sphere) in each of the above cases (Satterfield, "Mass transfer in heterogeneous catalysts", 142-145, 1970):

$\Phi_{Inlet} = 0.88$, $\eta = 1$

$\Phi_{Outlet} = 5.09$, $\eta = 0.65$

The values of reaction Φ for all the experiental runs are listed on Tables 4.10 through 4.13.

Appendix G: Rate models examined for kinetic study with Sono 3/11.5.

Table G.1: HDS Langmuir - Hinshelwood model: $r_{hds} = \dfrac{k_{hds} C_S^{1.4}}{(1 + K_{hds} C_S)^2}$

Temperature, °C	k_{hds}, $m^{1.2}$/s-$mol^{0.4}$	K_{hds}, m^3/mol
340	0.039 ± 0.007	66.285 ± 2.463
360	0.121 ± 0.154	30.233 ± 4.488
380	0.328 ± 0.131	45.514 ± 22.235

Figure G.1: HDS Power Law model: $r_{hds} = k_{hds} C_S^n$

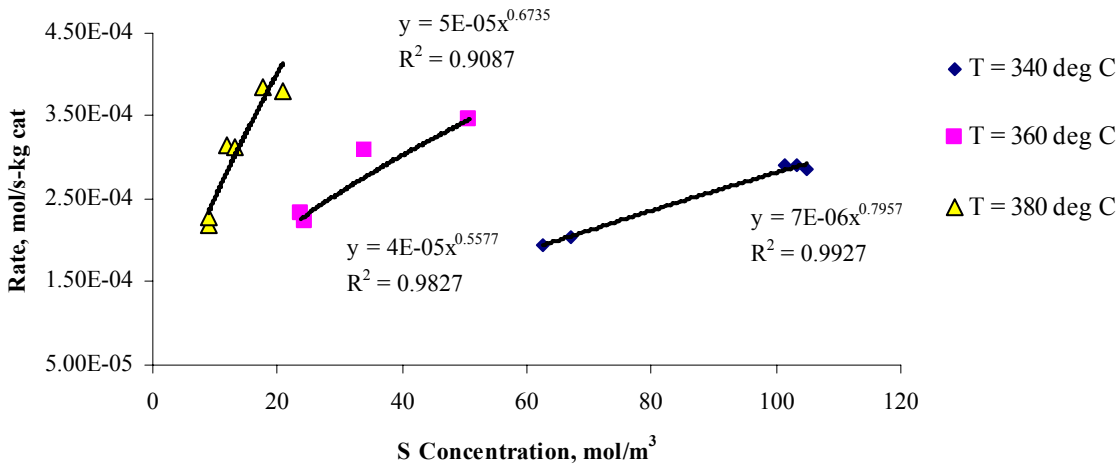

Table G.2: HDS Power Law model: $r_{hds} = k_{hds} C_S^{0.57}$

Temperature, °C	k_{hds}, $mol^{0.43}$-$m^{1.71}$/s-kg cat.
340	2.00e-5 ± 1.37e-6
360	3.70e-5 ± 2.49e-6
380	7.04e-5 ± 5.49e-6

Figure G.2: HDN Power Law model: $r_{hdn} = k_{hdn} C_N^n$

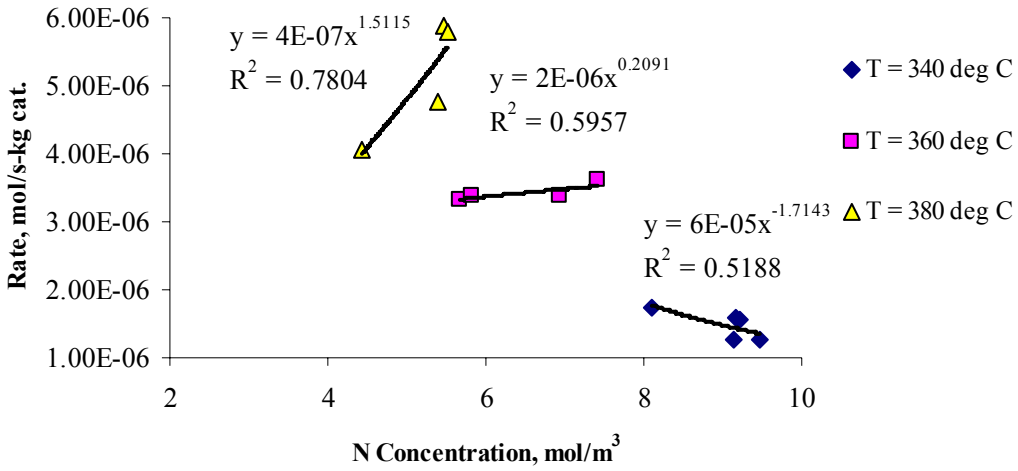

Table G.3: HDN Langmuir - Hinshelwood model: $r_{hdn} = \dfrac{k_{hdn} C_N^{1.2}}{(1 + K_{hdn} C_N)^{2.5}}$

Temperature, °C	k_{hdn}, $m^{0.6}/s\text{-}mol^{0.2}$	K_{hdn}, m^3/mol
340	0.03 ± 0.0159	16.140 ± 3.843
360	1.28e-6 ± 1.21e-6	0.100 ± 0.096
380	1.36e-6 ± 8.7e-9	0.055 ± 0.006

Appendix H: Rate models examined for kinetic study of results with Imp 3/10.

Table H.1: HDS Langmuir - Hinshelwood model: $r_{hds} = \dfrac{k_{hds} C_S^{1.6}}{(1 + K_{hds} C_S)}$

Temperature, °C	k_{hds}, $m^{1.8}$/s-$mol^{0.6}$	K_{hds}, m^3/mol
340	0.083 ± 0.002	15.203 ± 0.446
360	0.538 ± 0.011	48.474 ± 0.869
380	4.456 ± 0.099	178.095 ± 3.304

Figure H.1: HDS Power Law model: $r_{hds} = k_{hds} C_S^n$

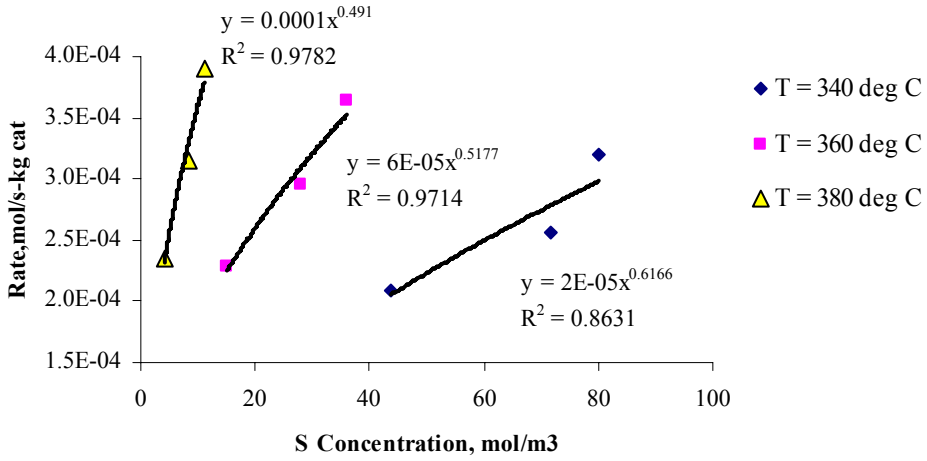

Table H.2: HDS Power Law model: $r_{hds} = k_{hds} C_S^{0.57}$

Temperature, °C	k_{hds}, $mol^{0.43}$-$m^{1.71}$/s-kg cat.
340	2.32e-5 ± 1.36e-6
360	4.67e-5 ± 2.49e-6
380	9.48e-5 ± 9.29e-6

.

Figure H.2: HDN Power Law model: $r_{hdn} = k_{hdn} C_N^n$

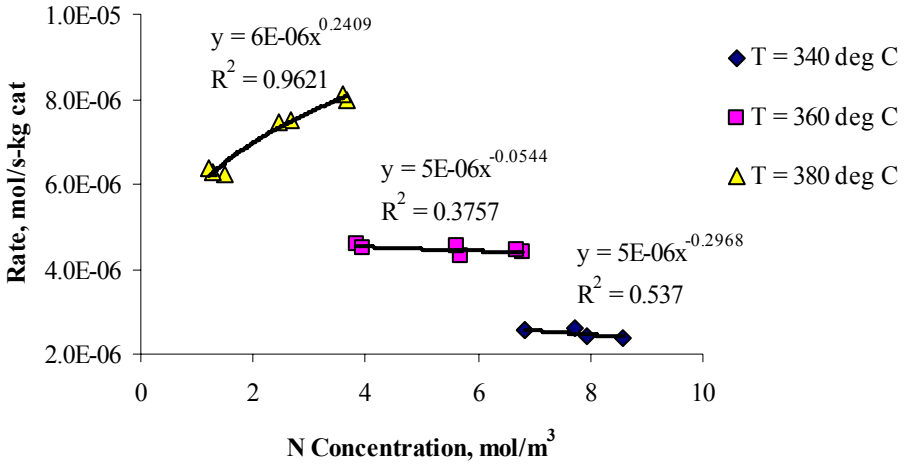

Table H.3: HDN Langmuir - Hinshelwood model: $r_{hdn} = \dfrac{k_{hdn} C_N^{0.5}}{(1 + K_{hdn} C_N)^2}$

Temperature, °C	k_{hdn}, mol$^{0.5}$/s-m$^{0.5}$	K_{hdn}, m^3/mol
340	2.62e-6 ± 1.77e-7	0.093 ± 0.007
360	3.80e-6 ± 2.94e-7	0.073 ± 0.010
380	6.46e-6 ± 5.34e-7	0.066 ± 0.018